Title
Pharmacological Targeting of a Metabolic Co-Dependency Pathway in Brain Cancers

Author
Villa, Genaro Rodriguez

Publication Date
2016

Peer reviewed|Thesis/dissertation

UNIVERSITY OF CALIFORNIA

Los Angeles

Pharmacological Targeting of a Metabolic Co-Dependency Pathway in Brain Cancers

A dissertation submitted in partial satisfaction of the
requirements for the degree of Doctor of Philosophy
in Molecular and Medical Pharmacology

By

Genaro Rodriguez Villa

2016

ABSTRACT OF THE DISSERTATION

Pharmacological Targeting of a Metabolic Co-Dependency Pathway in Brain Cancers

by

Genaro Rodriguez Villa
Doctor of Philosophy in Molecular and Medical Pharmacology
University of California, Los Angeles, 2016
Professor Harvey R. Herschman, Co-Chair
Professor Paul Mischel, Co-Chair

Oncogenic mutations in growth factor receptor signaling pathways are common in cancer, including in tumors that arise from or metastasize to the brain. However, most small-molecule inhibitors targeting growth factor receptors have failed to show efficacy for brain cancers, potentially due to inability to achieve sufficient drug levels in the central nervous system (CNS). Targeting tumor co-dependencies provides an alternative approach, particularly if drugs with high brain penetration can be identified. Here we demonstrate that EGFR-mutant cancers, including a highly lethal form of brain cancer glioblastoma (GBM), are remarkably dependent on cholesterol for survival, rendering them sensitive to Liver X receptor (LXR) agonist-dependent cell death. We show that LXR-623, a clinically viable, highly brain-penetrant LXRα-partial/LXRβ-full agonist selectively kills GBM cells in an LXRβ- and cholesterol-dependent fashion, causing significant tumor regression and prolonged survival in mouse models. Thus, a metabolic co-dependency provides a pharmacological means to kill growth factor-activated cancers in the CNS.

The dissertation of Genaro Rodriguez Villa is approved.

Steven J. Bensinger

Heather R. Christofk

Peter John Tontonoz

Harvey R. Herschman, Committee Co-Chair

Paul Mischel, Committee Co-Chair

University of California, Los Angeles

2016

For my loving parents,

Genaro M. Villa and Martha E. Villa

Table of Contents

Figures and Tables

Acknowledgements

Many exceptional individuals contributed to the work presented in this dissertation as well as my graduate school experience. First, I would like to give thanks to the members of the Mischel laboratory, past and present, who contributed to this work.

In addition, I would like to acknowledge and give thanks to members of the Ludwig Institute for Cancer Research including Andrew Shiau, Timothy Gahman, and Webster Cavenee. These outstanding scientists contributed immensely to the work in this dissertation and I am indebted to them for their support and mentoring throughout my time at the Ludwig Institute.

I would also like to thank Benjamin Cravatt for helpful discussions regarding experimental design and presentation of data, as well as the framing of the work for both this dissertation and the associated manuscript.

To the members of my committee, including Harvey Herschman, Heather Christofk, Peter Tontonoz, and Steve Bensinger, thank you for your support and guidance. To Harvey, for reminding me to be bold with my hypotheses, but careful with my experiments. To Heather, for her technical support and guidance, and her humility in explaining her own challenges in graduate school. To Peter, for challenging me to think critically and creatively, including with finding a pharmacologic advantage of the compound described in this dissertation. Lastly, to Steve for guidance with experiments and for suggesting I apply for grants.

Importantly, I would like to thank my advisor, Paul Mischel, for being such a great mentor to me, both professionally and personally. The work in this dissertation is the direct result of advice and support from Paul. His enthusiasm for scientific discovery has been infectious and inspiring.

I am grateful to Paul for encouraging me to be fearless in the face of uncertainty. It has been an honor and a privilege to have had Paul as a mentor and I will always be thankful to him for making my graduate school experience truly exceptional.

Lastly, I would like to thank my parents for their support and love throughout my journey in higher education. Your faith in me was a constant source of motivation throughout this process. To my father for reminding me to be myself and to my mother for reminding me to stop and smell the roses – it was your absence of opportunity and unconditional support that told me I could succeed in higher education.

The work for this dissertation was performed under the direction of Dr. Paul S. Mischel and supported by the National Cancer Institute grant F31CA186668 to G.R.V. My contributions were to the conception, design and execution of the experiments, with assistance from co-authors in some cases, in each of the following studies.

Chapters 1-4 of this dissertation are based upon work from the manuscript:

Villa GR, Hulce JJ, Zanca C, Ikegami S, Cahill GL, Gu Y, Bi J, Lum KM, Masui K, Yang, H, Rong X, Hong C, Turner K, Liu F, Hon GC, Jenkins D, Martini M, Armando AM, Quehenberger O, Cloughesy TF, Furnari FB, Cavenee WK, Tontonoz P, Gahman TC, Shiau AK, Cravatt BF, Mischel PS. An LXR-Cholesterol Axis Creates a Metabolic Co-Dependency for Brain Cancers. Submitted, *Cancer Cell*. 2016.

Vita

Education

2007 B.S. Molecular, Cell, and Developmental Biology

University of California, Los Angeles

Publications

Villa GR, Hulce JJ*, Zanca C*, Ikegami S, Cahill GL, Gu Y, Bi J, Lum KM, Masui K, Yang, H, Rong X, Hong C, Turner K, Liu F, Hon GC, Jenkins D, Martini M, Armando AM, Quehenberger O, Cloughesy TF, Furnari FB, Cavenee WK, Tontonoz P, Gahman TC, Shiau AK, Cravatt BF, Mischel PS. An LXR-Cholesterol Axis Creates a Metabolic Co-Dependency for Brain Cancers. Submitted, *Cancer Cell*. 2016

Villa GR, Mischel PS. Old Player, New Partner: EGFRvIII and Cytokine Receptor Signaling in Glioblastoma. *Nature Neuroscience*. 2016

Zanca C, **Villa GR**, et al. Tumor heterogeneity contributes to resistance to anti-EGFR therapy in glioblastoma. In preparation. 2016.

Lucki N, **Villa GR**, et al. Selective induction of RIPK2-mediated apoptosis in glioblastoma cancer stem cells. In Preparation. 2016.

Villa GR, Mischel PS. Shared Intelligence: A Patient-Derived, Deeply Characterized Glioblastoma Cell Line Resource. *EBioMedicine*. 2015

Liu F*, Hon GC*, **Villa GR**, et al. EGFR Mutation Promotes Glioblastoma through Epigenome and Transcription Factor Network Remodeling. *Molecular Cell*. 2015

Wykosky J, Hu J, Gomez GG, Taylor T, **Villa GR**, et al. A urokinase receptor-Bim signaling axis emerges during EGFR inhibitor resistance in mutant EGFR glioblastoma. *Cancer Research*. 2015

Masui K, Tanaka K, Akhavan D, Babic I, Gini B, Matsutani T, Iwanami A, Liu F, **Villa GR**, et al. mTOR complex 2 controls glycolytic metabolism in glioblastoma through FoxO acetylation and upregulation of c-Myc. *Cell Metabolism*. 2013

Gini B, Zanca C, Guo D, Matsutani T, Masui K, Ikegami S, Yang H, Nathanson D, **Villa GR**, et al. The mTOR kinase inhibitors, CC214-1 and CC214-2, preferentially block the growth of EGFRvIII-activated glioblastomas. *Clinical Cancer Research*. 2013

Babic I, Anderson ES, Tanaka K, Guo D, Masui K, Li B, Zhu S, Gu Y, **Villa GR**, et al. EGFR mutation-induced alternative splicing of Max contributes to growth of glycolytic tumors in brain cancer. *Cell Metabolism*. 2013

Akhavan D, Pourzia AL, Nourian AA, Williams KJ, Nathanson D, Babic I, **Villa GR**, et al. De-repression of PDGFRβ transcription promotes acquired resistance to EGFR tyrosine kinase inhibitors in glioblastoma patients. *Cancer Discovery*. 2013

*These authors contributed equally.

Introduction

Oncogenic Signaling, Metabolism, and Glioblastoma

Growth factor receptor mutations and amplifications are a hallmark of many cancers, including in those that arise from or metastasize to the brain (Ciriello et al., 2013; Kandoth et al., 2013). Cancer cells harboring growth factor receptor mutations are characterized by constitutive or hyperactive signaling cascades that have essential roles in tumorigenesis and tumor cell survival. The cancer field has established that these signaling cascades converge to promote tumor growth and survival, at least in part, through reprogramming of epigenetic, transcriptional, and metabolic networks (Hanahan and Weinberg, 2011; Lee and Young, 2013; Pavlova and Thompson, 2016).

Malignant brain tumors are among the most devastating types of cancer. Despite improvements in surgical techniques, development of various cytotoxic chemotherapy regimens, and advances in the delivery of focused radiation, the survival of most brain cancer patients has not appreciably improved over the past 50 years (Ohgaki and Kleihues, 2005; Owonikoko et al., 2014).

Glioblastoma (GBM) is the most common primary malignant brain tumor in adults and is among the most lethal of all cancers. GBMs are highly invasive and rapidly develop resistance to conventional therapy (Furnari et al., 2007; Wen and Kesari, 2008). Despite surgery and aggressive treatment with alkylating chemotherapy and radiation, the median patient survival ranges from 12-15 months from initial diagnosis (Stupp et al., 2005). Only minimal improvement in median survival has been achieved in patients with GBM for reasons ranging from the ineffectiveness of drugs traversing the blood brain barrier to the lack of treatments effectively targeting tumor heterogeneity (Furnari et al., 2007, 2015; Inda et al., 2010; Wen and Kesari, 2008). Therefore, new treatments tailored to the biology of GBM are urgently needed.

Genomically, GBM is one of the most deeply characterized forms of cancer. Mutations in coding genes that occur at frequencies greater than 5% above background are likely to have already been identified (Lawrence et al., 2014), revealing a landscape of potentially actionable drug targets. Growth factor receptor amplification and mutations, including epidermal growth factor receptor (EGFR) alterations, PIK3CA mutations and PTEN deletion and mutation are especially common(Brennan et al., 2013). EGFRvIII is the most common gain of function EGFR mutation in GBM, arising through a genomic deletion of exons 2-7 in EGFR amplified tumors (Furnari et al., 2007). EGFRvIII lacks the ligand binding domain and is persistently activated, promoting tumor formation by activating aberrant signaling pathways (Huang et al., 1997, 2007). Growth factor receptor signaling is activated by copy number alterations and mutations in close to 90% of tumors sampled (Brennan et al., 2013). Despite the compelling nature of EGFRvIII and other EGFR mutations as actionable drug targets, EGFR tyrosine kinase inhibitors have so far proven ineffective (Cloughesy et al., 2014). The current generation of EGFR inhibitors do not reach therapeutic levels in tumors in the central nervous system (CNS) (Vivanco et al., 2012), leading to the appearance of multiple resistance mechanisms (Furnari et al., 2015). Thus, to date, this information has yet to translate into new treatments or better outcomes for patients. Acting upon insights gained by the genomic road map will require a deeper understanding of how specific mutations cause tumors through reprogramming of signaling, metabolic and epigenetic networks, particularly with regard to identifying therapeutic vulnerabilities (Cloughesy et al., 2014).

GBMs, like many other cancer types, are characterized by major alterations in their cellular metabolism, increasing their uptake and utilization of glucose coupled to enhanced lipogenesis to meet the coordinately elevated anabolic and energetic demands imposed by rapid

tumor growth (Babic et al., 2013; Guo et al., 2009; Masui et al., 2013, 2015a). These metabolic alterations and the signaling pathways that control them, appear to be direct consequences of the genetic alterations that drive tumor growth and progression, thus providing a new array of potentially more specific and efficacious drug targets. Dissecting the molecular circuitry by which oncogenes and tumor suppressor losses alter cellular metabolism to support tumor growth and survival could lead to the development of new, highly specific and more effective GBM treatments.

GBM metabolic reprogramming drives changes in the uptake and utilization of cellular nutrients, as a consequence of upstream mutations in the EGFR–phosphoinositide 3-kinase (PI3K)–v-akt murine thymoma viral oncogene (Akt)–mechanistic target of rapamycin (mTOR) signaling network (Masui et al., 2015b). Dysregulated EGFR signaling activates two distinct mTOR complexes, namely mTORC1 and mTORC2, which drive alterations in nutrient availability and utilization by controlling protein levels of c-Myc, a master transcriptional regulator of genes involved in glucose and glutamine metabolism (Dang, 2013; Dang et al., 2009; Miller et al., 2012). A set of interlacing molecular mechanisms are responsible for EGFR-dependent mTORC1 and mTORC2 regulation of c-Myc. First, aberrant EGFR signaling induces mTORC1-dependent splicing of the obligate binding partner of c-Myc, delta max, which promotes Myc-dependent glycolysis and tumor growth in vivo (Babic et al., 2013). Second, c-Myc expression is maintained by mTORC2-dependent acetylation and inhibition of FoxO1 and FoxO3, transcriptional regulators that drive expression of a microRNA that antagonizes c-Myc (Appendix; Masui et al., 2013).

GBMs also integrate their growth factor signaling with extracellular nutrient availability. Glucose and acetate, two abundant nutrients in the brain, promote EGFRvIII-dependent

activation of mTORC2 to drive tumor growth (Masui et al., 2015a). Intriguingly, oncogenic EGFR signaling increases the uptake and utilization of nutrients that can be converted into acetyl-CoA in GBM cells. Glucose, or acetate-dependent, acetylation of Rictor, a core component of mTORC2, renders signaling downstream of mTORC2 constitutively active (Appendix; Masui et al., 2013) even when upstream components of the pathway are inhibited, demonstrating that elevated nutrient levels and their utilization can drive resistance to targeted cancer treatments by maintaining signaling downstream of mTORC2.

Our understanding of the oncogene-dependent dysregulation of metabolism in GBM has greatly increased in the past ten years. The majority of these advances have focused on the mechanisms by which aberrant EGFR signaling regulates the availability and utilization of nutrients that readily cross the blood-brain-barrier, including glucose, glutamine, and acetate. However, the role of oncogenic signaling in promoting GBM pathogenesis through altered metabolism of nutrients that cannot penetrate the CNS, and are thus confined to the closed environment in the brain, is not well understood. Addressing this critical question may provide new insight into unappreciated metabolic vulnerabilities that can be targeted by brain penetrant compounds, potentially leading to better GBM treatments.

The blood-brain barrier prevents many circulating molecules from entering into the brain. This includes most cytotoxic chemotherapies and targeted agents, and contributes to treatment failure (Deeken and Löscher, 2007). Thus, despite compelling drug targets such as the EGFR, which is amplified and/or mutated in nearly 60% of cases (Brennan et al., 2013), EGFR tyrosine kinase inhibitors have so far proven ineffective (Cloughesy et al., 2014; Furnari et al., 2015) due to insufficient tumor and CNS penetrance (Vivanco et al., 2012).

Cancer cells, due to alterations in their biochemical and signaling state, may become dependent on specific enzymes or transcription factors that are not themselves oncogenic, opening up new treatment possibilities. This process, known as non-oncogene addiction (Galluzzi et al., 2013; Luo et al., 2009; Solimini et al., 2007) or non-oncogene co-dependency (Raj et al., 2011), may extend the pharmacopeia of cancer drugs to include brain-penetrant compounds that act on non-traditional targets. Importantly, co-dependencies can be shaped both by specific oncogenes that reprogram cellular metabolism and signaling and by the local biochemical environment in which tumor cells grow (Galluzzi et al., 2013).

The unique metabolic environment of the brain may generate actionable vulnerabilities. The brain, for instance, is the most cholesterol rich organ of the body, containing approximately 20% of total body cholesterol (Dietschy, 2009). However, the brain cholesterol pool is virtually separate from cholesterol metabolism in the periphery. Because cholesterol cannot be transported across the blood-brain barrier into the CNS, almost all brain cholesterol is synthesized de novo (Björkhem and Meaney, 2004; Dietschy and Turley, 2001). Astrocytes synthesize the majority of brain cholesterol from glucose, glutamine or acetate-derived acetyl-CoA and supply cholesterol to neighboring cells, including neurons, in the form of ApoE-containing HDL-like lipoprotein particles (Hayashi et al., 2004; Karten et al., 2006; Wahrle et al., 2004). Neurons and astrocytes both produce, as products of cholesterol metabolism, oxysterols which act as endogenous ligands for the liver X receptors (LXRs) to decrease excess cellular cholesterol levels by promoting efflux through sterol transporters such as ABCA1 and suppressing uptake through IDOL-dependent degradation of LDLR (Chen et al., 2013; Repa et al., 2000; Venkateswaran et al., 2000; Zelcer et al., 2009). This negative feedback system complements suppression of HMG-CoA reductase (HMGCR), the rate-limiting enzyme for sterol synthesis, when cholesterol levels

rise (Björkhem, 2006; Brown and Goldstein, 1980) to maintain cholesterol homeostasis within distinct cell types in the brain. Statins, which block HMCGR, and synthetic LXR agonists have been suggested as anti-cancer agents. A recent study reported that LXR agonists suppressed metastasis in the periphery through an APOE-dependent mechanism (Pencheva et al., 2014). In the brain, the efficacy of targeting either cholesterol synthesis or LXR activation may depend both on the specific tumor genotype and on the tissue-specific context required for cancer cell survival.

We reasoned that tumor cells in the brain may behave in a parasitic fashion with regard to cholesterol, obtaining CNS-derived cholesterol while suppressing endogenous LXR-ligand synthesis, enabling GBM cells to access a nearly limitless supply of cholesterol to fuel their growth. If this hypothesis is correct, GBM cells may be exquisitely vulnerable to synthetic brain-penetrant LXR ligands that would otherwise spare normal brain cell constituents, including astrocytes and neurons.

Here, we show that GBM cells rely on exogenous cholesterol and suppress the production of endogenous LXR ligands. LXR-623, a clinical stage LXRα-partial/LXRβ-full agonist that concentrates at high levels in the brain, causes cholesterol depletion in GBM and massive cell death through an LXRβ-dependent mechanism. We further show that LXR-623 has minimal effects on LXR target gene expression in peripheral tissues, which may limit undesirable metabolic side effects. Most importantly, treatment with LXR-623 causes substantial tumor cell death and prolongs survival of mice bearing patient-derived GBM intracranial xenografts. These results nominate LXR-623 as a candidate treatment for GBM.

References

Babic, I., Anderson, E.S., Tanaka, K., Guo, D., Masui, K., Li, B., Zhu, S., Gu, Y., Villa, G.R., Akhavan, D., et al. (2013). EGFR mutation-induced alternative splicing of Max contributes to growth of glycolytic tumors in brain cancer. Cell Metab. *17*, 1000–1008.

Björkhem, I. (2006). Crossing the barrier: oxysterols as cholesterol transporters and metabolic modulators in the brain. J. Intern. Med. *260*, 493–508.

Björkhem, I., and Meaney, S. (2004). Brain cholesterol: long secret life behind a barrier. Arterioscler. Thromb. Vasc. Biol. *24*, 806–815.

Brennan, C.W., Verhaak, R.G.W., McKenna, A., Campos, B., Noushmehr, H., Salama, S.R., Zheng, S., Chakravarty, D., Sanborn, J.Z., Berman, S.H., et al. (2013). The somatic genomic landscape of glioblastoma. Cell *155*, 462–477.

Brown, M.S., and Goldstein, J.L. (1980). Multivalent feedback regulation of HMG CoA reductase, a control mechanism coordinating isoprenoid synthesis and cell growth. J. Lipid Res. *21*, 505–517.

Chen, J., Zhang, X., Kusumo, H., Costa, L.G., and Guizzetti, M. (2013). Cholesterol efflux is differentially regulated in neurons and astrocytes: implications for brain cholesterol homeostasis. Biochim. Biophys. Acta *1831*, 263–275.

Ciriello, G., Miller, M.L., Aksoy, B.A., Senbabaoglu, Y., Schultz, N., and Sander, C. (2013). Emerging landscape of oncogenic signatures across human cancers. Nat. Genet. *45*, 1127–1133.

Cloughesy, T.F., Cavenee, W.K., and Mischel, P.S. (2014). Glioblastoma: from molecular pathology to targeted treatment. Annu. Rev. Pathol. *9*, 1–25.

Dang, C.V. (2013). MYC, metabolism, cell growth, and tumorigenesis. Cold Spring Harb. Perspect. Med. *3*.

Dang, C.V., Le, A., and Gao, P. (2009). MYC-induced cancer cell energy metabolism and therapeutic opportunities. Clin. Cancer Res. Off. J. Am. Assoc. Cancer Res. *15*, 6479–6483.

Deeken, J.F., and Löscher, W. (2007). The Blood-Brain Barrier and Cancer: Transporters, Treatment, and Trojan Horses. Clin. Cancer Res. *13*, 1663–1674.

Dietschy, J.M. (2009). Central nervous system: cholesterol turnover, brain development and neurodegeneration. Biol. Chem. *390*, 287–293.

Dietschy, J.M., and Turley, S.D. (2001). Cholesterol metabolism in the brain. Curr. Opin. Lipidol. *12*, 105–112.

Furnari, F.B., Fenton, T., Bachoo, R.M., Mukasa, A., Stommel, J.M., Stegh, A., Hahn, W.C., Ligon, K.L., Louis, D.N., Brennan, C., et al. (2007). Malignant astrocytic glioma: genetics, biology, and paths to treatment. Genes Dev. *21*, 2683–2710.

Furnari, F.B., Cloughesy, T.F., Cavenee, W.K., and Mischel, P.S. (2015). Heterogeneity of epidermal growth factor receptor signalling networks in glioblastoma. Nat. Rev. Cancer *15*, 302–310.

Galluzzi, L., Kepp, O., Heiden, M.G.V., and Kroemer, G. (2013). Metabolic targets for cancer therapy. Nat. Rev. Drug Discov. *12*, 963–963.

Guo, D., Hildebrandt, I.J., Prins, R.M., Soto, H., Mazzotta, M.M., Dang, J., Czernin, J., Shyy, J.Y.-J., Watson, A.D., Phelps, M., et al. (2009). The AMPK agonist AICAR inhibits the growth of EGFRvIII-expressing glioblastomas by inhibiting lipogenesis. Proc. Natl. Acad. Sci. U. S. A. *106*, 12932–12937.

Hanahan, D., and Weinberg, R.A. (2011). Hallmarks of cancer: the next generation. Cell *144*, 646–674.

Hayashi, H., Campenot, R.B., Vance, D.E., and Vance, J.E. (2004). Glial lipoproteins stimulate axon growth of central nervous system neurons in compartmented cultures. J. Biol. Chem. *279*, 14009–14015.

Huang, H.S., Nagane, M., Klingbeil, C.K., Lin, H., Nishikawa, R., Ji, X.D., Huang, C.M., Gill, G.N., Wiley, H.S., and Cavenee, W.K. (1997). The enhanced tumorigenic activity of a mutant epidermal growth factor receptor common in human cancers is mediated by threshold levels of constitutive tyrosine phosphorylation and unattenuated signaling. J. Biol. Chem. *272*, 2927–2935.

Huang, P.H., Mukasa, A., Bonavia, R., Flynn, R.A., Brewer, Z.E., Cavenee, W.K., Furnari, F.B., and White, F.M. (2007). Quantitative analysis of EGFRvIII cellular signaling networks reveals a combinatorial therapeutic strategy for glioblastoma. Proc. Natl. Acad. Sci. U. S. A. *104*, 12867–12872.

Inda, M.-M., Bonavia, R., Mukasa, A., Narita, Y., Sah, D.W.Y., Vandenberg, S., Brennan, C., Johns, T.G., Bachoo, R., Hadwiger, P., et al. (2010). Tumor heterogeneity is an active process maintained by a mutant EGFR-induced cytokine circuit in glioblastoma. Genes Dev. *24*, 1731–1745.

Kandoth, C., McLellan, M.D., Vandin, F., Ye, K., Niu, B., Lu, C., Xie, M., Zhang, Q., McMichael, J.F., Wyczalkowski, M.A., et al. (2013). Mutational landscape and significance across 12 major cancer types. Nature *502*, 333–339.

Karten, B., Campenot, R.B., Vance, D.E., and Vance, J.E. (2006). Expression of ABCG1, but not ABCA1, correlates with cholesterol release by cerebellar astroglia. J. Biol. Chem. *281*, 4049–4057.

Lawrence, M.S., Stojanov, P., Mermel, C.H., Robinson, J.T., Garraway, L.A., Golub, T.R., Meyerson, M., Gabriel, S.B., Lander, E.S., and Getz, G. (2014). Discovery and saturation analysis of cancer genes across 21 tumour types. Nature *505*, 495–501.

Lee, T.I., and Young, R.A. (2013). Transcriptional regulation and its misregulation in disease. Cell *152*, 1237–1251.

Luo, J., Solimini, N.L., and Elledge, S.J. (2009). Principles of Cancer Therapy: Oncogene and Non-oncogene Addiction. Cell *136*, 823–837.

Masui, K., Tanaka, K., Akhavan, D., Babic, I., Gini, B., Matsutani, T., Iwanami, A., Liu, F., Villa, G.R., Gu, Y., et al. (2013). mTOR complex 2 controls glycolytic metabolism in glioblastoma through FoxO acetylation and upregulation of c-Myc. Cell Metab. *18*, 726–739.

Masui, K., Tanaka, K., Ikegami, S., Villa, G.R., Yang, H., Yong, W.H., Cloughesy, T.F., Yamagata, K., Arai, N., Cavenee, W.K., et al. (2015a). Glucose-dependent acetylation of Rictor promotes targeted cancer therapy resistance. Proc. Natl. Acad. Sci. U. S. A. *112*, 9406–9411.

Masui, K., Cavenee, W.K., and Mischel, P.S. (2015b). mTORC2 and Metabolic Reprogramming in GBM: at the Interface of Genetics and Environment. Brain Pathol. Zurich Switz. *25*, 755–759.

Miller, D.M., Thomas, S.D., Islam, A., Muench, D., and Sedoris, K. (2012). c-Myc and cancer metabolism. Clin. Cancer Res. Off. J. Am. Assoc. Cancer Res. *18*, 5546–5553.

Ohgaki, H., and Kleihues, P. (2005). Population-based studies on incidence, survival rates, and genetic alterations in astrocytic and oligodendroglial gliomas. J. Neuropathol. Exp. Neurol. *64*, 479–489.

Owonikoko, T.K., Arbiser, J., Zelnak, A., Shu, H.-K.G., Shim, H., Robin, A.M., Kalkanis, S.N., Whitsett, T.G., Salhia, B., Tran, N.L., et al. (2014). Current approaches to the treatment of metastatic brain tumours. Nat. Rev. Clin. Oncol. *11*, 203–222.

Pavlova, N.N., and Thompson, C.B. (2016). The Emerging Hallmarks of Cancer Metabolism. Cell Metab. *23*, 27–47.

Pencheva, N., Buss, C.G., Posada, J., Merghoub, T., and Tavazoie, S.F. (2014). Broad-spectrum therapeutic suppression of metastatic melanoma through nuclear hormone receptor activation. Cell *156*, 986–1001.

Raj, L., Ide, T., Gurkar, A.U., Foley, M., Schenone, M., Li, X., Tolliday, N.J., Golub, T.R., Carr, S.A., Shamji, A.F., et al. (2011). Selective killing of cancer cells by a small molecule targeting the stress response to ROS. Nature *475*, 231–234.

Repa, J.J., Turley, S.D., Lobaccaro, J.A., Medina, J., Li, L., Lustig, K., Shan, B., Heyman, R.A., Dietschy, J.M., and Mangelsdorf, D.J. (2000). Regulation of absorption and ABC1-mediated efflux of cholesterol by RXR heterodimers. Science *289*, 1524–1529.

Solimini, N.L., Luo, J., and Elledge, S.J. (2007). Non-Oncogene Addiction and the Stress Phenotype of Cancer Cells. Cell *130*, 986–988.

Stupp, R., Mason, W.P., van den Bent, M.J., Weller, M., Fisher, B., Taphoorn, M.J.B., Belanger, K., Brandes, A.A., Marosi, C., Bogdahn, U., et al. (2005). Radiotherapy plus concomitant and adjuvant temozolomide for glioblastoma. N. Engl. J. Med. *352*, 987–996.

Venkateswaran, A., Laffitte, B.A., Joseph, S.B., Mak, P.A., Wilpitz, D.C., Edwards, P.A., and Tontonoz, P. (2000). Control of cellular cholesterol efflux by the nuclear oxysterol receptor LXR alpha. Proc. Natl. Acad. Sci. U. S. A. *97*, 12097–12102.

Vivanco, I., Robins, H.I., Rohle, D., Campos, C., Grommes, C., Nghiemphu, P.L., Kubek, S., Oldrini, B., Chheda, M.G., Yannuzzi, N., et al. (2012). Differential sensitivity of glioma- versus lung cancer-specific EGFR mutations to EGFR kinase inhibitors. Cancer Discov. *2*, 458–471.

Wahrle, S.E., Jiang, H., Parsadanian, M., Legleiter, J., Han, X., Fryer, J.D., Kowalewski, T., and Holtzman, D.M. (2004). ABCA1 is required for normal central nervous system ApoE levels and for lipidation of astrocyte-secreted apoE. J. Biol. Chem. *279*, 40987–40993.

Wen, P.Y., and Kesari, S. (2008). Malignant gliomas in adults. N. Engl. J. Med. *359*, 492–507.

Zelcer, N., Hong, C., Boyadjian, R., and Tontonoz, P. (2009). LXR regulates cholesterol uptake through Idol-dependent ubiquitination of the LDL receptor. Science *325*, 100–104.

Chapter 1

Dysregulated Cholesterol Metabolism Renders GBM Cells Selectively Vulnerable to an Exogenous LXR Agonist

INTRODUCTION

Glioblastoma (GBM) is a devastating diagnosis. Despite aggressive surgery, radiation, and chemotherapy, median patient survival is 12-15 months from diagnosis (Cloughesy et al., 2014; Stupp et al., 2005). GBMs arise from the constituent cells of the brain, generating a series of difficult therapeutic challenges. GBMs spread diffusely throughout the surrounding brain, making complete surgical resection almost impossible (Young et al., 2015). The blood-brain-barrier limits access to many anti-cancer drugs and further, GBM cells are also among the most radiation and cytotoxic chemotherapy-resistant types of cancer cells (Wen and Kesari, 2008). Therefore, new treatments tailored to the biology of GBM are urgently needed.

GBMs are characterized by major alterations in their cellular metabolism, frequently as a consequence of oncogenic epidermal growth factor receptor (EGFR) signaling (Babic et al., 2013; Guo et al., 2009; Masui et al., 2013, 2015). Dissecting the molecular circuitry by which mutations in the growth factor receptor signaling system, which occurs in nearly 90% of GBMs, alters cellular metabolism to support tumor growth and survival may yield a panoply of actionable therapeutic targets. The development of CNS-penetrant drugs whose pharmacological properties permit persistent target inhibition in the brain, by exploiting vulnerabilities distinguishing GBMs from the normal brain tissue physiology in which they reside, is especially promising.

Non-cancerous cells obtain cholesterol from either *de novo* synthesis or via uptake of exogenous cholesterol bound to lipoproteins in the plasma, especially low density lipoprotein (LDL) (Goldstein and Brown, 2015). The majority of LDL uptake is mediated by LDL receptors (LDLR), which recognize the apoprotein B-100 constituent of LDL (Twisk et al., 2000). Normal cells, including neurons and astrocytes in the brain, have finely tuned, elegant, feedback

mechanisms to maintain cholesterol levels within a narrow range (Brown and Goldstein, 1980; Goldstein and Brown, 2015). In the presence of excess cholesterol, non-cancerous cells produce oxysterols as products of cholesterol metabolism, which act as endogenous ligands for the liver X receptors (LXRs) to decrease excess cellular cholesterol levels by promoting efflux through sterol transporters such as ABCA1 and suppressing uptake through IDOL-dependent degradation of LDLR (Chen et al., 2013; Repa et al., 2000; Venkateswaran et al., 2000; Zelcer et al., 2009). This negative feedback system complements suppression of HMG-CoA reductase (HMGCR), the rate-limiting enzyme for sterol synthesis, when cholesterol levels rise in order to maintain cholesterol homeostasis within distinct cell types in the brain (Björkhem, 2006; Brown and Goldstein, 1980).

We have recently discovered that the mutant form of the epidermal growth factor receptor EGFRvIII stimulates tumor growth by up-regulating expression of the LDLR to promote uptake of cholesterol into the cell (Guo et al., 2011). However, whether dysregulated EGFR signaling alters additional cholesterol metabolic pathways, and how GBM cell cholesterol metabolism differs from that of normal cells in the brain, are not well understood.

Here, we set out to dissect the cholesterol metabolic circuitry of GBM and normal tissue counterparts utilizing both clinical samples and relevant cell culture models, including established and patient-derived *ex vivo* GBM cells and normal human astrocytes (NHAs). We first determined the relative dependency of GBM cells on endogenous cholesterol synthesis versus uptake by: 1) examining the status of the *de novo* cholesterol biosynthetic pathway in GBM and normal brain specimens using data from The Cancer Genome Atlas (TCGA) (Brennan et al., 2013; Cancer Genome Atlas Research Network, 2008), 2) assessing the sensitivity of GBM cells and NHAs to suppression of *de novo* cholesterol synthesis using statins, which target

HMGCR, 3) measuring LDLR protein levels in GBM clinical samples relative to normal brain in tissue microarray analyses, 4) performing mass spectrometric analysis of GBM cell lines and NHAs to measure endogenous LXR ligand levels, and 5) surveying the mRNA expression of the enzymes that produce these endogenous LXR ligands in the aforementioned cells, as well as more broadly across GBMs in the TCGA dataset.

RESULTS

GBM cells display dysregulated cholesterol metabolism

We previously demonstrated that mutant EGFR signaling in GBM cells upregulates LDLR expression (Guo et al., 2011), suggesting that these tumor cells may rely on exogenous cholesterol for survival. Therefore, to determine the relative dependency of GBM cells on endogenous cholesterol synthesis versus uptake, we examined the status of the *de novo* cholesterol biosynthetic pathway in GBM and normal brain specimens using data from The Cancer Genome Atlas (TCGA) (Brennan et al., 2013; Cancer Genome Atlas Research Network, 2008). We determined the expression of mRNAs encoding three key enzymes: HMGCS1 that converts acetyl-CoA to HMG-CoA; HMGCR, the rate limiting step in the pathway that converts HMG-CoA to mevalonate, and DHCR24 which ultimately converts desmosterol to cholesterol. Expression of these critical enzymes was coordinately suppressed in GBM clinical samples relative to normal brain ($p < 0.001$ for each) (Figure 1-1). We reasoned that if GBM cells suppress *de novo* cholesterol synthesis, then they should be relatively resistant to statins, which target HMCGR. In contrast, NHAs, which rely primarily on endogenous synthesis, should be highly vulnerable. Consistent with this hypothesis, both lovastatin and atorvastatin caused significant cell death of NHAs while showing limited activity against two independent models of EGFRvIII-expressing GBMs – U87EGFRvIII cells, which are derived by overexpression of

EGFRvIII in an established GBM cell line (Wang et al., 2006), and GBM39, which is a patient-derived GBM line that maintains endogenous EGFR amplification and EGFRvIII expression in neurosphere culture (Sarkaria et al., 2007) (Figure 1-2).

Consistent with the notion that GBM cells obtain cholesterol primarily through uptake, LDLR protein was significantly elevated in GBM clinical samples relative to normal brain in tissue microarray analyses (Figure 1-3). LDLR protein was also substantially elevated in GBM cells relative to NHAs in culture (Figure 1-4A), and GBM cells took up three- to four-fold more LDL than did NHAs (1-4B-D). Removal of lipids from the culture medium caused extensive GBM cell death while having no effect on the viability of NHAs, (Figure 1-5), motivating us to further examine the role of cholesterol uptake in GBM survival.

In non-cancerous cells, excess cholesterol is used to synthesize oxysterols, which act as endogenous LXR ligands to suppress LDL uptake and promote the efflux of cholesterol from the cell (Figure 1-6A) (Repa et al., 2000; Venkateswaran et al., 2000). However, the activity of this pathway in GBM cells and in many other cancer types (Lin and Gustafsson, 2015) is not well understood. Therefore, we performed mass spectrometric analysis of GBM cell lines and NHAs to measure endogenous LXR ligand levels and surveyed the mRNA expression of the enzymes that produce these endogenous LXR ligands, both in the aforementioned cell lines, as well as more broadly across GBMS in the TCGA dataset. The levels of 24(S)-hydroxycholesterol (24-OHC), 22(R)-hydroxycholesterol (22-OHC), 4β-hydroxycholesterol (4b-OHC), 27-hydroxycholesterol (27-OHC), and the downstream product of 7α-hydroxycholesterol, 7α-hydroxy-4-cholesten-3-one (7a-OH-ONE), were significantly reduced in GBM cells relative to NHAs (Figure 1-6B), as were the mRNA levels of the enzymes that catalyze their production (Figure 1-7). In particular, CYP46A1, the most highly expressed enzyme that catalyzes oxysterol

synthesis in the brain, was reduced nearly ten-fold in GBMs in the TCGA dataset (Figure 1-7C). Taken together, these data suggest that GBM cells have a decreased capacity to produce endogenous LXR ligands.

GBM cells show selective vulnerability to LXR agonists

We hypothesized that the relatively low levels of endogenous LXR ligands in GBM cells would render them selectively sensitive to exogenous LXR ligands. We first tested the effect of exogenous administration of LXR ligands that are normally synthesized by cells in the presence of excess cholesterol. 24-OHC induced a dramatic dose-dependent increase in GBM cell death in vitro (Figure 1-8). Importantly, NHAs, which synthesize 24-OHC (Figure 1-6), were insensitive to exogenous 24-OHC administration (Figure 1-8). Therefore, we reasoned that synthetic LXR agonists might also kill GBM cells while sparing NHAs.

We focused our initial investigation on LXR-623 (Figure 1-9), a compound originally developed for cardiovascular indications and the first synthetic LXR agonist tested in patients (Hong and Tontonoz, 2014). A phase I clinical trial raised the possibility of brain penetration (Katz et al., 2009), motivating our focus on this drug. Consistent with our proposed model, LXR-623 potently killed U87vIII and GBM39 cells in vitro while completely sparing NHAs (Figure 1-10) and induced LXR target gene expression in all three cell lines (Figure 1-11). Altogether, these data suggest that the exploitation of differences in cholesterol access between GBM cells and normal tissue counterparts (Figure 1-12) may be an effective therapeutic strategy, and warrant deeper investigation of LXR-623 as a candidate treatment for patients with GBM.

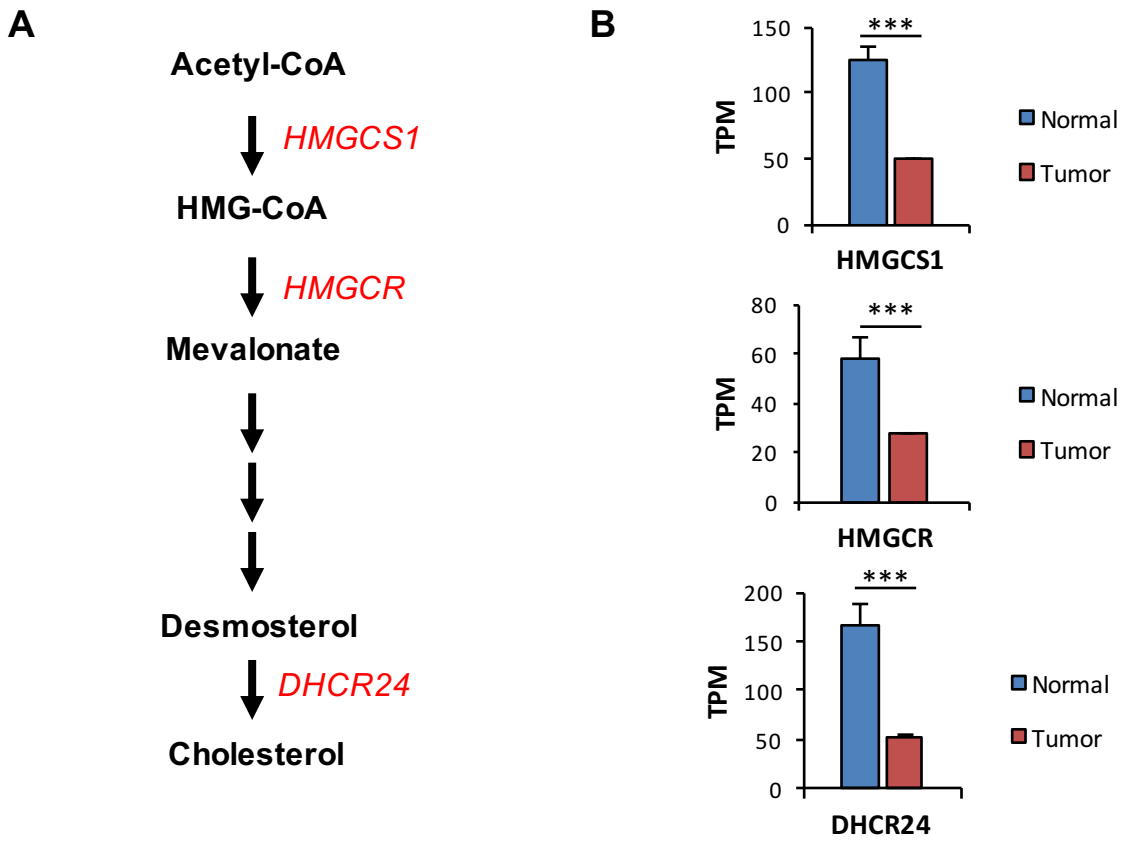

Figure 1-1. **GBM tumors suppress the mRNA expression of key cholesterol biosynthetic enzymes**. (**A**) Cholesterol biosynthetic enzymes and their respective contributions to cholesterol synthesis. (**B**) Analysis of TCGA RNA sequencing gene expression data shows significantly reduced expression of cholesterol synthesis genes in GBMs vs. normal brain. TPM = transcripts per million. *$p < 0.05$; **$p < 0.01$; ***$p < 0.001$.

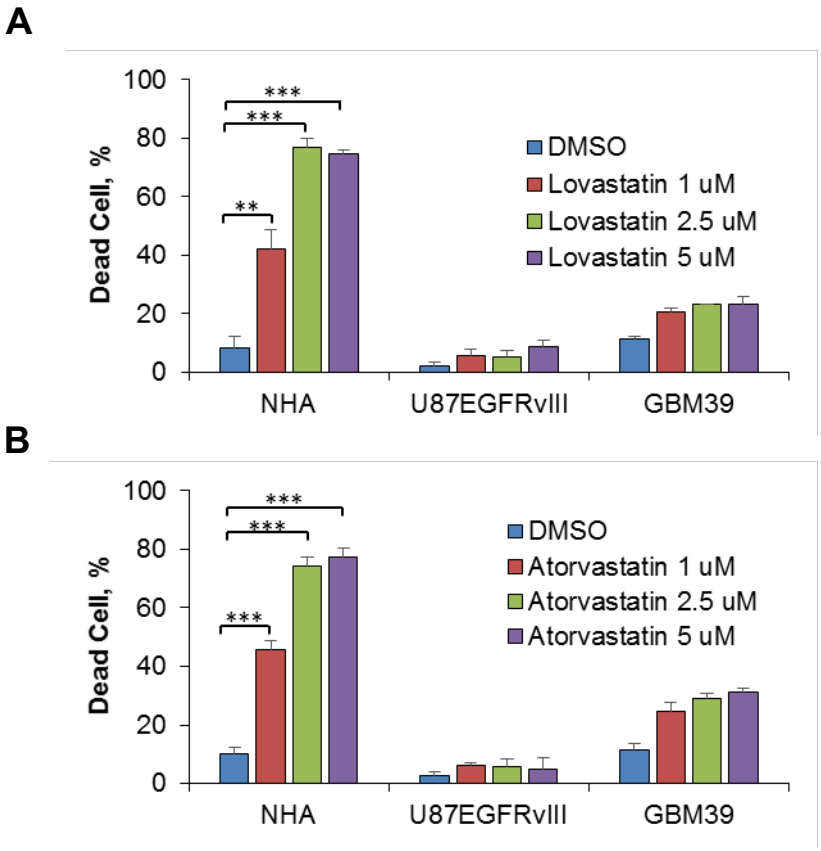

Figure 1-2. **GBM cells display reduced sensitivity to inhibition of endogenous cholesterol synthesis**. In contrast to normal human astrocytes, GBM cells are not dependent on endogenous cholesterol synthesis for survival; three day treatment with the (**A**) brain penetrant HMGCR inhibitor lovastatin or (**B**) non-brain penetrant HMGCR inhibitor atorvastatin. *$p < 0.05$; **$p < 0.01$; ***$p < 0.001$.

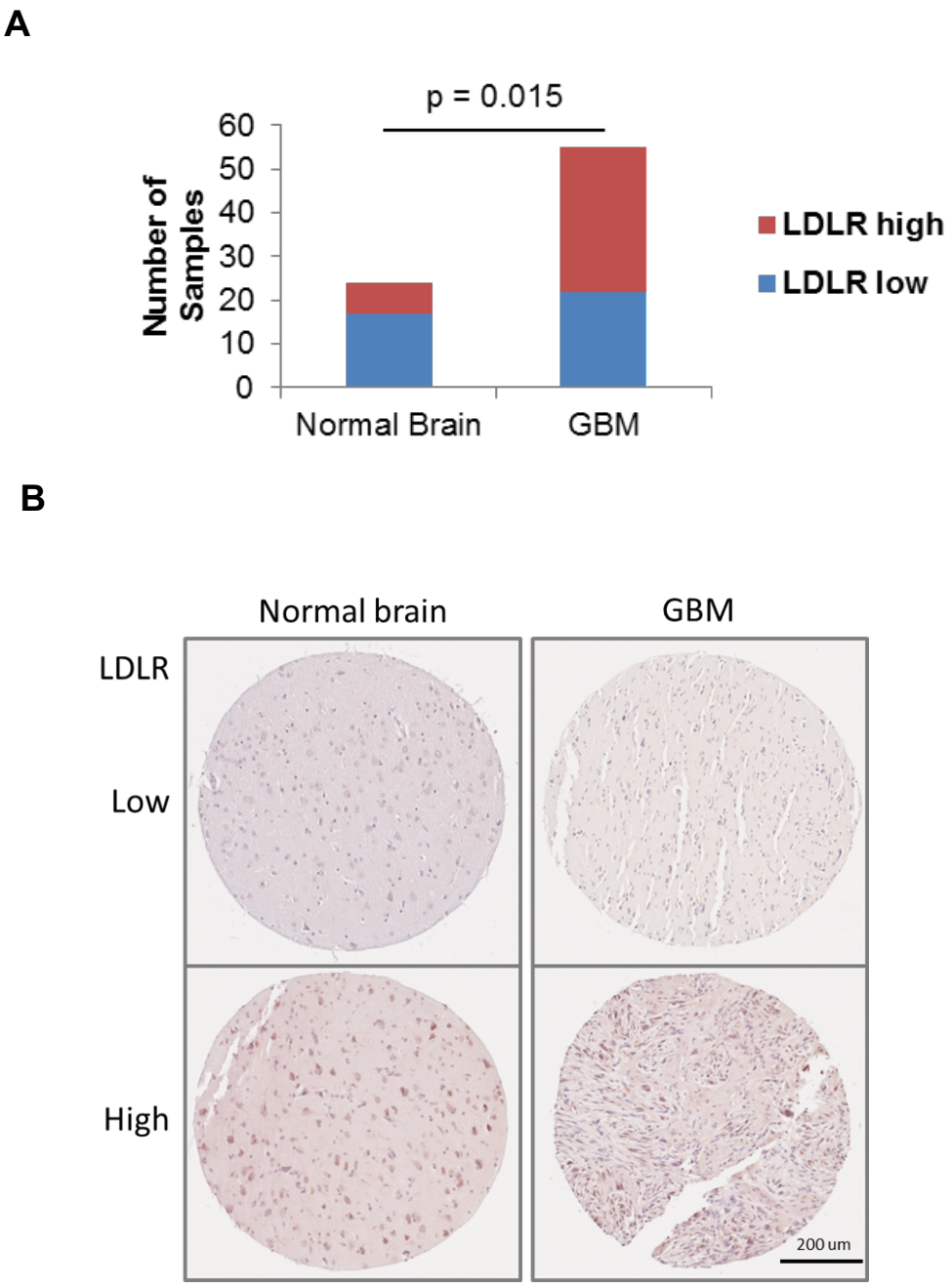

Figure 1-3. **GBMs express higher levels of the LDLR relative to normal brain**. (**A**) Tissue microarray analysis for LDLR indicates GBMs express higher levels relative to normal brain. Samples were scored by an independent pathologist (see methods). n = 24 for normal brain, n = 55 for GBM. Fischer's exact test was used for statistical analysis. *p < 0.05. (**B**) Representative images from TMA analysis.

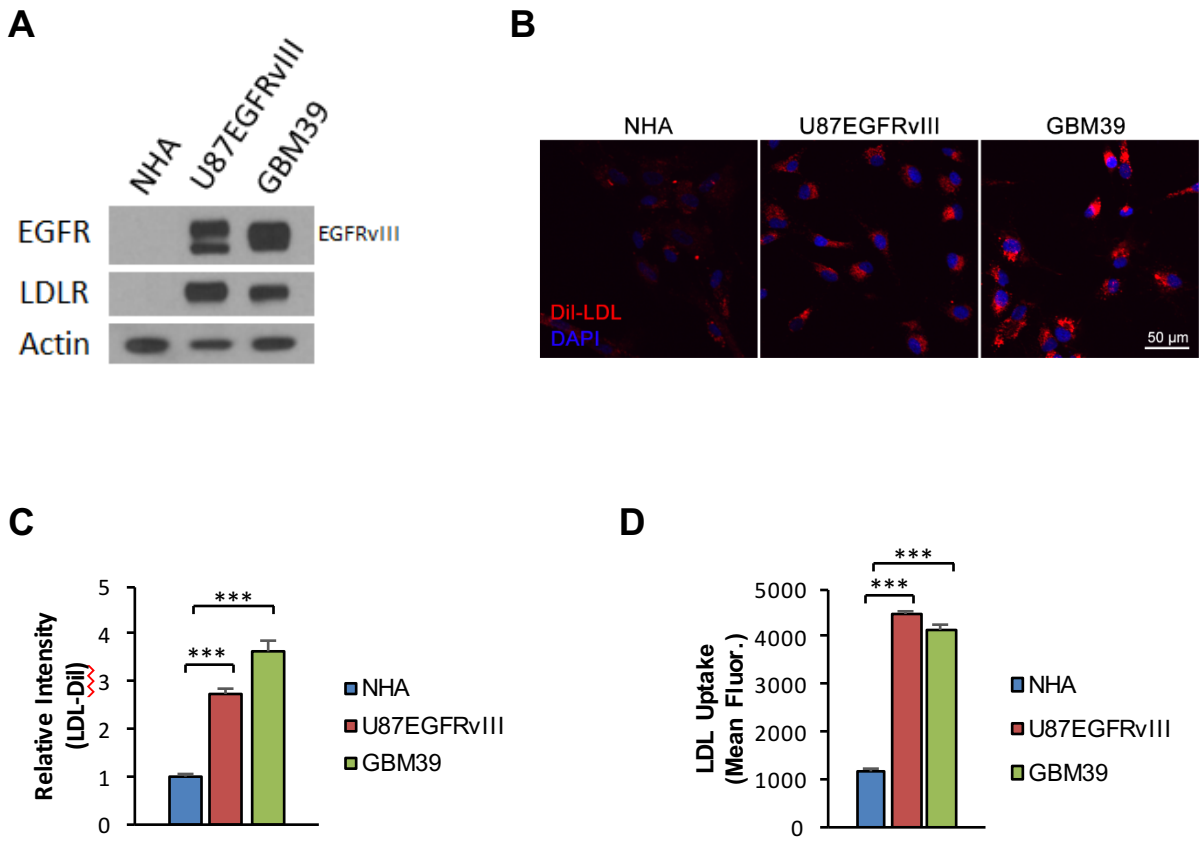

Figure 1-4. **GBM cells take up substantially more LDL than do normal human astrocytes**. (**A**) Immunoblotting indicates GBM cells express markedly higher levels of the LDLR in contrast to NHA. (**B-C**) NHA, U87EGFRvIII, and GBM39 were treated with fluorescently labeled LDL for four hours after which LDL uptake was assessed via confocal microscopy. (**B**) Confocal representative images and (**C**) quantification of LDL uptake showing GBM cells take up far more LDL than do normal astrocytes. (**D**) NHA, U87EGFRvIII, and GBM39 were treated as indicated in (B-C) and LDL uptake was assessed via fluorescence activated cell sorting (FACS) analysis. ***$p < 0.001$.

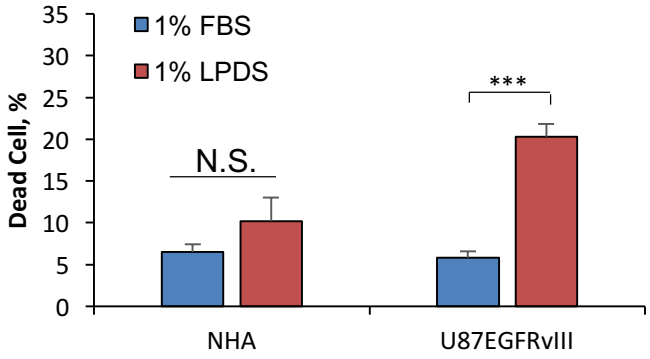

Figure 1-5. **Lipoprotein deficient media causes extensive GBM cell death while having no effect on the viability of NHAs**. NHA and U87EGFRvIII were placed in 1% lipoprotein deficient serum (LPDS) and cell death was assessed via trypan blue on day five. ***$p < 0.001$.

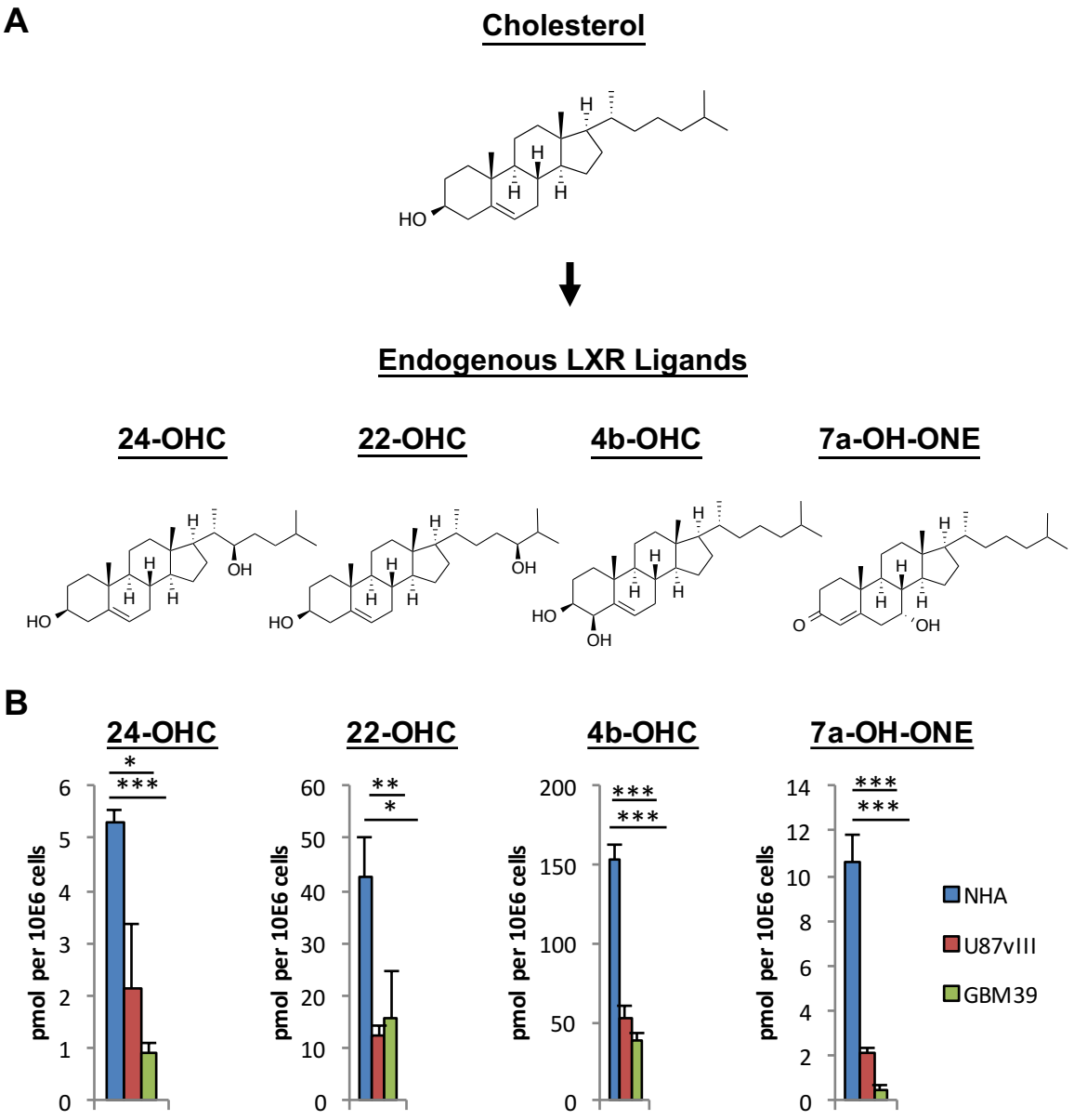

Figure 1-6. **GBM cells synthesize reduced levels of endogenous LXR ligands**. (**A**) Schematic model and molecular structures of cholesterol synthesis into endogenous LXR ligands. (**B**) Liquid chromatography-tandem mass spectrometry (LC/MS-MS) data demonstrating significant reduction in the level of endogenous LXR ligands in GBM cells relative to astrocytes. *$p < 0.05$; **$p < 0.01$; ***$p < 0.001$.

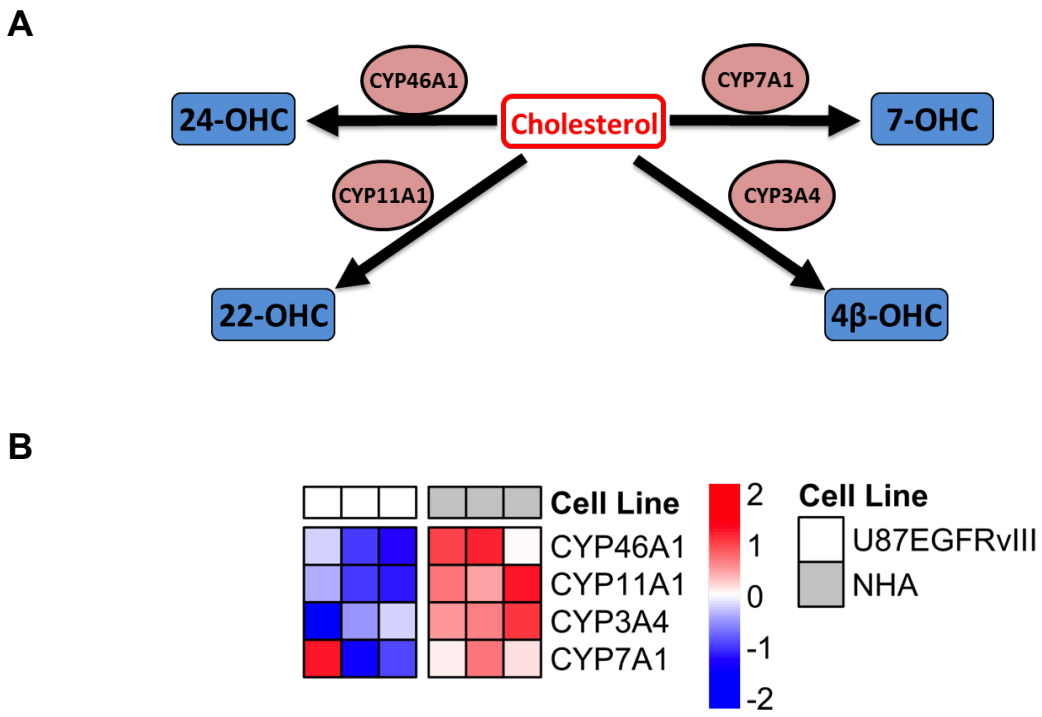

Figure 1-7. **mRNA expression of the enzymes that produce endogenous LXR ligands are substantially reduced in GBM.** (**A**) Schematic illustrating the enzymes that catalyze the formation of LXR ligands. (**B**) Microarray expression analysis showing GBM cells express lower levels of endogenous LXR ligand synthetic enzymes relative to NHA. (C) The Cancer Genome Atlas (TCGA) GBM RNASeq expression data indicating endogenous LXR ligand synthetic enzymes are expressed at lower levels in GBM relative to normal brain tissue. *p < 0.05; **p < 0.01; ***p < 0.001.

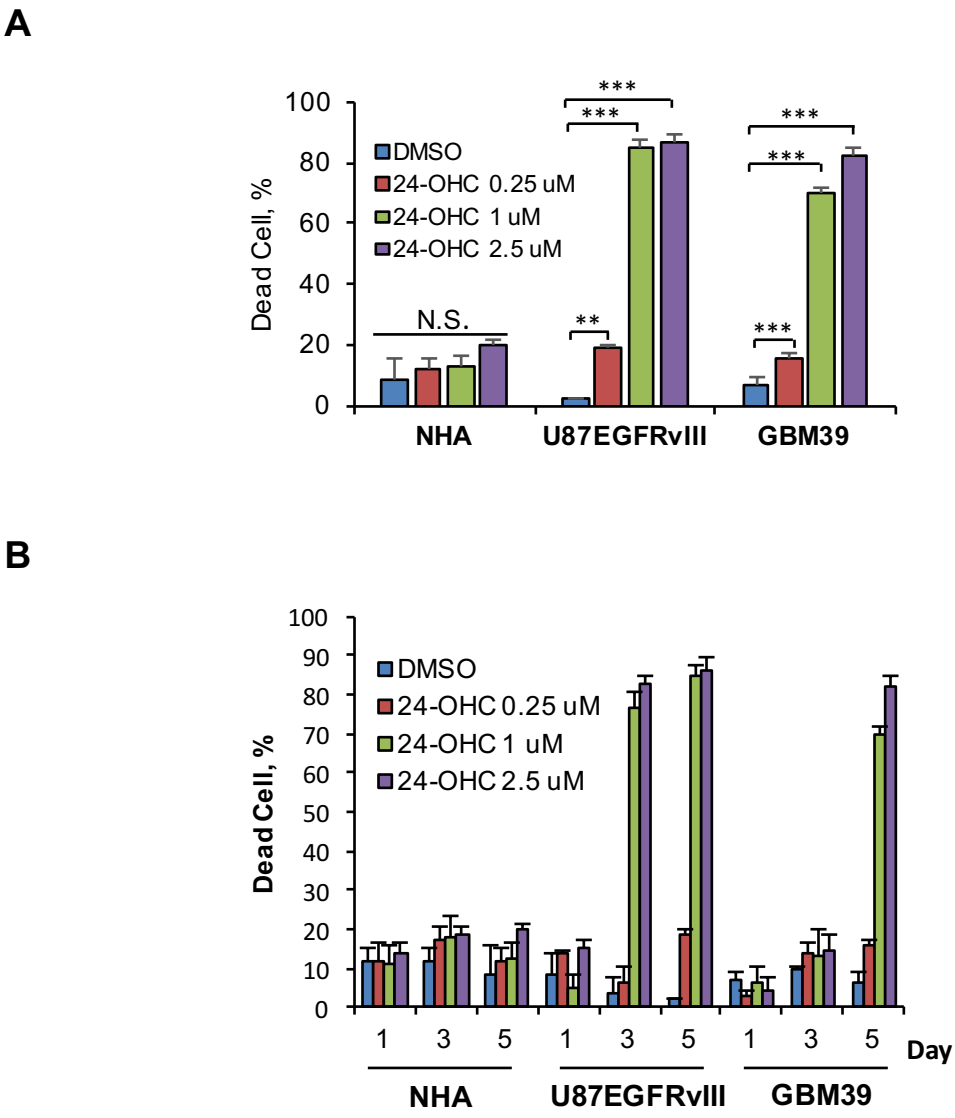

Figure 1-8. **GBM cells show selective vulnerability to an endogenous LXR agonist**. (A) GBM and NHA cells were treated with the indicated concentrations of the endogenous LXR agonist, 24-OHC, and cell death was quantified on day five of treatment. (B) Cell death was assessed over five-day treatment with 24-OHC. GBM cells undergo substantial cell death in response to an endogenous LXR agonist, no cell death is observed in astrocytes. *$p < 0.05$; **$p < 0.01$; ***$p < 0.001$.

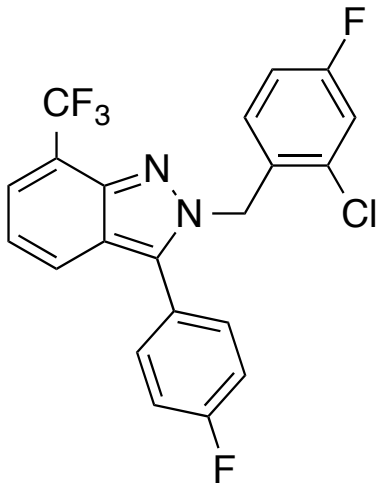

Figure 1-9. **The structure of the LXR agonist LXR-623.** LXR-623, 2-(2-chloro-4-fluorobenzyl)-3-(4-fluorophenyl)-7-(trifluoromethyl)-2H-indazole, is an indazole-based LXR agonist.

A

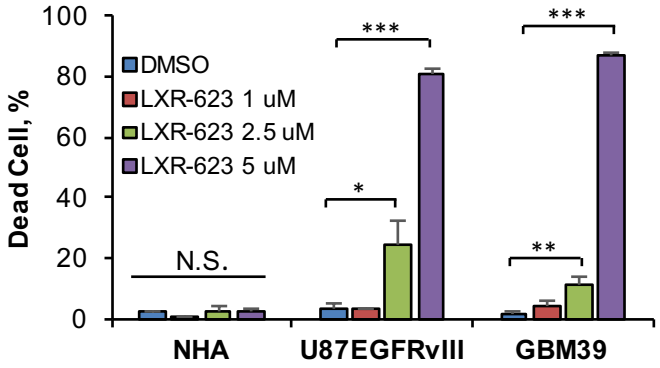

B

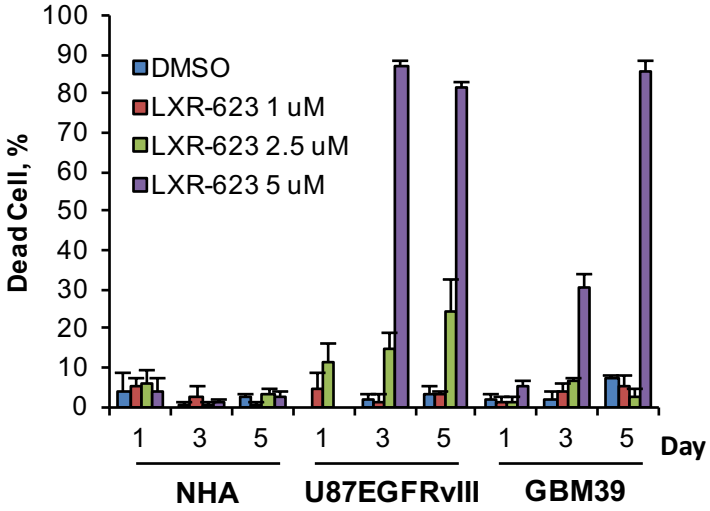

Figure 1-10. **GBM cells show selective vulnerability to a pharmacologic LXR agonist**. (A) GBM and NHA cells were treated with the indicated concentrations of the pharmacologic LXR agonist, LXR-623, and cell death was quantified on day five of treatment. (B) Cell death was assessed over five-day treatment with LXR-623. Similar to treatment with an endogenous LXR agonist, GBM cells undergo substantial cell death in response to a pharmacologic LXR agonist and no cell death is observed in astrocytes. *$p < 0.05$; **$p < 0.01$; ***$p < 0.001$.

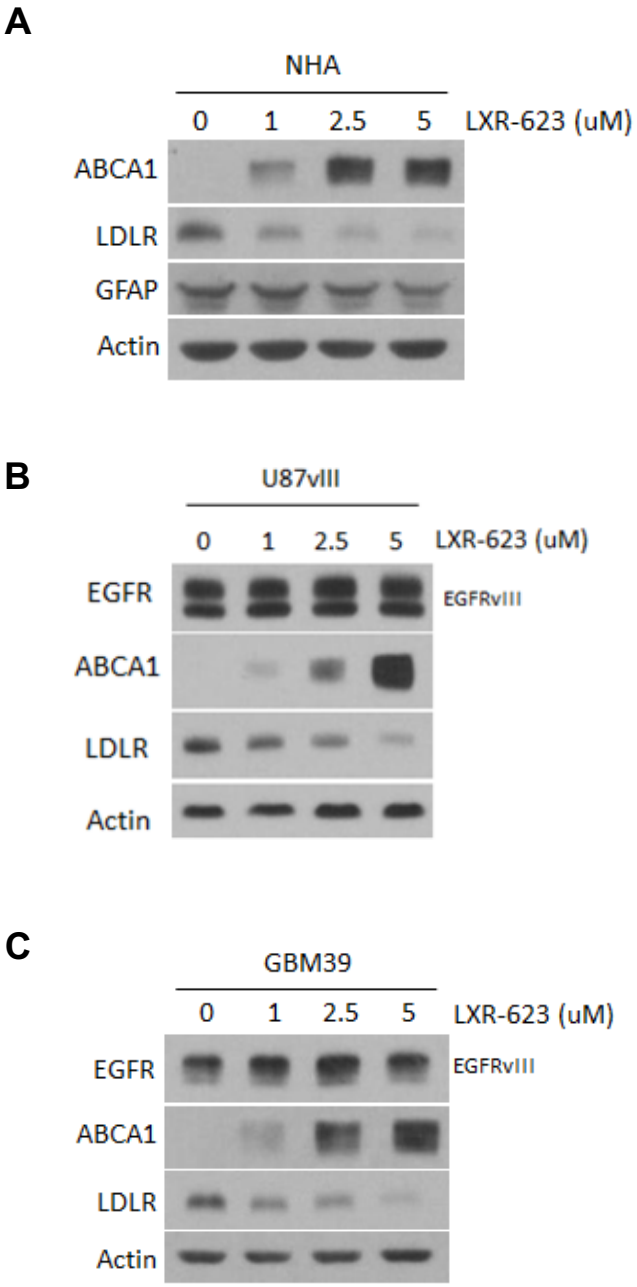

Figure 1-11. **LXR-623 induces target gene expression in NHA and GBM cell lines**. (A) NHA, (B) U87EGFRvIII, and (C) GBM39 cells were treated with the indicated concentrations of LXR-623 for 48 h and immunoblotting was performed with the indicated antibodies.

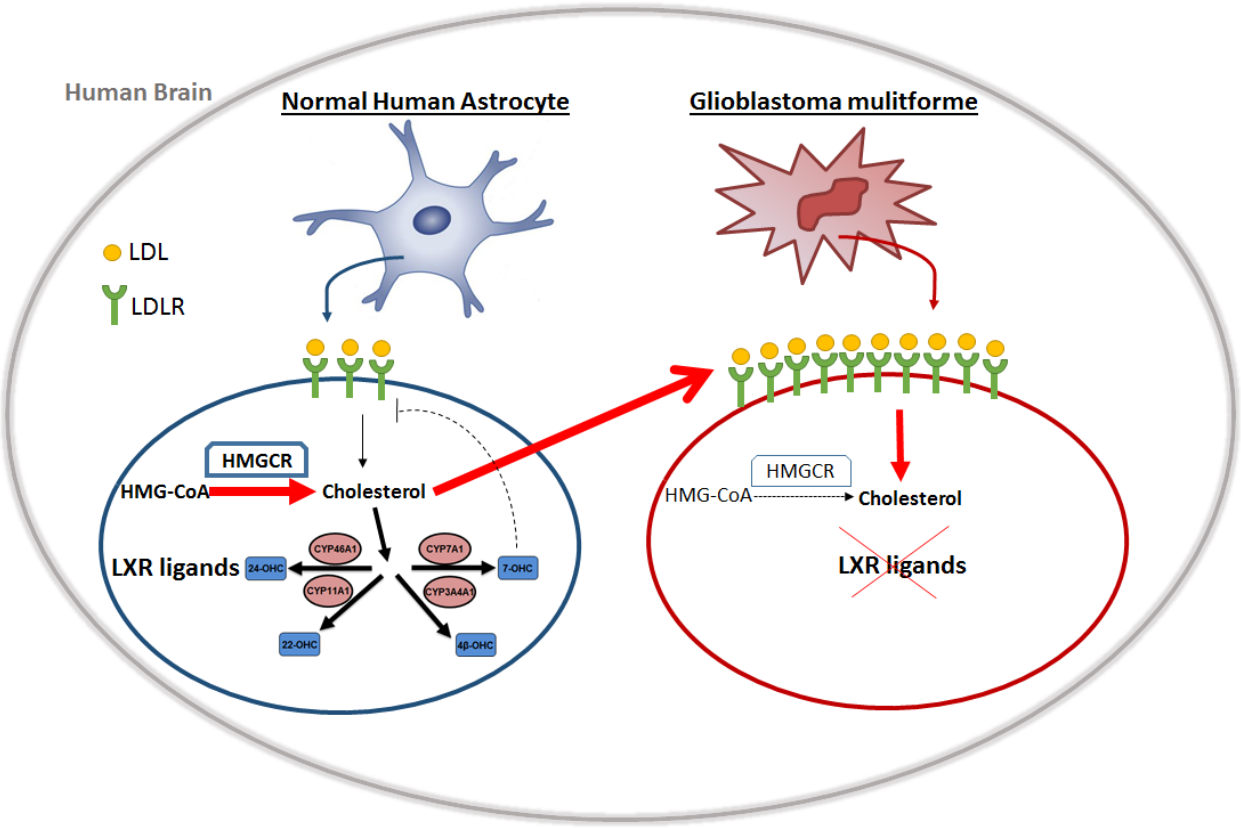

Figure 1-12. **Schematic model of differences in cholesterol regulation between GBM and NHAs**. GBM cells, in contrast to NHAs, express higher LDLR protein, uptake greater levels of LDL, suppress mRNA expression of critical enzymes involved in cholesterol biosynthesis, and synthesize reduced levels of endogenous LXR ligands. Astrocyte model modified from (Friedmann-Morvinski and Verma, 2014).

DISCUSSION

Motivated by the persistent clinical failure and the lack of therapeutic options for brain cancers, we adopted an alternative strategy designed to take advantage of a targetable metabolic dependency using a potentially brain penetrant drug. We focused on cholesterol homeostasis because: 1) GBM cells are highly dependent on cholesterol for survival (Bovenga et al., 2015); 2) EGFR mutations can regulate cholesterol homeostasis in GBM and possibly in other types of cancers (Gabitova et al., 2015; Guo et al., 2011); 3) the brain has a unique mechanism of cholesterol regulation that may expose a targetable vulnerability specific to tumor cells in this organ (Dietschy and Turley, 2001); and 4) anecdotal evidence from a Phase 1 clinical trial raised the possibility that a potentially brain penetrant compound, LXR-623, could be used to exploit this vulnerability (Katz et al., 2009).

Most of the cells in the brain are dependent on astrocyte-synthesized cholesterol for survival (Nieweg et al., 2009). Here we show that GBM cells exploit this tissue-specific physiology to fuel their growth. By upregulating LDLR to enhance cholesterol uptake while concurrently suppressing de novo synthesis of cholesterol and oxysterols, GBMs evade two key negative feedback mechanisms of cholesterol homeostasis: 1) feedback inhibition of HMGCR, the rate limiting enzyme in cholesterol synthesis, and 2) activation of LXRs by oxysterols to inhibit LDL uptake and induce cholesterol efflux. These coordinated metabolic adaptations give tumor cells access to an abundant and uninterrupted source of cholesterol. De novo cholesterol synthesis consumes 26 reducing equivalents of NADPH (Lunt and Vander Heiden, 2011), and it is tempting to speculate that the reliance of GBM cells on CNS-derived cholesterol enables them to direct their cellular NADPH, a key reducing agent in relatively short supply (Pavlova and Thompson, 2016), towards buffering ROS and synthesizing other macromolecules (Vander

Heiden et al., 2009). It is remarkable that CYP46A1, the main oxysterol-synthesizing enzyme in the brain, was suppressed ten-fold in GBM tissue relative to normal brain (Figure 1-7). Notably, the concentrations of 24-OHC, the product of CYP46A1 mediated oxidation of cholesterol, required to elicit GBM cell death surpassed those normally found in the CNS (Lütjohann et al., 1996). These coordinated metabolic adaptations give tumor cells access to an abundant and uninterrupted source of cholesterol, but also make them exquisitely and selectively vulnerable to exogenous LXR agonists (Figure 1-10). Together, these results warrant a deeper examination of LXR-623 as a potential therapy for GBM.

EXPERIMENTAL PROCEDURES

Antibodies and Reagents

Antibodies used include mouse anti-ABCA1 (Abcam, ab18180), rabbit anti-LDLR (Abcam, ab30532), rabbit anti-EGFR (Millipore, 06847MI), mouse anti-ACTIN (Sigma, A4700), mouse anti-GFAP (Cell Signaling, 3670), HRP-linked anti-rabbit IgG antibody (Cell Signaling, 7074), and HRP-linked anti-mouse IgG antibody (Cell Signaling, 7076). Reagents used include low density lipoprotein dil (Dil LDL) complex (Thermo Scientific, L-3482), 24(S)-hydroxycholesterol (Cayman Chemical, 10009931), lovastatin (Sigma, PHR1285), atorvastatin (Selleckchem, S2077), and lipoprotein deficient serum (Sigma, S5519). LXR-623 was synthesized by Sundia MediTech (Shanghai, China).

Western Blotting

Cultured cells were lysed and homogenized with RIPA lysis buffer from Boston BioProducts (50mM Tris-HCl, 150mM NaCl, 1% NP-40, 0.5% Sodium deoxycholate, 0.1% SDS) supplemented with protease and phosphatase inhibitor cocktail (Thermo Scientific). Protein concentration of each sample was determined by BCA assay using the BCA kit (Pierce) per manufacturer's instructions. Equal amounts of protein extracts were separated by electrophoresis on 4-12% NuPAGE Bis-Tris Mini Gel (Invitrogen), and then transferred to a nitrocellulose membrane (GE Healthcare) with XCell II Blot Module (Invitrogen). The membrane was probed with various primary antibodies, followed by secondary antibodies conjugated to horseradish peroxidase. The immunoreactivity was detected with Super Signal West Pico Chemiluminescent Substrate or Super Signal West Femto Kit (Thermo Scientific).

Cell Culture

The human glioma cell line U87 (or U-87MG) was purchased from ATCC and the U87EGFRvIII isogenic GBM cell line was obtained as described previously (Wang et al., 2006). U87EGFRvIII were cultured in Dulbecco's Modified Eagle Media (DMEM, Cellgro) supplemented with 10% fetal bovine serum (FBS, Hyclone) and 1% penicillin/streptomycin/glutamine (Invitrogen) in a humidified 5% CO2 incubator at 37°C. GBM39 were cultured in Neurocult media (Stemcell Technologies) supplemented with EGF (Sigma), FGF (Sigma) and heparin (Sigma) in a humidified 5% CO2 incubator at 37°C. Normal human astrocytes were purchased from Lonza and cultured per manufacturer's guidelines.

Tissue Microarray

Tissue microarrays (TMA) were constructed as reported previously (Guo et al., 2009), and immunohistochemical staining was performed, as described under immunohistochemistry methods, to analyze the expression of LDLR in 55 GBM samples and 24 normal brain samples. Images of LDLR-stained tissue sections were reviewed in a blinded fashion and dichotomized as either undetectable or barely detectable – "low", or as readily detectable or abundant – "high".

Immunohistochemistry

Immunohistochemistry was performed according to standard procedures. Antigen was retrieved by boiling slides in 0.01 M of sodium citrate (pH 6.0) in a microwave for 15 min. Sections were incubated with primary antibodies at 4 °C overnight, followed by incubation with biotinylated secondary antibodies at room temperature for 30 min. Three representative images from each stained section were captured using DP 25 camera mounted on an Olympus BX43 microscope at

40x magnification. Quantitative analysis of the IHC images was performed using image analyzing software (Visiopharm).

TCGA Data Analysis

Processed TCGA data were downloaded through the TCGA data portal. The EGFR status of TCGA GBM samples are designated as euploid, regionally amplified, focally amplified, or EGFRvIII based on annotations previously published (Brennan et al., 2013). Specifically, EGFRvIII samples are samples with non-zero Δ2–7 values, and euploid / regionally amplified / focally amplified samples are non-EGFRvIII samples labeled as "Euploid" / "Regional gain" / "Focal Amplification."

Microarray Analysis

Total RNA was isolated in triplicate for each condition using the RNeasy Plus Mini Kit (QIAGEN). Primeview affymetrix arrays were obtained from Affymetrix, and labeled samples were hybridized and scanned, and gene expression was analyzed in the UCSD VA/VMRF Microarray and NGS Core.

LDL Uptake

For confocal imaging analysis, cells were plated at a density of 1-2,000 cells in an eight well chamber slide (Lab-Tek). Cells were treated with 5 ug/ml Dil-LDL resuspended in DMEM media with 1% lipoprotein deficient serum (LPDS) for 4 h and then washed twice by PBS and fixed in 4% PFA for 15 minutes. After fixing, cells were washed twice by PBS and slides were mounted in antifade reagent with DAPI (Life Technologies) for imaging. Cell imaging was performed on an Olympus FV1000 confocal microscope and fluorescence intensity of 50 cells for each cell line was quantified by ImageJ. For FACS analysis, cells were seeded at a density of

80,000-100,000 in each well of 6-well plates and treated as above with 5 ug/ml Dil-LDL 5 for 4 h. After treatment, cells were washed twice with PBS, harvested, and LDL uptake was assessed via flow cytometry recording signals using the PE channel. Data analyses were performed using FlowJo.

Oxysterol Analysis

Extraction: Cells (~500,000) were pelleted and re-suspended in 100 ul PBS. A mixture of deuterated desmosterol, 25-hydroxycholesterol and campesterol (Avanti Polar Lipids, Alabaster, AL) was added to each sample to serve as internal standards. The sterols/oxysterols were extracted by addition of 1 ml of dichloromethane/methanol (50:50; v/v) and bath sonication for 10 min. The samples were centrifuged for 5 min @ 5000 rpm, the organic extracts were collected and the pellets were re-extracted with dichloromethane/methanol. The combined extracts were brought to dryness under vacuum, resolubilized in 50 ul methanol/water (90:10; v/v), and 10 ul were injected for liquid chromatography and mass spectrometry.

Reverse-phase liquid chromatography and mass spectrometry: Sterols were analysed according to a modified method previously (McDonald et al., 2012; Quehenberger et al., 2010). Briefly, the extracted sterols/oxysterols were separated by reverse phase chromatography using a 1.7uM 2.1x150 mm Kinetex C18 column (Phenomenex, Torrance, CA) and an Acquity UPLC system (Waters, Milford, MA). The column was equilibrated with buffer A consisting of acetonitrile/water (70:30; v/v) and 5 mM ammonium acetate and sterols/oxysterols were separated with a linear gradient over 10 min to 100% buffer B consisting of acetonitrile/2-propanol (50:50; v/v) and 5 mM ammonium acetate.

The liquid chromatography effluent was interfaced with a mass spectrometer and mass spectral analysis was performed on an AB SCIEX 6500 QTrap mass spectrometer equipped with an APCI (Atmospheric Pressure Chemical Ionization) probe (SCIEX, Framingham, MA). The instrument was operated in the positive ion mode. The curtain gas, nebulizer current, ion source gas and temperature settings were optimize by infusion under chromatographic flow conditions using early eluting 25-hydroxycholesterol and late eluting desmosterol for calibration. The sterols/oxysterols were measured using multiple reaction monitoring (MRM) with the transitions set for specificity and sensitivity (McDonald et al., 2012). The collision energy and the declustering potential was determined for each metabolite. The sterols/oxysterols were identified by matching the MRM signal and chromatographic retention times with that of pure standards analyzed identical under conditions.

Quantification: Sterols/oxysterols were quantified by the isotope dilution method. Briefly, identical amounts of deuterated internal standards were added to each sample and to the dilutions of primary standard used to generate standard curves. To calculate the amount of sterols/oxysterols in a sample, ratios of peak areas between endogenous metabolites and deuterated internal standards were calculated and the ratios were converted to absolute amounts by linear regression analysis of the standard curve generated under identical conditions. The lower detection limit for oxysterols was on average 0.06 ng on the column and for the sterols about 0.6 ng on the column.

Cell Viability Assay

Cells were seeded in triplicate for each condition in 24-well culture plates at 10,000 cells per well. DMSO or LXR-623 was added to cells in DMEM media containing 0.5%-1% FBS for established cell lines or Neurocult media without supplement for patient derived neurosphere

lines. Total and live cells in each well were quantified by Trypan blue (Gibco) assay using a TC10 automatic cell counter (Bio-Rad).

Data Analysis

The Fischer's exact test was used for statistical analysis of tissue microarray staining. All other statistical comparisons were carried out using Student's t tests. Throughout all figures, *$p < 0.05$, **$p < 0.01$, and ***$p < 0.001$. Significance was concluded at $p < 0.05$.

REFERENCES

Babic, I., Anderson, E.S., Tanaka, K., Guo, D., Masui, K., Li, B., Zhu, S., Gu, Y., Villa, G.R., Akhavan, D., et al. (2013). EGFR mutation-induced alternative splicing of Max contributes to growth of glycolytic tumors in brain cancer. Cell Metab. *17*, 1000–1008.

Björkhem, I. (2006). Crossing the barrier: oxysterols as cholesterol transporters and metabolic modulators in the brain. J. Intern. Med. *260*, 493–508.

Bovenga, F., Sabbà, C., and Moschetta, A. (2015). Uncoupling nuclear receptor LXR and cholesterol metabolism in cancer. Cell Metab. *21*, 517–526.

Brennan, C.W., Verhaak, R.G.W., McKenna, A., Campos, B., Noushmehr, H., Salama, S.R., Zheng, S., Chakravarty, D., Sanborn, J.Z., Berman, S.H., et al. (2013). The somatic genomic landscape of glioblastoma. Cell *155*, 462–477.

Brown, M.S., and Goldstein, J.L. (1980). Multivalent feedback regulation of HMG CoA reductase, a control mechanism coordinating isoprenoid synthesis and cell growth. J. Lipid Res. *21*, 505–517.

Cancer Genome Atlas Research Network (2008). Comprehensive genomic characterization defines human glioblastoma genes and core pathways. Nature *455*, 1061–1068.

Chen, J., Zhang, X., Kusumo, H., Costa, L.G., and Guizzetti, M. (2013). Cholesterol efflux is differentially regulated in neurons and astrocytes: implications for brain cholesterol homeostasis. Biochim. Biophys. Acta *1831*, 263–275.

Cloughesy, T.F., Cavenee, W.K., and Mischel, P.S. (2014). Glioblastoma: from molecular pathology to targeted treatment. Annu. Rev. Pathol. *9*, 1–25.

Dietschy, J.M., and Turley, S.D. (2001). Cholesterol metabolism in the brain. Curr. Opin. Lipidol. *12*, 105–112.

Friedmann-Morvinski, D., and Verma, I.M. (2014). Dedifferentiation and reprogramming: origins of cancer stem cells. EMBO Rep. *15*, 244–253.

Gabitova, L., Restifo, D., Gorin, A., Manocha, K., Handorf, E., Yang, D.-H., Cai, K.Q., Klein-Szanto, A.J., Cunningham, D., Kratz, L.E., et al. (2015). Endogenous Sterol Metabolites Regulate Growth of EGFR/KRAS-Dependent Tumors via LXR. Cell Rep. *12*, 1927–1938.

Goldstein, J.L., and Brown, M.S. (2015). A century of cholesterol and coronaries: from plaques to genes to statins. Cell *161*, 161–172.

Guo, D., Hildebrandt, I.J., Prins, R.M., Soto, H., Mazzotta, M.M., Dang, J., Czernin, J., Shyy, J.Y.-J., Watson, A.D., Phelps, M., et al. (2009). The AMPK agonist AICAR inhibits the growth of EGFRvIII-expressing glioblastomas by inhibiting lipogenesis. Proc. Natl. Acad. Sci. U. S. A. *106*, 12932–12937.

Guo, D., Reinitz, F., Youssef, M., Hong, C., Nathanson, D., Akhavan, D., Kuga, D., Amzajerdi, A.N., Soto, H., Zhu, S., et al. (2011). An LXR agonist promotes glioblastoma cell death through inhibition of an EGFR/AKT/SREBP-1/LDLR-dependent pathway. Cancer Discov. *1*, 442–456.

Hong, C., and Tontonoz, P. (2014). Liver X receptors in lipid metabolism: opportunities for drug discovery. Nat. Rev. Drug Discov. *13*, 433–444.

Katz, A., Udata, C., Ott, E., Hickey, L., Burczynski, M.E., Burghart, P., Vesterqvist, O., and Meng, X. (2009). Safety, pharmacokinetics, and pharmacodynamics of single doses of LXR-623, a novel liver X-receptor agonist, in healthy participants. J. Clin. Pharmacol. *49*, 643–649.

Lin, C.-Y., and Gustafsson, J.-Å. (2015). Targeting liver X receptors in cancer therapeutics. Nat. Rev. Cancer *15*, 216–224.

Lunt, S.Y., and Vander Heiden, M.G. (2011). Aerobic glycolysis: meeting the metabolic requirements of cell proliferation. Annu. Rev. Cell Dev. Biol. *27*, 441–464.

Lütjohann, D., Breuer, O., Ahlborg, G., Nennesmo, I., Sidén, A., Diczfalusy, U., and Björkhem, I. (1996). Cholesterol homeostasis in human brain: evidence for an age-dependent flux of 24S-hydroxycholesterol from the brain into the circulation. Proc. Natl. Acad. Sci. U. S. A. *93*, 9799–9804.

Masui, K., Tanaka, K., Akhavan, D., Babic, I., Gini, B., Matsutani, T., Iwanami, A., Liu, F., Villa, G.R., Gu, Y., et al. (2013). mTOR complex 2 controls glycolytic metabolism in glioblastoma through FoxO acetylation and upregulation of c-Myc. Cell Metab. *18*, 726–739.

Masui, K., Tanaka, K., Ikegami, S., Villa, G.R., Yang, H., Yong, W.H., Cloughesy, T.F., Yamagata, K., Arai, N., Cavenee, W.K., et al. (2015). Glucose-dependent acetylation of Rictor promotes targeted cancer therapy resistance. Proc. Natl. Acad. Sci. U. S. A. *112*, 9406–9411.

McDonald, J.G., Smith, D.D., Stiles, A.R., and Russell, D.W. (2012). A comprehensive method for extraction and quantitative analysis of sterols and secosteroids from human plasma. J. Lipid Res. *53*, 1399–1409.

Nieweg, K., Schaller, H., and Pfrieger, F.W. (2009). Marked differences in cholesterol synthesis between neurons and glial cells from postnatal rats. J. Neurochem. *109*, 125–134.

Pavlova, N.N., and Thompson, C.B. (2016). The Emerging Hallmarks of Cancer Metabolism. Cell Metab. *23*, 27–47.

Quehenberger, O., Armando, A.M., Brown, A.H., Milne, S.B., Myers, D.S., Merrill, A.H., Bandyopadhyay, S., Jones, K.N., Kelly, S., Shaner, R.L., et al. (2010). Lipidomics reveals a remarkable diversity of lipids in human plasma. J. Lipid Res. *51*, 3299–3305.

Repa, J.J., Turley, S.D., Lobaccaro, J.A., Medina, J., Li, L., Lustig, K., Shan, B., Heyman, R.A., Dietschy, J.M., and Mangelsdorf, D.J. (2000). Regulation of absorption and ABC1-mediated efflux of cholesterol by RXR heterodimers. Science *289*, 1524–1529.

Sarkaria, J.N., Yang, L., Grogan, P.T., Kitange, G.J., Carlson, B.L., Schroeder, M.A., Galanis, E., Giannini, C., Wu, W., Dinca, E.B., et al. (2007). Identification of molecular characteristics correlated with glioblastoma sensitivity to EGFR kinase inhibition through use of an intracranial xenograft test panel. Mol. Cancer Ther. *6*, 1167–1174.

Stupp, R., Mason, W.P., van den Bent, M.J., Weller, M., Fisher, B., Taphoorn, M.J.B., Belanger, K., Brandes, A.A., Marosi, C., Bogdahn, U., et al. (2005). Radiotherapy plus concomitant and adjuvant temozolomide for glioblastoma. N. Engl. J. Med. *352*, 987–996.

Twisk, J., Gillian-Daniel, D.L., Tebon, A., Wang, L., Barrett, P.H., and Attie, A.D. (2000). The role of the LDL receptor in apolipoprotein B secretion. J. Clin. Invest. *105*, 521–532.

Vander Heiden, M.G., Cantley, L.C., and Thompson, C.B. (2009). Understanding the Warburg effect: the metabolic requirements of cell proliferation. Science *324*, 1029–1033.

Venkateswaran, A., Laffitte, B.A., Joseph, S.B., Mak, P.A., Wilpitz, D.C., Edwards, P.A., and Tontonoz, P. (2000). Control of cellular cholesterol efflux by the nuclear oxysterol receptor LXR alpha. Proc. Natl. Acad. Sci. U. S. A. *97*, 12097–12102.

Wang, M.Y., Lu, K.V., Zhu, S., Dia, E.Q., Vivanco, I., Shackleford, G.M., Cavenee, W.K., Mellinghoff, I.K., Cloughesy, T.F., Sawyers, C.L., et al. (2006). Mammalian target of rapamycin inhibition promotes response to epidermal growth factor receptor kinase inhibitors in PTEN-deficient and PTEN-intact glioblastoma cells. Cancer Res. *66*, 7864–7869.

Wen, P.Y., and Kesari, S. (2008). Malignant gliomas in adults. N. Engl. J. Med. *359*, 492–507.

Young, R.M., Jamshidi, A., Davis, G., and Sherman, J.H. (2015). Current trends in the surgical management and treatment of adult glioblastoma. Ann. Transl. Med. *3*, 121.

Zelcer, N., Hong, C., Boyadjian, R., and Tontonoz, P. (2009). LXR regulates cholesterol uptake through Idol-dependent ubiquitination of the LDL receptor. Science *325*, 100–104.

Chapter 2

In Vivo Pharmacologic Characterization of the Synthetic LXR Agonist LXR-623

INTRODUCTION

A strong case has been made for nuclear hormone receptor modulators as potential cancer drugs (Gronemeyer et al., 2004), including LXR modulators that show activity against melanoma, intestinal cancers, squamous cell cancers, prostate cancers cells and breast cancer cell lines (Flaveny et al., 2015; Gabitova et al., 2015; Lin and Gustafsson, 2015; Lo Sasso et al., 2013; Nguyen-Vu et al., 2013; Pencheva et al., 2014; Pommier et al., 2013). Hormone receptor modulators are FDA-approved therapies for breast and prostate cancers (Masters et al., 2015). In contrast, LXR modulators, which were originally developed for the treatment of atherosclerosis, have failed to move forward clinically, due in large part to an undesirable pre-clinical side effect profile, which includes elevated plasma triglyceride levels and hepatic steatosis (Bradley et al., 2007; Collins et al., 2002; Joseph et al., 2002a, 2002b; Schultz et al., 2000). To date, no LXR agonist has been developed specifically as a cancer therapeutic (Lin and Gustafsson, 2015).

The lipogenic activity of LXR results from the upregulation of the master transcriptional regulator of lipogenesis, Sterol Response Element Binding Protein 1 C (SREBP1C). Treatment of mice with synthetic LXR agonists promotes transcriptional induction of Srebp1c and several of its downstream targets, including fatty acid synthase (Fas) and stearoyl-CoA desaturase 1 (Scd1), which together result in triglyceride synthesis in the liver and elevated plasma triglyceride levels (Chu et al., 2006; Joseph et al., 2002a). LXR exists as two isotypes, and activation of LXRα, rather than the ubiquitously expressed LXRβ, is responsible for hepatic triglyceride synthesis. Thus, a major goal for the clinical advancement of synthetic LXR agonists has been the development of synthetic LXR ligands that more selectively activate LXRβ.

The first identified LXR agonist was T0901317 (Schultz et al., 2000), which was also found to activate the farnesoid X receptor (FXR) and the pregnane X receptor (PXR) (Houck et al., 2004;

Mitro et al., 2007). GW3965, a more selective synthetic LXR agonist, was later developed and is most commonly used in mechanistic studies of LXR (Collins et al., 2002). LXR-623, an LXRα-partial/LXRβ-full agonist, was more recently developed (Hu et al., 2010; Wrobel et al., 2008) and was the first synthetic LXR agonist tested in patients (Hong and Tontonoz, 2014; Katz et al., 2009). Patients treated in a healthy participant trial of LXR-623 experienced mild to moderate CNS side effects. This generated our interest, as it suggested the compound was potentially brain-penetrant (Katz et al., 2009).

Determining the preclinical activity of LXR-623 in a relevant *in vivo* system is a *sine qua non* for clinical testing. The microenvironment plays a critical role in brain tumors and must be taken into consideration to better understand tumor behavior in response to treatment modalities (Blouw et al., 2003). Therefore, we established an orthotopic GBM xenograft mouse model utilizing fluorescence molecular tomography (FMT), a non-invasive and quantitative method to measure tumor growth over time.

A major pharmacologic challenge in the treatment of GBM has been the development of compounds with high CNS penetration. Therapies targeting EGFR in GBM demonstrated poor inhibition of the EGFR signaling axis in tumor tissue, in part due to an inability to achieve sufficient intratumoral concentrations (Hegi et al., 2011; Lassman et al., 2005; Vivanco et al., 2012). To address this issue we examined the potential relationship between intracranial GBM growth, as monitored by non-invasive FMT imaging and intratumoral LXR-623 levels. We further pharmacologically characterized LXR-623 *in vivo* by examining known toxicities associated with LXR agonists.

RESULTS

LXR-623 crosses the blood-brain barrier with minimal activity in the periphery

In a healthy participant trial of LXR-623, subjects experienced mild to moderate CNS side effects, suggesting that this compound crosses the blood-brain barrier (Katz et al., 2009). Consistent with this premise, at two or eight hours after dosing LXR-623 levels in the brains of nude mice treated daily by oral gavage were higher than plasma levels (Figure 2-1).

Many of the undesirable hyperlipidemic effects of synthetic LXR agonists are mediated through LXRα in the liver and adipose tissue (Bradley et al., 2007; Joseph et al., 2002a, 2002b; Schultz et al., 2000). Previous studies indicated that LXR-623, unlike structurally distinct LXR agonists such as GW3965, does not activate hepatic lipogenesis (Quinet et al., 2009) because it is an LXRα-partial/LXRβ-full agonist with a unique transcriptional cofactor recruitment profile (Quinet et al., 2009; Wrobel et al., 2008). Therefore, we compared the abilities of LXR-623 and GW3965 to induce target gene expression in the brain and peripheral tissues. LXR-623 significantly induced LXR target gene expression in cerebral cortex tissue in a fashion similar to GW3965, albeit to a lesser degree for Abca1 and with the exception of Srebp1c (Figure 2A). On the other hand, LXR-623 did not induce target gene expression in the liver and epididymal white adipose tissue (eWAT) (Figure 2B, 2C). These data suggested that at least two ligand-specific properties of LXR-623 – high CNS penetrance and reduced activity on LXRα – may provide a therapeutic window for treating GBM, and possibly other brain cancers.

LXR-623 achieves therapeutic levels in GBM cells in the brain

We next performed a pilot study of LXR-623 treatment in an *in vivo* intracranial GBM xenograft model (Figure 2-3). We examined the potential relationship between intracranial GBM growth,

as monitored by non-invasive fluorescence molecular tomography (FMT) imaging, and intratumoral LXR-623 levels. As shown in Figure 2-4A, LXR-623 reached low-μM concentrations within intracranial GBMs, meeting or exceeding the concentrations required to kill GBM cells in culture (Figure 1-10), and significantly reduced GBM tumor growth *in vivo* (Figure 2-4B). These data demonstrate favorable brain penetration and potent anti-GBM activity for LXR-623 *in vivo*.

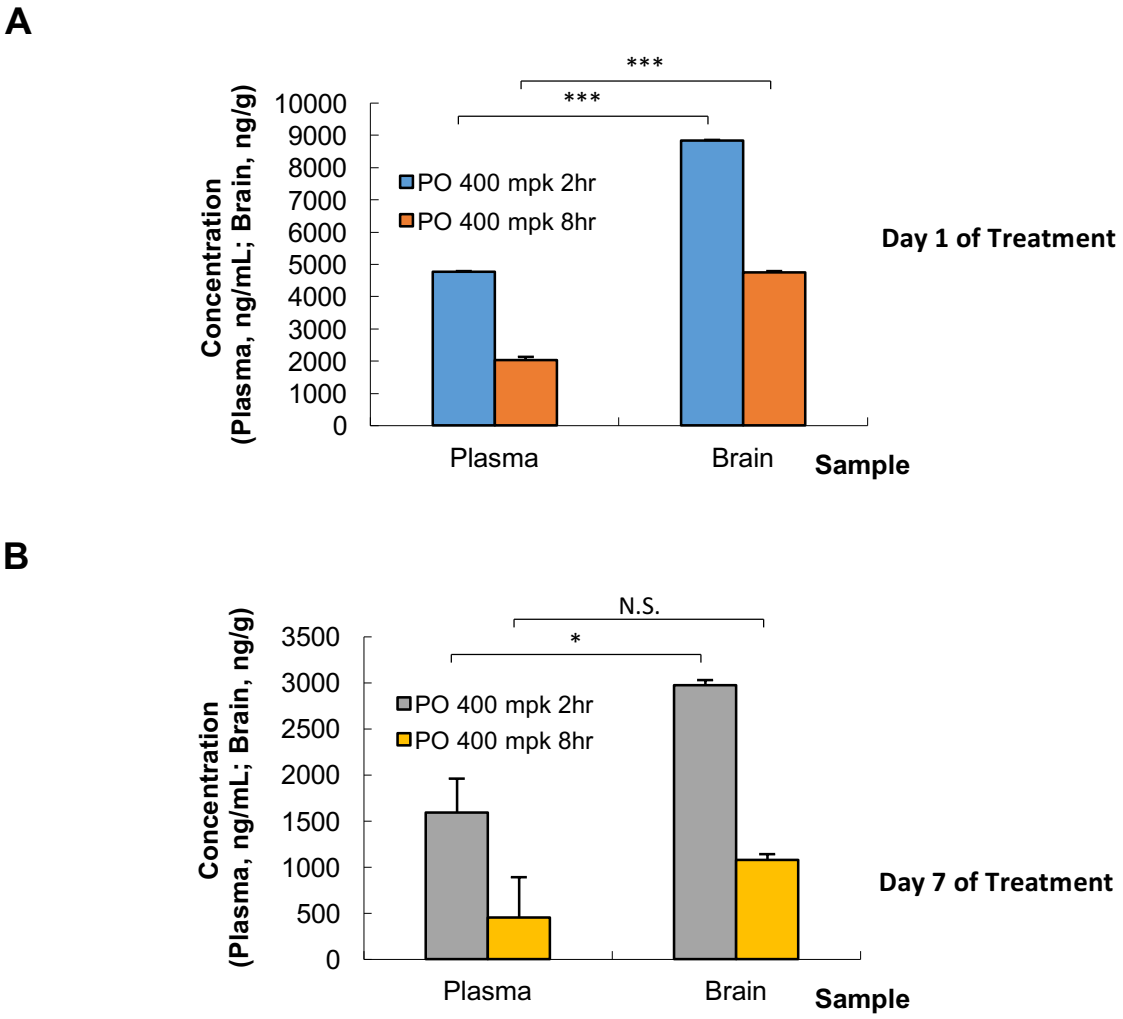

Figure 2-1. **LXR-623 cross the blood-brain barrier in mice**. (**A**) Mice were treated with a single dose of LXR-623 by oral gavage (p.o.), 400 mg/kg (mpk). Plasma and brain were extracted from mice at 2 or 8 hours post-gavage. n = 5 for each time point. (**B**) Mice were treated with LXR-623 by oral gavage (p.o.), 400 mg/kg (mpk) daily for seven continuous days. Plasma and brain were extracted from mice on day seven at 2 or 8 hours after gavage. n = 5 for each time point. LXR-623 levels were assessed via liquid chromatography-tandem mass spectrometry (LC-MS/MS). *p < 0.05; **p < 0.01; ***p < 0.001. N.S. = not significant.

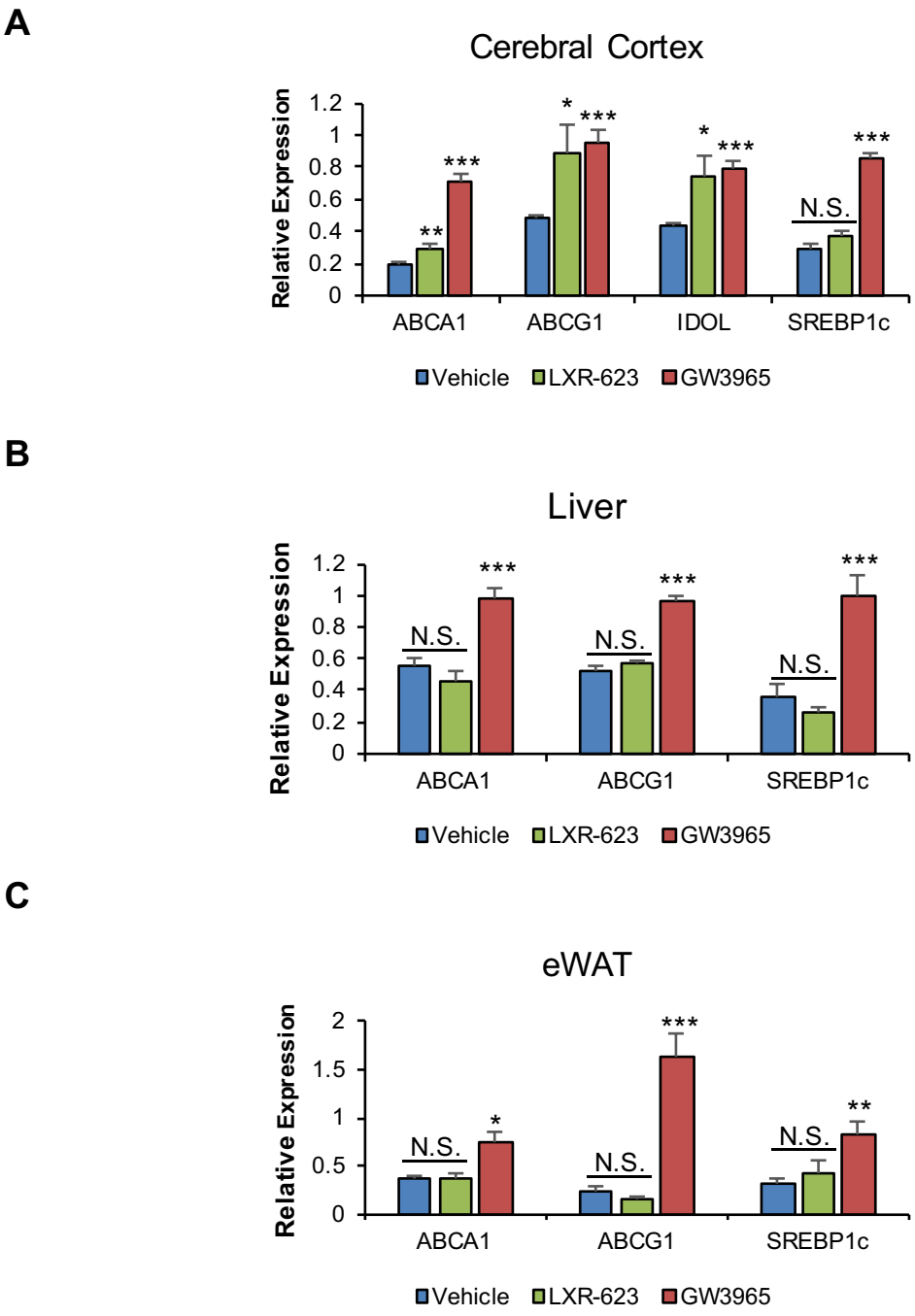

Figure 2-2. **LXR-623 induces target gene expression in the brain with minimal activity in the periphery**. Mice were treated with LXR-623 or GW3965 (40 mg/kg) by oral gavage daily for three days. RNA was extracted from (**A**) cerebral cortex, (**B**) liver, and (**C**) epididymal white adipose tissue (eWAT), and qPCR was performed for the indicated genes. n = 4 for each group. *p < 0.05; **p < 0.01; ***p < 0.001. N.S. = not significant.

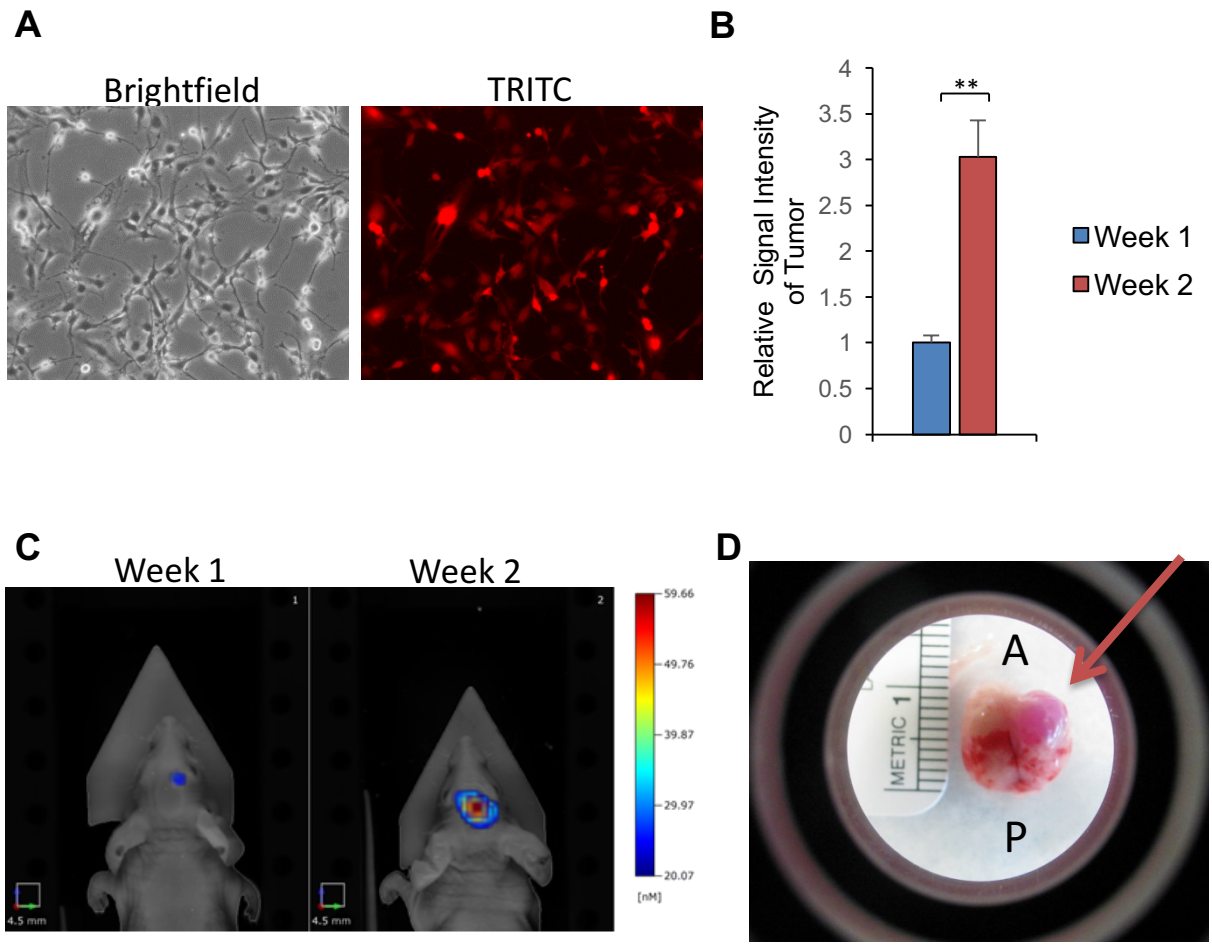

Figure 2-3. **Intracranial xenograft model of GBM**. (**A**) U87vIII GBM cells were engineered to express the Turbo FP 635 fluorescent protein. Brightfield (left) and tetramethylrhodamine (TRITC) fluorescent (right) images. (**B**) U87vIII Turbo FP 635 cells were injected orthotopically into five-week old nude mice. Signal intensity was quantified via Fluorescence Molecular Tomography (FMT) technology one or two weeks post-injection (n=6 for each group). A two-tailed paired t-test was used to calculate the p-value. (**C**) Representative image of a mouse from (**B**). (**D**) Excised mouse brain containing a well-established intracerebral tumor from a mouse in (**B**). The tumor appears red due to the presence of the Turbo FP 635 protein. Arrow indicates tumor location. A: Anterior, P: Posterior of mouse, respectively. **$p < 0.01$.

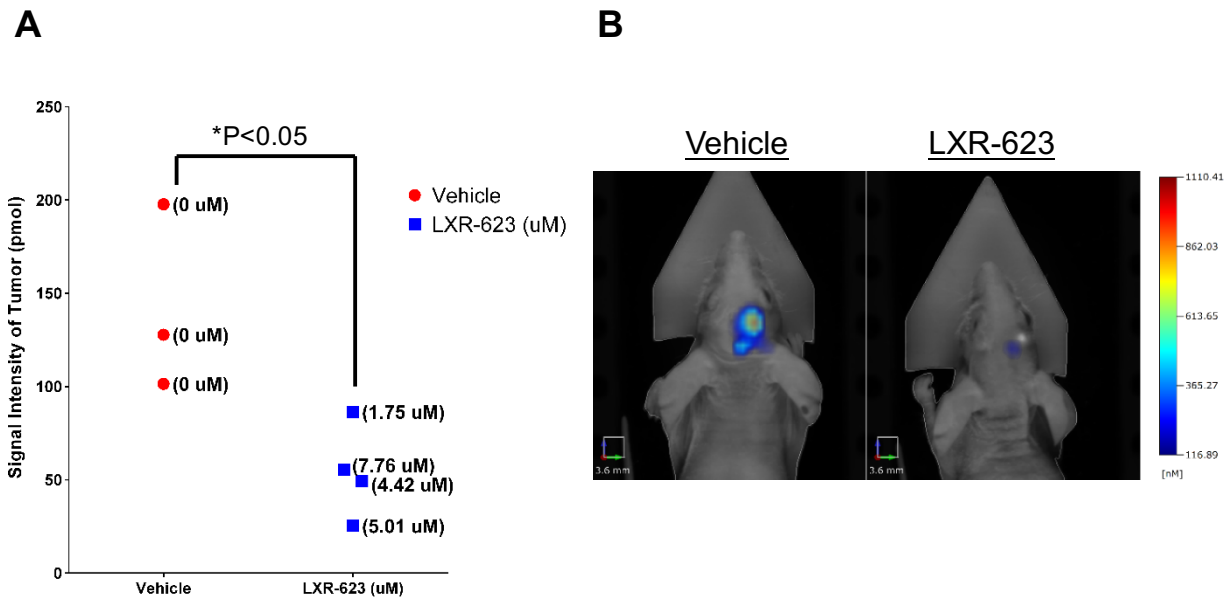

Figure 2-4. **LXR-623 achieves therapeutic levels in GBM cells in the brain and inhibits tumor growth**. (**A**) U87EGFRvIII Turbo FP 635 orthotopic mouse xenograft. Mice were treated with vehicle or LXR-623 400 mpk p.o. daily. Tumor size was assessed via FMT technology on day five of treatment. Tumors were excised from mice and the intratumor concentration of LXR-623 was assessed via (LC-MS/MS). Intratumoral LXR-623 concentrations are indicated within parentheses. n = 3 for vehicle and n = 4 for LXR-623 treated mice. (**B**) Representative FMT images of mice from (**A**). *p < 0.05; **p < 0.01; ***p < 0.001; N.S. = not significant.

DISCUSSION

Growth factor receptor mutations are common in cancer, including in tumors that arise from or metastasize to the brain. Therapies targeting oncogenic signaling have been a mainstay strategy for cancers harboring activating growth factor receptor signaling mutations. However, most small-molecule inhibitors targeting growth factor receptors have failed to show efficacy for brain cancers, potentially due to both inadequate CNS penetration and upregulation of resistance mechanisms (Akhavan et al., 2013; Furnari et al., 2015; Vivanco et al., 2012). Targeting non-oncogene metabolic dependencies that result from dysregulated receptor tyrosine (RTK) signaling provides an alternative approach, particularly if drugs with brain and tumor penetration can be identified.

Here, LXR-623 displayed significant brain penetration in mice treated by oral gavage (Figure 2-1). LXR-623 also induced LXR target gene expression in the cerebral cortex while having limited effects on extracerebral tissues, consistent with a model of CNS accumulation of this compound (Figure 2-2). However, it should be noted that a drug clearance response occurs as evidenced by a decrease in total brain levels of LXR-623 after seven days of continuous dosing (Figure 2-1). Thus, future studies will need to delineate an optimal dosing regimen, which includes, but is not limited to, continuous dosing at 200 mg/kg daily.

GBM patients treated with small molecules targeting EGFR have demonstrated poor responses due to incomplete inhibition of the EGFR signaling axis in tumor tissue, which occurs as a result of inability to achieve sufficient intratumoral concentrations (Hegi et al., 2011; Lassman et al., 2005; Vivanco et al., 2012). Here, therapeutic levels of LXR-623 were achieved intratumorally concomitant with inhibition of tumor growth (Figure 2-4), overcoming a major pharmacologic barrier to GBM treatment.

To date, no LXR agonist has been developed specifically as a cancer therapeutic (Lin and Gustafsson, 2015). While the mild to moderate CNS effects observed in patients treated with LXR-623 are not to be underestimated, the considerable anti-GBM activity and favorable pharmacologic profile of LXR-623 merits further pre-clinical investigation.

EXPERIMENTAL PROCEDURES

Pharmacokinetic Analysis

Plasma and brain concentrations of LXR-623 (0.5% methylcellulose, 2% Tween-80 in water) in female nu/nu mice after oral dosing (day 1 and 7) were determined by standard LC-MS/MS-based methods by WuXi AppTec (Shanghai, China).

Pharmacodynamic Analysis

Mice were treated with vehicle (0.5% methylcellulose, 2% Tween-80 in water), LXR-623 or GW3965 (40 mg/kg) by oral gavage daily for three days. RNA was extracted from cerebral cortex, liver, and epididymal white adipose tissue (eWAT), and qPCR was performed.

Real-Time RT-PCR

Total RNA was extracted by using the RNeasy Plus Mini Kit (QIAGEN). First-strand cDNA was synthesized using the using the SuperScript VILO cDNA synthesis kit (Invitrogen). Real-time RT-PCR was performed using the iQ SYBR Green Supermix (Bio-Rad) on the the CFX96 Touch Real Time PCR Detection system (Bio-Rad) following the manufacturer's instructions. Results were normalized to the 36B4 reference gene for *in vivo* studies. Primer sequences are available upon request.

Cell Culture

U87EGFRvIII and U87EGFRvIII Turbo FP 635 were cultured in Dulbecco's Modified Eagle Media (DMEM, Cellgro) supplemented with 10% fetal bovine serum (FBS, Hyclone) and 1% penicillin/streptomycin/glutamine (Invitrogen) in a humidified 5% CO2 incubator at 37°C.

Lentivirus Production and Infection

The Turbo FP 635 protein cDNA (Evrogen) was PCR-cloned into the Nhe I and Xho I restriction enzyme sites of the pLV lentiviral plasmid vector. The construct was then co-transfected with lentivirus packaging plasmids to Lenti-X 293T cells (Clontech), using X-tremeGENE DNA transfection reagents (Roche). Supernatants containing high titer lentiviruses were collected between 24-72 hours after transfection and were filtered through a 0.45 μm syringe filter before use. For infection, $5x10^5$ U87EGFRvIII cells were seeded. The following day, 1/10 volume of high titer lentivirus and 12.5 ng/ml (final concentration) of polybrene were mixed and added to cultured cells. After 8 hours of incubation in 37 °C, the supernatant containing virus was replaced by fresh culture media (DMEM/10%FBS). Infected cells were selected by blasticidin (2 μg /ml) and then fluorescence-activated cell sorting (FACS) using the Sony Sorter SH800Z was used to enrich the top 5% of total fluorescent cell population.

Intracranial Xenograft

Five-week-old female athymic nu/nu mice were purchased from Harlan Sprague Dawley Inc. 1×10^5 U87EGFRvIII Turbo FP 635 cells in 5 μl of phosphate-buffered saline (PBS) were intracranially injected into the mouse brain as described previously (Ozawa and James, 2010). Tumor growth was monitored using an FMT 2500 Fluorescence Tomography System (PerkinElmer). For drug treatment studies, vehicle (0.5% methylcellulose, 2% Tween-80 in water) or LXR-623 (400 mg/kg) resuspended in vehicle were administered to mice orally via daily gavage starting at day seven post-injection. All procedures were reviewed and approved by the Institutional Animal Use and Care Committee at the University of California, San Diego.

Data Analysis

Statistical comparisons were carried out using Student's t-tests. Throughout all figures, *$p < 0.05$, **$p < 0.01$, and ***$p < 0.001$. Significance was concluded at $p < 0.05$.

REFERENCES

Akhavan, D., Pourzia, A.L., Nourian, A.A., Williams, K.J., Nathanson, D., Babic, I., Villa, G.R., Tanaka, K., Nael, A., Yang, H., et al. (2013). De-repression of PDGFRβ transcription promotes acquired resistance to EGFR tyrosine kinase inhibitors in glioblastoma patients. Cancer Discov. *3*, 534–547.

Blouw, B., Song, H., Tihan, T., Bosze, J., Ferrara, N., Gerber, H.P., Johnson, R.S., and Bergers, G. (2003). The hypoxic response of tumors is dependent on their microenvironment. Cancer Cell *4*, 133–146.

Bradley, M.N., Hong, C., Chen, M., Joseph, S.B., Wilpitz, D.C., Wang, X., Lusis, A.J., Collins, A., Hseuh, W.A., Collins, J.L., et al. (2007). Ligand activation of LXR beta reverses atherosclerosis and cellular cholesterol overload in mice lacking LXR alpha and apoE. J. Clin. Invest. *117*, 2337–2346.

Chu, K., Miyazaki, M., Man, W.C., and Ntambi, J.M. (2006). Stearoyl-coenzyme A desaturase 1 deficiency protects against hypertriglyceridemia and increases plasma high-density lipoprotein cholesterol induced by liver X receptor activation. Mol. Cell. Biol. *26*, 6786–6798.

Collins, J.L., Fivush, A.M., Watson, M.A., Galardi, C.M., Lewis, M.C., Moore, L.B., Parks, D.J., Wilson, J.G., Tippin, T.K., Binz, J.G., et al. (2002). Identification of a nonsteroidal liver X receptor agonist through parallel array synthesis of tertiary amines. J. Med. Chem. *45*, 1963–1966.

Flaveny, C.A., Griffett, K., El-Gendy, B.E.-D.M., Kazantzis, M., Sengupta, M., Amelio, A.L., Chatterjee, A., Walker, J., Solt, L.A., Kamenecka, T.M., et al. (2015). Broad Anti-tumor Activity of a Small Molecule that Selectively Targets the Warburg Effect and Lipogenesis. Cancer Cell *28*, 42–56.

Furnari, F.B., Cloughesy, T.F., Cavenee, W.K., and Mischel, P.S. (2015). Heterogeneity of epidermal growth factor receptor signalling networks in glioblastoma. Nat. Rev. Cancer *15*, 302–310.

Gabitova, L., Restifo, D., Gorin, A., Manocha, K., Handorf, E., Yang, D.-H., Cai, K.Q., Klein-Szanto, A.J., Cunningham, D., Kratz, L.E., et al. (2015). Endogenous Sterol Metabolites Regulate Growth of EGFR/KRAS-Dependent Tumors via LXR. Cell Rep. *12*, 1927–1938.

Gronemeyer, H., Gustafsson, J.-A., and Laudet, V. (2004). Principles for modulation of the nuclear receptor superfamily. Nat. Rev. Drug Discov. *3*, 950–964.

Hegi, M.E., Diserens, A.-C., Bady, P., Kamoshima, Y., Kouwenhoven, M.C.M., Delorenzi, M., Lambiv, W.L., Hamou, M.-F., Matter, M.S., Koch, A., et al. (2011). Pathway analysis of glioblastoma tissue after preoperative treatment with the EGFR tyrosine kinase inhibitor gefitinib--a phase II trial. Mol. Cancer Ther. *10*, 1102–1112.

Hong, C., and Tontonoz, P. (2014). Liver X receptors in lipid metabolism: opportunities for drug discovery. Nat. Rev. Drug Discov. *13*, 433–444.

Houck, K.A., Borchert, K.M., Hepler, C.D., Thomas, J.S., Bramlett, K.S., Michael, L.F., and Burris, T.P. (2004). T0901317 is a dual LXR/FXR agonist. Mol. Genet. Metab. *83*, 184–187.

Hu, B., Bernotas, R., Unwalla, R., Collini, M., Quinet, E., Feingold, I., Goos-Nilsson, A., Wilhelmsson, A., Nambi, P., Evans, M., et al. (2010). Quinoline-3-carboxamide containing sulfones as liver X receptor (LXR) agonists with binding selectivity for LXRbeta and low blood-brain penetration. Bioorg. Med. Chem. Lett. *20*, 689–693.

Joseph, S.B., Laffitte, B.A., Patel, P.H., Watson, M.A., Matsukuma, K.E., Walczak, R., Collins, J.L., Osborne, T.F., and Tontonoz, P. (2002a). Direct and indirect mechanisms for regulation of fatty acid synthase gene expression by liver X receptors. J. Biol. Chem. *277*, 11019–11025.

Joseph, S.B., McKilligin, E., Pei, L., Watson, M.A., Collins, A.R., Laffitte, B.A., Chen, M., Noh, G., Goodman, J., Hagger, G.N., et al. (2002b). Synthetic LXR ligand inhibits the development of atherosclerosis in mice. Proc. Natl. Acad. Sci. U. S. A. *99*, 7604–7609.

Katz, A., Udata, C., Ott, E., Hickey, L., Burczynski, M.E., Burghart, P., Vesterqvist, O., and Meng, X. (2009). Safety, pharmacokinetics, and pharmacodynamics of single doses of LXR-623, a novel liver X-receptor agonist, in healthy participants. J. Clin. Pharmacol. *49*, 643–649.

Lassman, A.B., Rossi, M.R., Raizer, J.J., Razier, J.R., Abrey, L.E., Lieberman, F.S., Grefe, C.N., Lamborn, K., Pao, W., Shih, A.H., et al. (2005). Molecular study of malignant gliomas treated with epidermal growth factor receptor inhibitors: tissue analysis from North American Brain Tumor Consortium Trials 01-03 and 00-01. Clin. Cancer Res. Off. J. Am. Assoc. Cancer Res. *11*, 7841–7850.

Lin, C.-Y., and Gustafsson, J.-Å. (2015). Targeting liver X receptors in cancer therapeutics. Nat. Rev. Cancer *15*, 216–224.

Lo Sasso, G., Bovenga, F., Murzilli, S., Salvatore, L., Di Tullio, G., Martelli, N., D'Orazio, A., Rainaldi, S., Vacca, M., Mangia, A., et al. (2013). Liver X receptors inhibit proliferation of human colorectal cancer cells and growth of intestinal tumors in mice. Gastroenterology *144*, 1497–1507, 1507.e1–e13.

Masters, G.A., Krilov, L., Bailey, H.H., Brose, M.S., Burstein, H., Diller, L.R., Dizon, D.S., Fine, H.A., Kalemkerian, G.P., Moasser, M., et al. (2015). Clinical cancer advances 2015: Annual report on progress against cancer from the American Society of Clinical Oncology. J. Clin. Oncol. Off. J. Am. Soc. Clin. Oncol. *33*, 786–809.

Mitro, N., Vargas, L., Romeo, R., Koder, A., and Saez, E. (2007). T0901317 is a potent PXR ligand: implications for the biology ascribed to LXR. FEBS Lett. *581*, 1721–1726.

Nguyen-Vu, T., Vedin, L.-L., Liu, K., Jonsson, P., Lin, J.Z., Candelaria, N.R., Candelaria, L.P., Addanki, S., Williams, C., Gustafsson, J.-Å., et al. (2013). Liver × receptor ligands disrupt breast cancer cell proliferation through an E2F-mediated mechanism. Breast Cancer Res. BCR *15*, R51.

Ozawa, T., and James, C.D. (2010). Establishing intracranial brain tumor xenografts with subsequent analysis of tumor growth and response to therapy using bioluminescence imaging. J. Vis. Exp. JoVE.

Pencheva, N., Buss, C.G., Posada, J., Merghoub, T., and Tavazoie, S.F. (2014). Broad-spectrum therapeutic suppression of metastatic melanoma through nuclear hormone receptor activation. Cell *156*, 986–1001.

Pommier, A.J.C., Dufour, J., Alves, G., Viennois, E., De Boussac, H., Trousson, A., Volle, D.H., Caira, F., Val, P., Arnaud, P., et al. (2013). Liver x receptors protect from development of prostatic intra-epithelial neoplasia in mice. PLoS Genet. *9*, e1003483.

Quinet, E.M., Basso, M.D., Halpern, A.R., Yates, D.W., Steffan, R.J., Clerin, V., Resmini, C., Keith, J.C., Berrodin, T.J., Feingold, I., et al. (2009). LXR ligand lowers LDL cholesterol in primates, is lipid neutral in hamster, and reduces atherosclerosis in mouse. J. Lipid Res. *50*, 2358–2370.

Schultz, J.R., Tu, H., Luk, A., Repa, J.J., Medina, J.C., Li, L., Schwendner, S., Wang, S., Thoolen, M., Mangelsdorf, D.J., et al. (2000). Role of LXRs in control of lipogenesis. Genes Dev. *14*, 2831–2838.

Vivanco, I., Robins, H.I., Rohle, D., Campos, C., Grommes, C., Nghiemphu, P.L., Kubek, S., Oldrini, B., Chheda, M.G., Yannuzzi, N., et al. (2012). Differential sensitivity of glioma- versus lung cancer-specific EGFR mutations to EGFR kinase inhibitors. Cancer Discov. *2*, 458–471.

Wrobel, J., Steffan, R., Bowen, S.M., Magolda, R., Matelan, E., Unwalla, R., Basso, M., Clerin, V., Gardell, S.J., Nambi, P., et al. (2008). Indazole-based liver X receptor (LXR) modulators with maintained atherosclerotic lesion reduction activity but diminished stimulation of hepatic triglyceride synthesis. J. Med. Chem. *51*, 7161–7168.

Chapter 3

LXR-623 Induces GBM Cell Death through LXRβ and Cholesterol Depletion

INTRODUCTION

Mutations in components of signal-transduction pathways are a hallmark of many cancers, including in those that arise from or metastasize to the brain (Ciriello et al., 2013; Kandoth et al., 2013). Glioblastoma (GBM) bulk tumor and single cell sequencing efforts have revealed a landscape of mutations that promote growth factor receptor signaling, with PI3K pathway-activating genetic lesions occurring in nearly 90% of patients as a consequence of amplifications or mutations in receptor tyrosine kinases (RTKs), activating mutations in the downstream effector PIK3CA, and loss of the negative regulator PTEN (Brennan et al., 2013; Patel et al., 2014). Mutations in the epidermal growth factor receptor (EGFR) occur in nearly 60% of GBM patients and 25% of lung cancer and up to 40% of breast cancer patients harboring mutations in the EGFR family develop brain metastases (Bendell et al., 2003; Brennan et al., 2013; Clayton et al., 2004; Lin et al., 2009; Rangachari et al., 2015). Targeting the EGFR in brain cancer has remained elusive, due in part to incomplete tumor penetrance of available small molecule inhibitors (Vivanco et al., 2012).

The EGFR, as well as other RTKs that can promote PI3K signaling, activate the master transcriptional regulator of lipogenesis, Sterol Response Element Binding Protein 1 (SREBP1) (Guo et al., 2009). SREBP1 activation stimulates GBM growth by up-regulating expression of the low-density lipoprotein receptor (LDLR) to promote uptake of cholesterol into the cell (Guo et al., 2011), thus pointing toward LDL uptake as an alternative point of therapeutic intervention.

Originally identified as orphan receptors, the liver X receptors (LXRs) are members of the nuclear receptor (NR) superfamily of ligand-activated transcription factors (Calkin and Tontonoz, 2012) that function, in part, to maintain whole-body cholesterol homeostasis (Zhang

et al., 2012). At the cellular level, excess cholesterol is hydroxylated to form oxysterols, oxidized derivatives of cholesterol, which serve as endogenous ligands for LXR (Janowski et al., 1996). Oxysterol-mediated activation of LXRs, which form obligate heterodimers with the retinoid X receptors (RXRs), results in induction of ABCA1 and IDOL, to efflux and inhibit cholesterol uptake, respectively (Chen et al., 2013; Repa et al., 2000; Venkateswaran et al., 2000; Zelcer et al., 2009).

Drug development of LXR agonists has been an intense subject of study, primarily for treatment of dyslipidemia and more recently for use as cancer therapeutics. However, LXR ligands may have tissue-specific activity (Figure 2-2) and potential mechanistic diversity across cancer types (Lin and Gustafsson, 2015), thus requiring a deep examination of the spectrum of activity and mechanism of action of compounds with potential for clinical utilization. Here, we determine if EGFR mutations sensitize GBM cells to the brain-penetrant LXR ligand, LXR-623, assessing its spectrum of activity and mechanism of action in relevant preclinical models of GBM, including established and patient-derived GBM neurosphere cell lines. We further extend our study and assess LXR-623 antitumor activity in brain-derived secondary metastatic cancer cell lines.

RESULTS

LXR-623 induces cell death in established and patient-derived GBMs

We extended our analysis of LXR-623 effects to a panel of established GBM cell lines (Figure 3-1) and patient-derived GBM neurosphere cultures (Figure 3-2) and found that LXR-623 suppressed LDLR expression, increased expression of the ABCA1 efflux transporter, and induced substantial cell death in all of the GBM samples tested. The brain metastatic breast cancer cell line MDA-MB-361, which harbors human epidermal growth factor 2 (HER2)

amplification was sensitive to LXR-623 (Figure 3-3). The EGFR-mutated PC9 brain metastatic (BRM) lung cancer cell line (Nguyen et al., 2009) was similarly sensitive to LXR-623 (Figure 3-4), raising the possibility that the drug could also have activity against systemic cancers that metastasize to the brain.

LXR-623 Induces GBM cell death through activation of LXRβ

To determine whether LXR-623 promotes its effects on GBM cells through activation of LXR, we first examined the effect of LXR-623 on gene expression. Gene microarray analysis demonstrated upregulation of mRNAs encoding the ABCA1 cholesterol efflux transporter and the E3 ligase IDOL, which targets the LDLR for degradation (Figure 3-5). Further, gene set enrichment analysis (GSEA) revealed the anticipated transcriptional effects on lipid metabolism that are characteristic of LXR activation (Figure 3-5). In contrast to GW3965, which induced ApoE-mediated suppression of metastasis in melanoma (Pencheva et al., 2014), we did not observe induction of APOE expression in GBM cells or NHA treated with LXR-623 (Figure 3-5), indicating an ApoE-independent mechanism. Validation of our microarray results via qPCR and immunoblotting revealed concentration-dependent increases in ABCA1 and IDOL expression, and enhanced LDLR degradation (Figures 3-6). Although LXR forms a heterodimer with RXRs, which are expressed in patient GBM samples (Figure 3-7A), treatment of U87EGFRvIII cells with the RXR agonist bexarotene did not induce cell death or LXR-target gene expression, despite inducing RXR-target gene expression (Figures 3-7B-D). This suggests a specific role for LXR activation in LXR-623 induced cell death.

The two LXR isotypes – LXRα and LXRβ – display different tissue distributions and have been shown to vary among some tumor types, but their relative expression in many cancers, including

glioblastoma, remains, to date, unknown (Lin and Gustafsson, 2015). We found that LXRβ expression was nearly eightfold greater than LXRα in U87EGFRvIII cells and nearly fourfold greater in the patient-derived GBM39 neurosphere culture (Figure 3-8A). Analysis of the TCGA dataset similarly showed that LXRβ is the predominant LXR isotype in GBM (Figure 3-8B) and that its expression is unaffected by EGFR mutational status (Figure 3-8C).

To determine whether LXR-623 mediates its effects in GBM through LXRβ, we knocked down both LXRs by RNA-interference and assessed the impact on LXR-623 biochemical and functional responses. siRNA-mediated knockdown of LXRβ, but not LXRα, in GBM cells inhibited the upregulation of ABCA1 expression, limited degradation of LDLR, and prevented cell death in response to LXR-623 (Figure 3-9A-C). Further, the LXR inverse agonist SR9243, which has been shown to promote tumor cell death in prostate, colon, and lung cancer models (Flaveny et al., 2015), failed to cause GBM cell death despite robust inhibition of LXR target genes (Figures 3-9D-E). These results show that LXR-623 promotes its anti-tumor activity in GBM specifically by activating LXRβ.

Depletion of cholesterol drives LXR-623-induced killing of GBM cells

Our finding that LXRβ activation suppressed LDLR and induced expression of the ABCA1 efflux transporter, concomitant with promotion of tumor cell death, raised the possibility that LXR-623 kills GBM cells by reducing cellular cholesterol. To test this idea, we measured the effect of LXR-623 on LDL uptake and cholesterol efflux. LXR-623 inhibited LDL uptake and induced cholesterol efflux in GBM cells ($p < 0.001$ for each) (Figure 3-10), resulting in a significant reduction in cellular cholesterol content (Figure 3-11).

We have described a chemical proteomic assay that uses a photoreactive, clickable, sterol-based probe to survey cholesterol-binding proteins in human cells (Hulce et al., 2013). Using this methodology, we found that LXR-623 induced a concentration-dependent increase in sterol probe binding to proteins in U87EGFRvIII cells (Figures 3-11). Because the sterol probe competes with endogenous cholesterol for interaction with cholesterol-binding proteins (Hulce et al., 2013), these results provide further evidence that LXR-623 depletes intracellular cholesterol and by doing so, enhances sterol probe-protein interactions in GBM cells.

We reasoned that if LXR-623 kills GBM by depleting cholesterol, the addition of exogenous cholesterol should prevent LXR-623-induced cell death. Consistent with this hypothesis, adding cholesterol to cultures fully rescued LXR-623-induced cell death in both established and patient-derived GBM cell lines (Figure 3-12A). Cholesterol repletion did not affect LDLR or ABCA1 levels (Figure 3-12B-C), indicating that the rescue effect of cholesterol was not mediated by altering LXR-623 activity. Further, exposure to methyl-β-cyclodextrin (MβCD), a chemical means of decreasing cellular cholesterol levels (Caliceti et al., 2012; Christian et al., 1997), also caused GBM cell death, an effect that was considerably greater in GBM cells than NHAs (Figures 3-12D-E). Taken together, these results demonstrate that GBM cells have an enhanced reliance on cholesterol for survival and that LXR-623 induces GBM cell death by depleting cellular cholesterol.

A

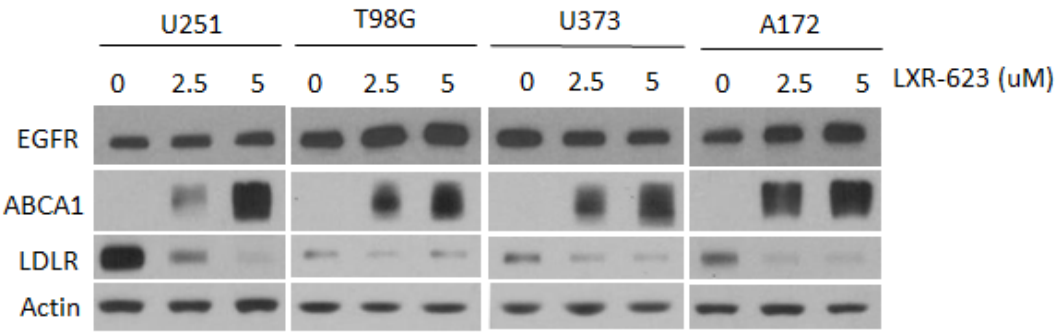
U251
T98G
U373
A172
0 2.5 5 0 2.5 5 0 2.5 5 0 2.5 5
LXR-623 (uM)
EGFR
ABCA1
LDLR
Actin

B

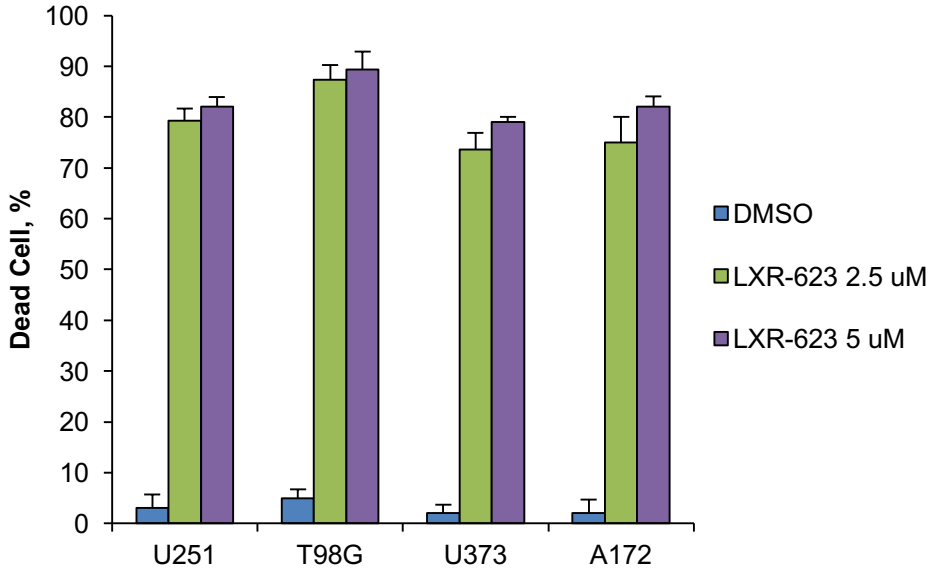
Dead Cell, %
100
90
80
70
60
50
40
30
20
10
0
U251
T98G
U373
A172
DMSO
LXR-623 2.5 uM
LXR-623 5 uM

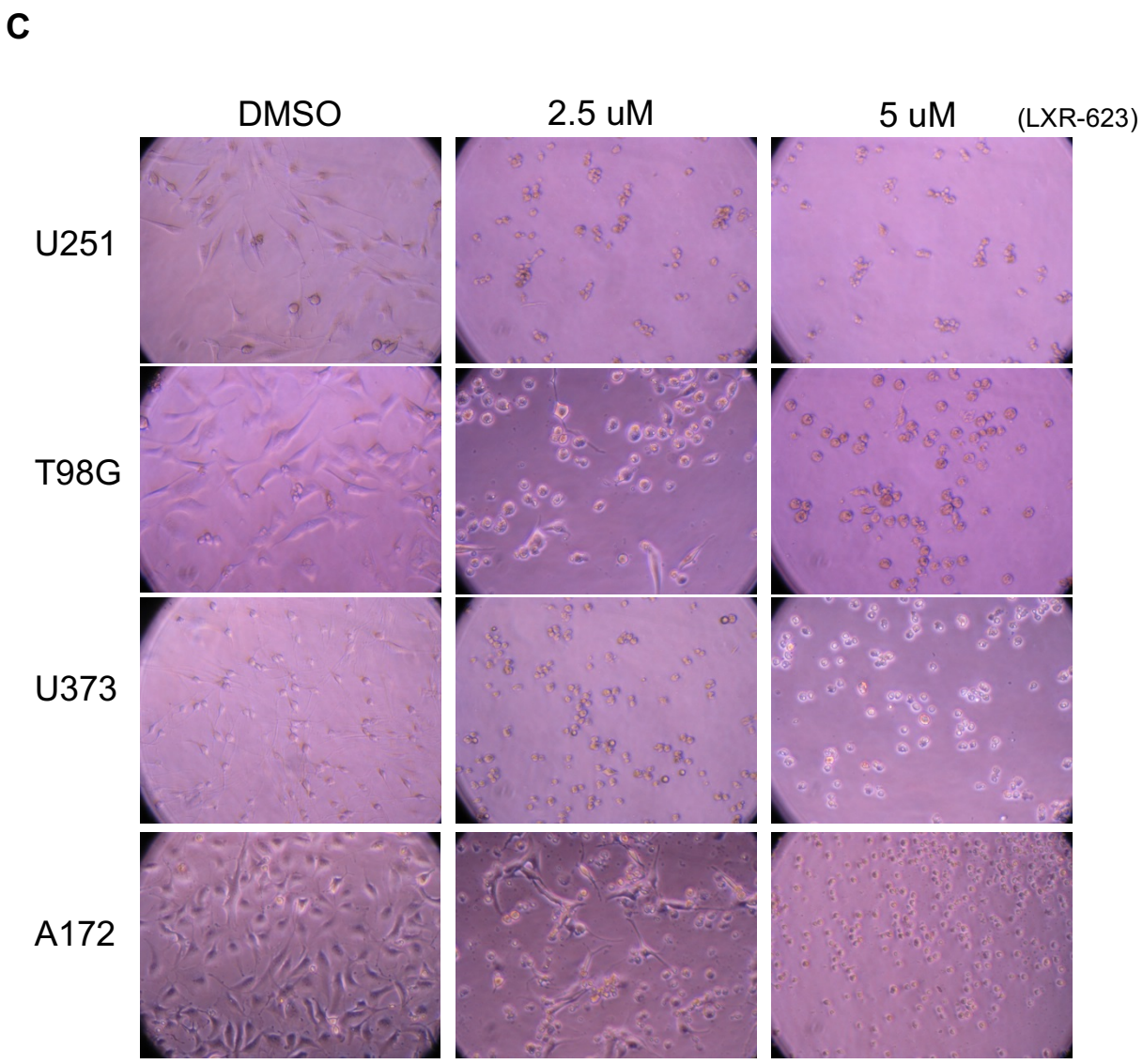

Figure 3-1. **LXR-623 induces cell death in established GBM cell lines**. (**A**) Established GBM cell lines were treated with the indicated concentration of LXR-623 for 48 hours and immunoblotting was performed with the indicated antibodies. (**B**) Trypan blue exclusion assay was carried out in parallel to (A) after three days of LXR-623 treatment. (**C**) Representative images from each treatment condition presented in (**B**).

A

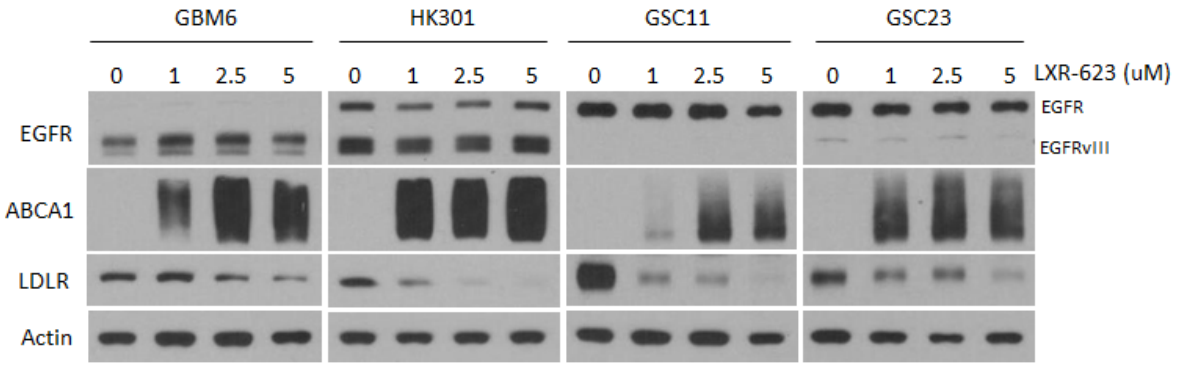
GBM6
HK301
GSC11
GSC23
0 1 2.5 5 0 1 2.5 5 0 1 2.5 5 0 1 2.5 5
LXR-623 (uM)
EGFR
EGFRvIII
ABCA1
LDLR
Actin

B

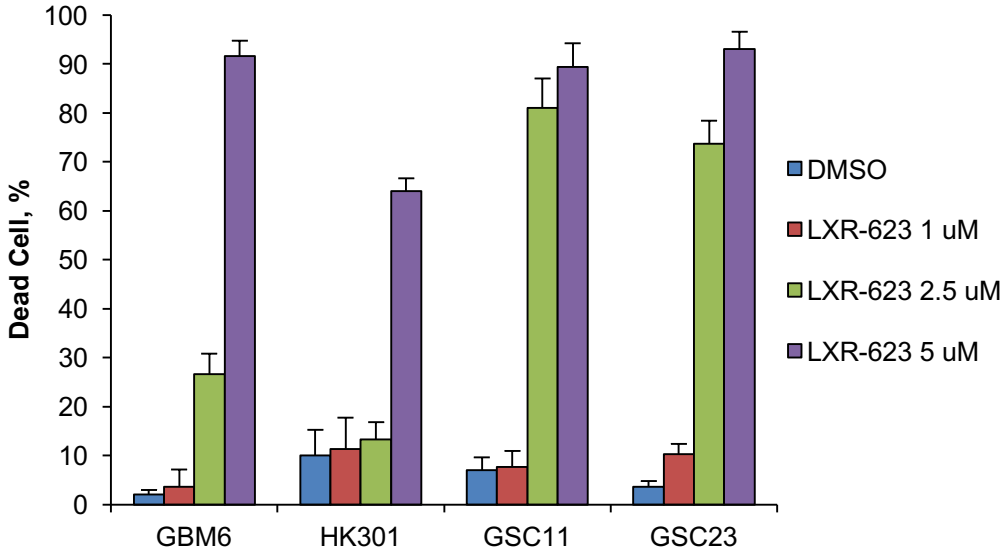
Dead Cell, %
100
90
80
70
60
50
40
30
20
10
0
GBM6
HK301
GSC11
GSC23
DMSO
LXR-623 1 uM
LXR-623 2.5 uM
LXR-623 5 uM

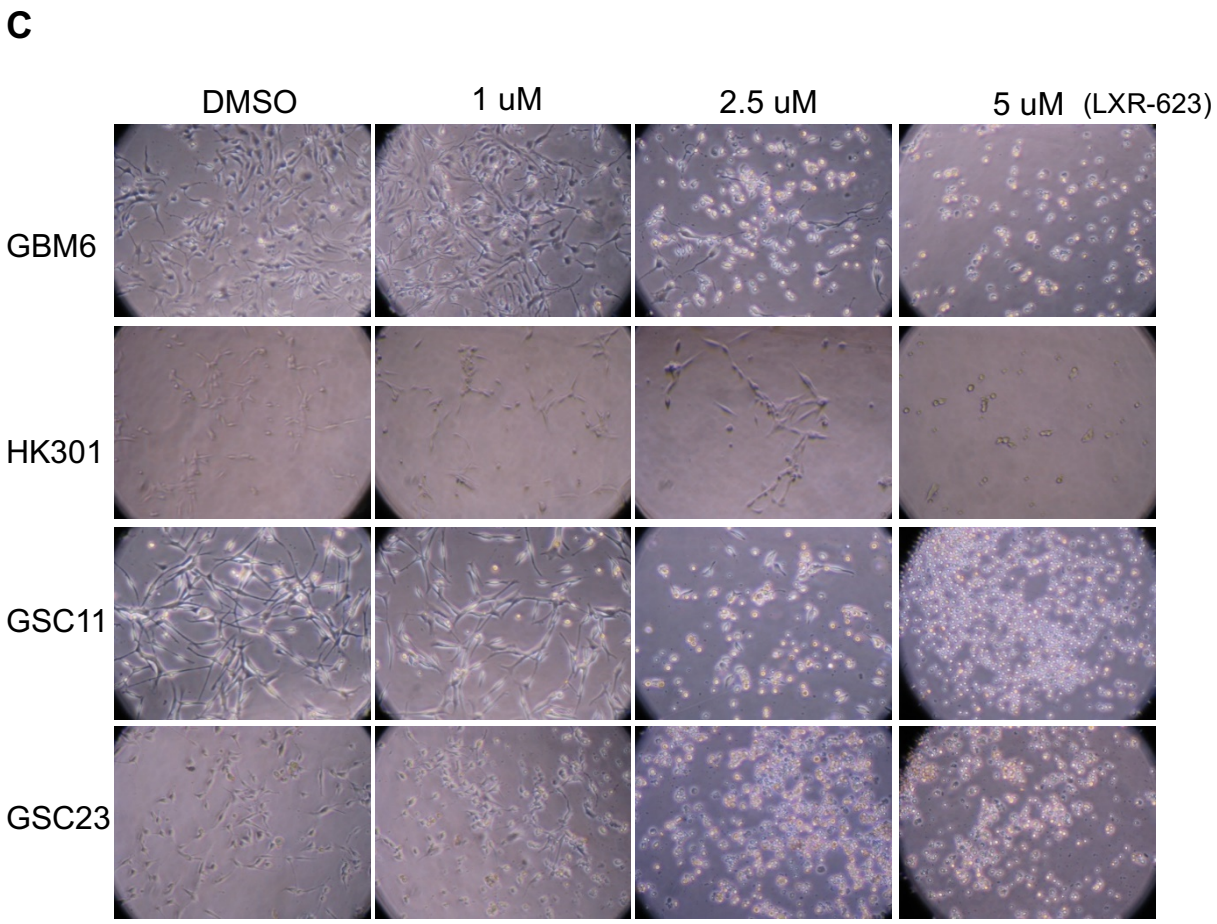

Figure 3-2. **LXR-623 induces cell death in patient-derived neurosphere GBM cell lines**. (**A**) Patient-derived neurosphere GBM cell lines were treated with the indicated concentration of LXR-623 for 48 hours and immunoblotting was performed with the indicated antibodies. (**B**) Trypan blue exclusion assay was carried out in parallel to (A) after five days of LXR-623 treatment. (**C**) Representative images from each treatment condition presented in (**B**).

A

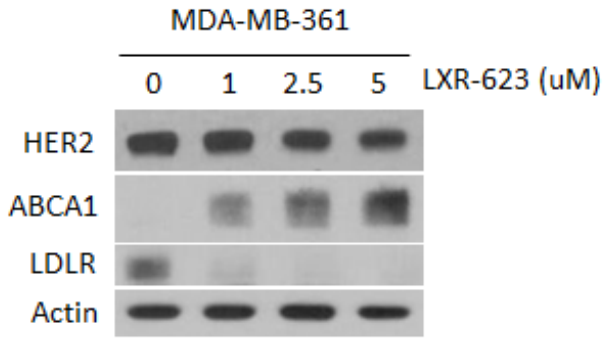

B

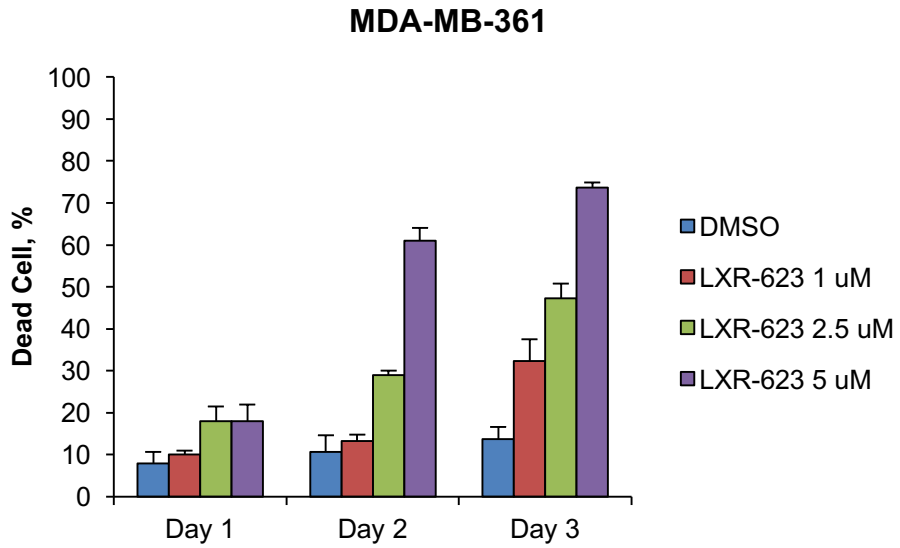

Figure 3-3. **LXR-623 induces cell death in an RTK-driven brain metastatic breast cancer cell line**. (A). MDA-MB361 brain metastatic breast cancer cells were treated with the indicated concentration of LXR-623 for 24 hours and immunoblotting was performed with the indicated antibodies. (B) MDA-MB-361 cells were treated with indicated concentrations of LXR-623 and cell death was assessed over three days via trypan blue exclusion assay.

A

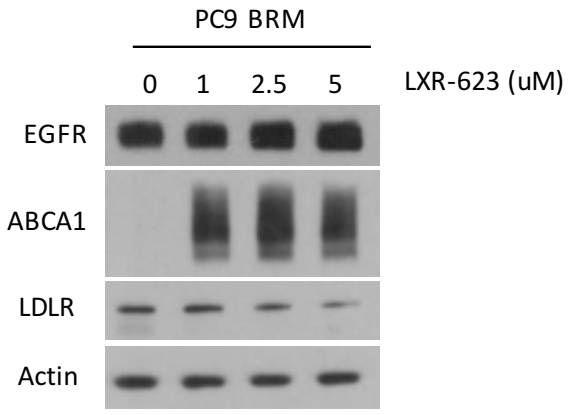

B

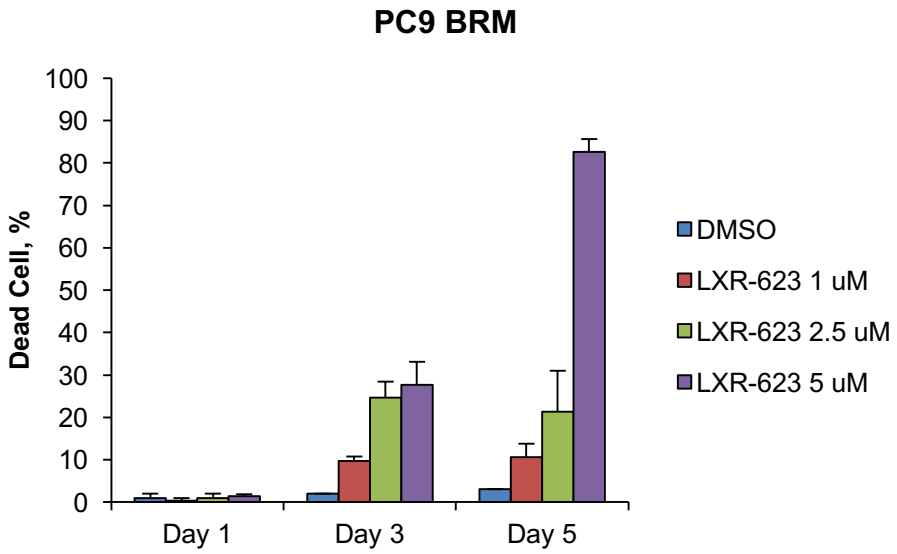

Figure 3-4. **LXR-623 induces cell death in an RTK-driven brain metastatic lung cancer cell line**. (A). PC9 brain metastatic (BRM) lung adenocarcinoma cancer cells were treated with the indicated concentration of LXR-623 for 48 hours and immunoblotting was performed with the indicated antibodies. (B) PC9 BRM cells were treated with indicated concentrations of LXR-623 and cell death was assessed over five days via trypan blue exclusion assay.

A

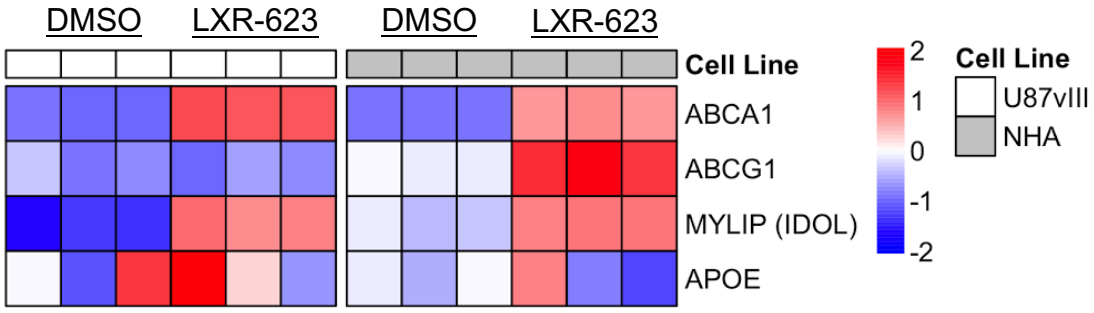

B

GO Term Biological Process	NES	NOM p-val	FDR q-val
LIPID METABOLIC PROCESS	3.12	<.001	<.001
PHOSPHOLIPID BIOSYNTHETIC PROCESS	2.85	<.001	.002
CELLULAR LIPID METABOLIC PROCESS	2.79	<.001	.001
MEMBRANE LIPID BIOSYNTHETIC PROCESS	2.74	<.001	.001
MEMBRANE LIPID METABOLIC PROCESS	2.57	<.001	.005
LIPID BIOSYNTHETIC PROCESS	2.49	<.001	.008

Figure 3-5. **LXR-623 induces characteristic LXR target genes**. (**A**) Microarray analysis of LXR target genes in U87EGFRvIII and NHA cells treated with LXR-623 5 uM for 24 h. Triplicates are shown. (**B**) Gene Set Enrichment Analysis (GSEA) for Gene Ontology (GO) pathways for microarray data in **(A)**.

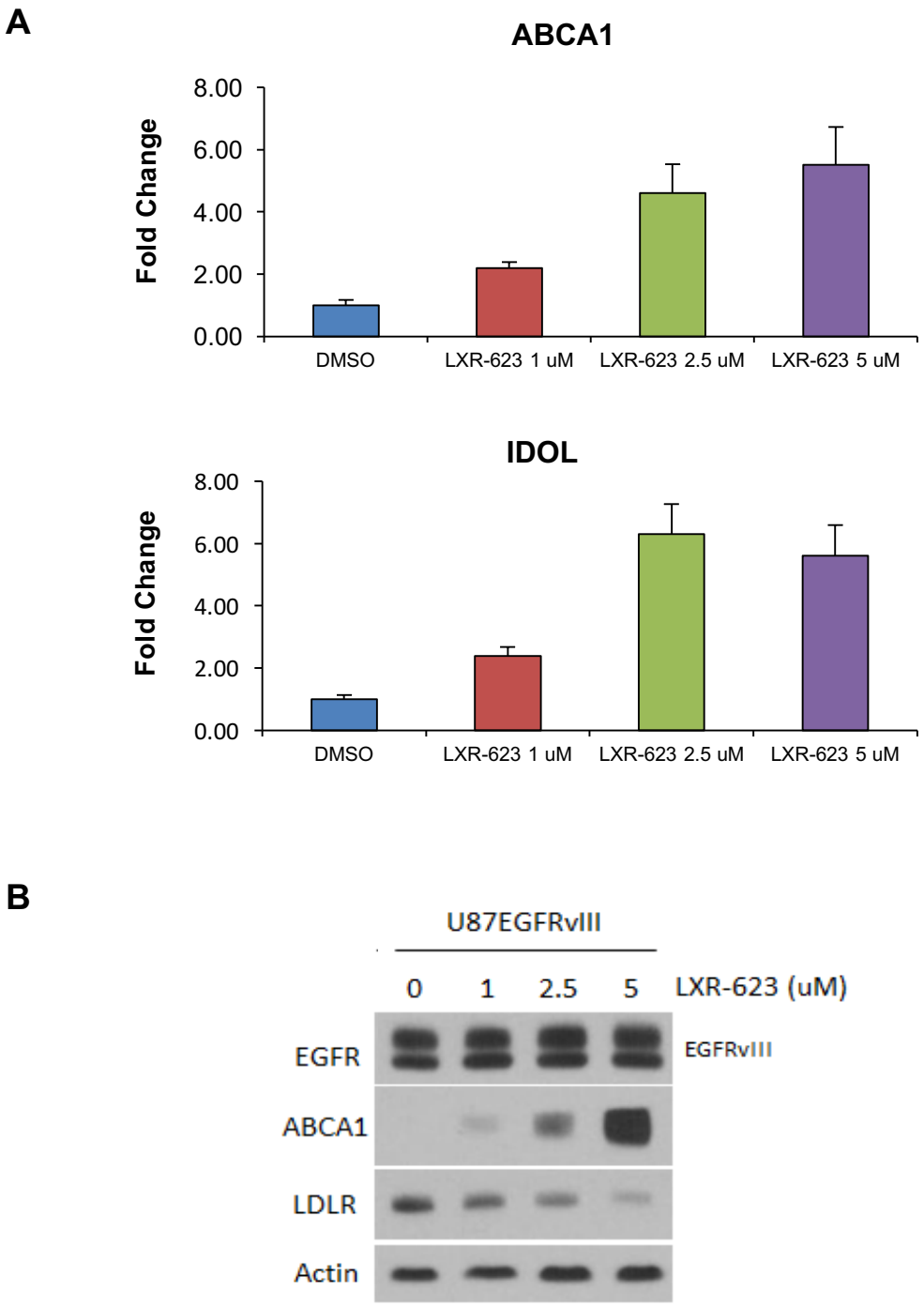

Figure 3-6. **LXR-623 induces ABCA1 and IDOL in U87EGFRvIII GBM cells.** (**A**) U87EGFRvIII cells were treated with LXR-623 for 48 h and qPCR was performed for LXR target genes. (**B**) U87EGFRvIII cells were treated as in (**A**) and immunoblotting was performed with the indicated antibodies.

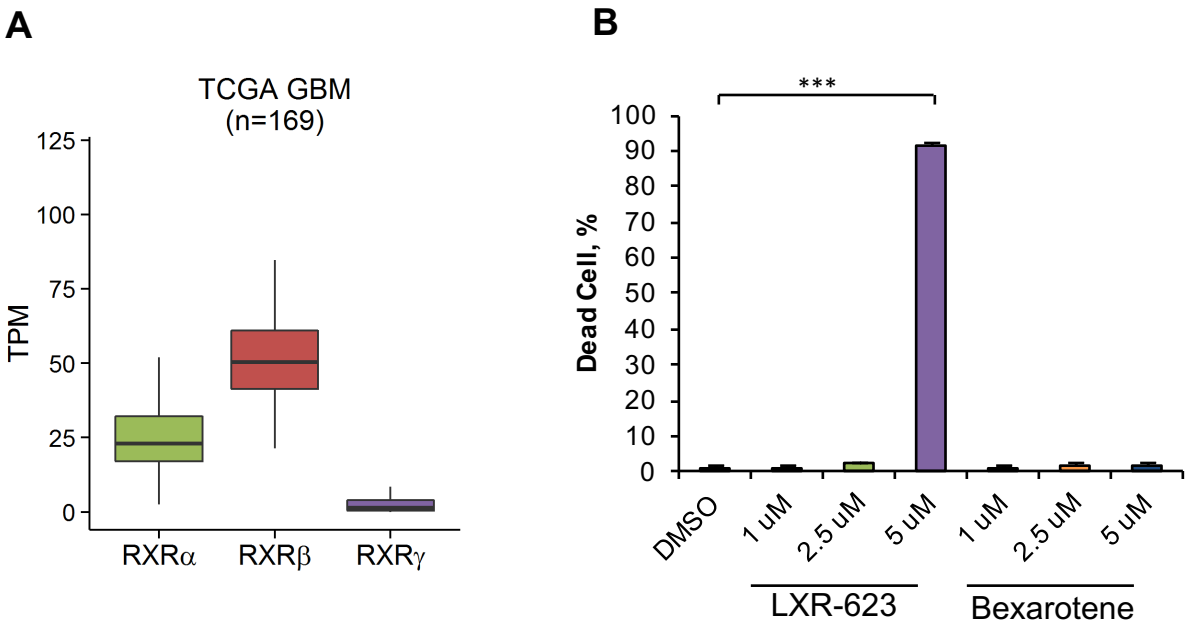
A
TCGA GBM
(n=169)
TPM
125
100
75
50
25
0
RXRα
RXRβ
RXRγ
B
***
Dead Cell, %
100
90
80
70
60
50
40
30
20
10
0
DMSO
1 uM
2.5 uM
5 uM
1 uM
2.5 uM
5 uM
LXR-623
Bexarotene

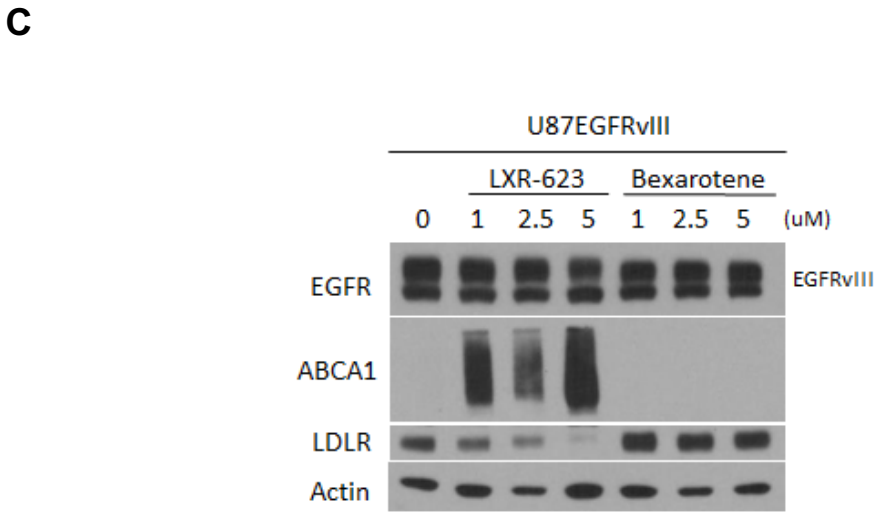
C
U87EGFRvIII
LXR-623
Bexarotene
0
1
2.5
5
1
2.5
5
(uM)
EGFR
EGFRvIII
ABCA1
LDLR
Actin

D

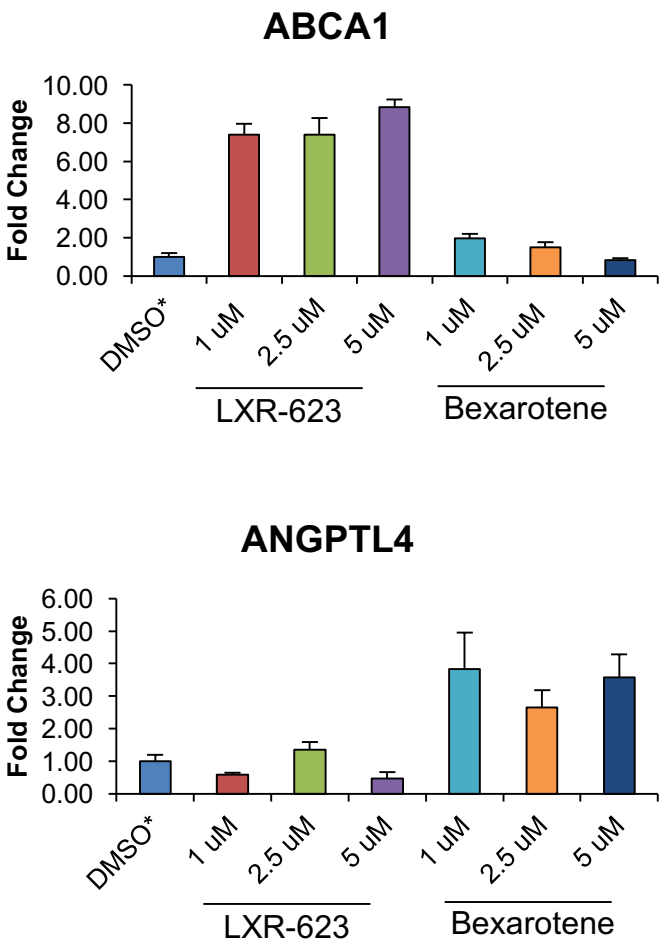

Figure 3-7. **RXR agonism does not induce GBM cell death**. (**A**) GBM TCGA RNA-seq data indicating the relative expression of retinoid x receptor (RXR) subtypes. (**B**) U87EGFRvIII cells were treated with the indicated concentrations of LXR-623 or the RXR agonist Bexarotene. Cell death was assessed via trypan blue exclusion assay on day three of treatment. (**C**) Immunoblotting of U87EGFRvIII cells treated with LXR-623 or Bexarotene treated for 48 hr. (**D**) qPCR of U87EGFRvIII cells treated as in (**C**) for the LXR target gene ABCA1 and the RXR target gene ANGPTL4. ***$p < 0.001$

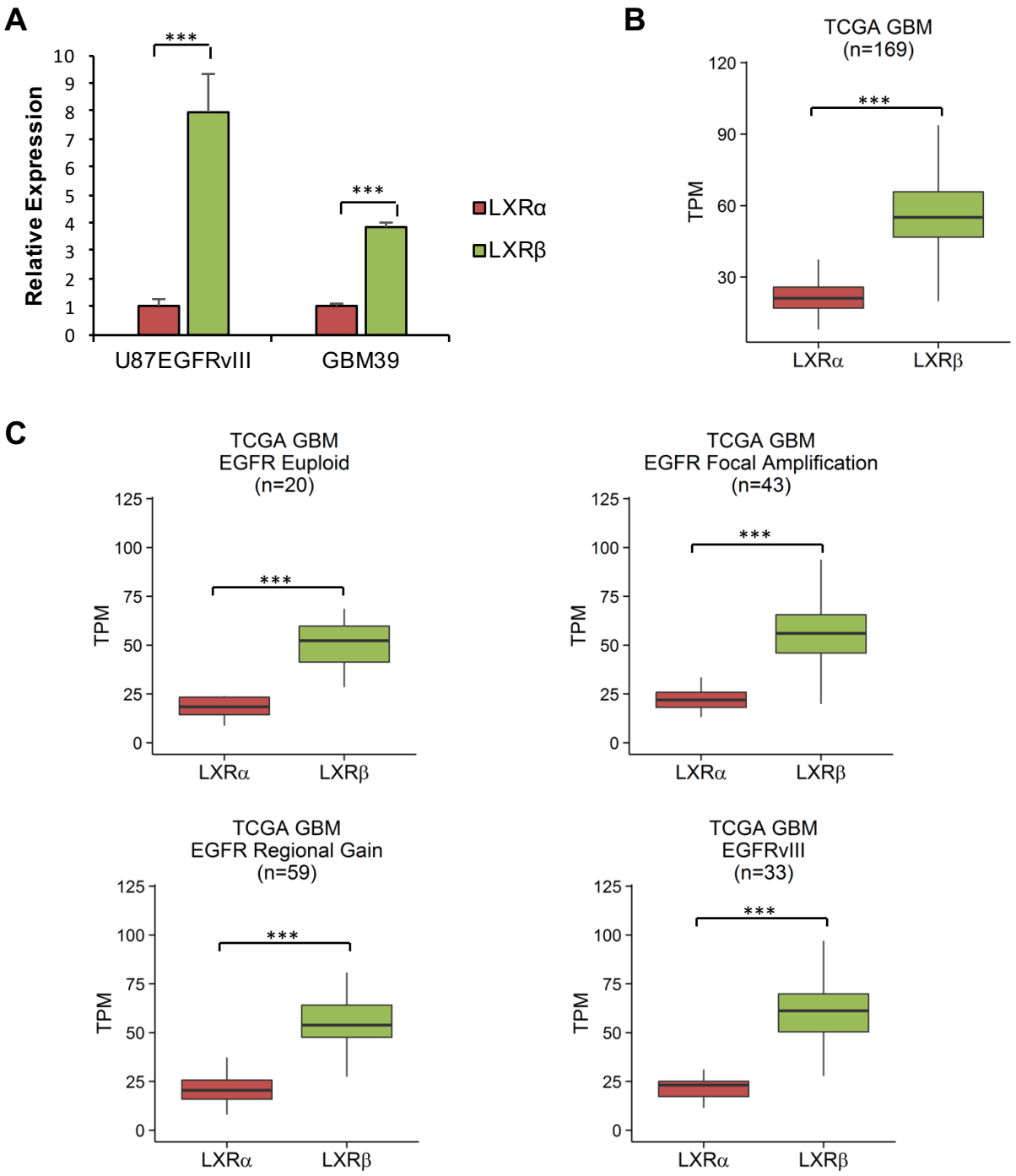

Figure 3-8. **LXRβ is the predominant LXR subtype in GBM**. (**A**) RNA was extracted from U87EGFRvIII and GBM39. qPCR was performed for LXRα and LXRβ. (**B**) TCGA RNASeq data from patients with GBM for LXRα and LXRβ. (**C**) GBM TCGA RNASeq data were separated by EGFR status and relative levels of LXRα and LXRβ were assessed. ***$p < 0.001$

A

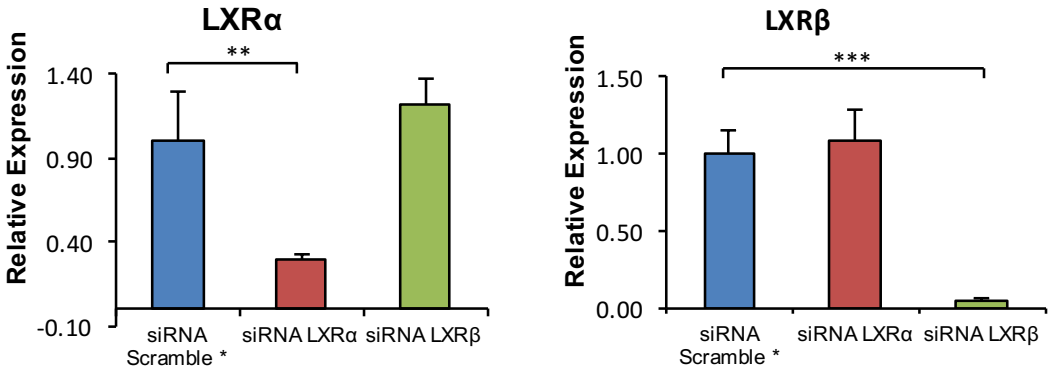
LXRα
**
Relative Expression
1.40
0.90
0.40
-0.10
siRNA Scramble *
siRNA LXRα
siRNA LXRβ
LXRβ
***
Relative Expression
1.50
1.00
0.50
0.00
siRNA Scramble *
siRNA LXRα
siRNA LXRβ

B

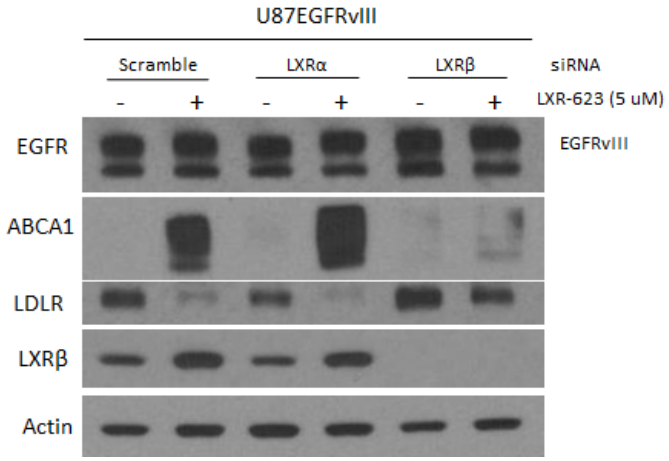
U87EGFRvIII
Scramble
LXRα
LXRβ
siRNA
- + - + - +
LXR-623 (5 uM)
EGFR
EGFRvIII
ABCA1
LDLR
LXRβ
Actin

C

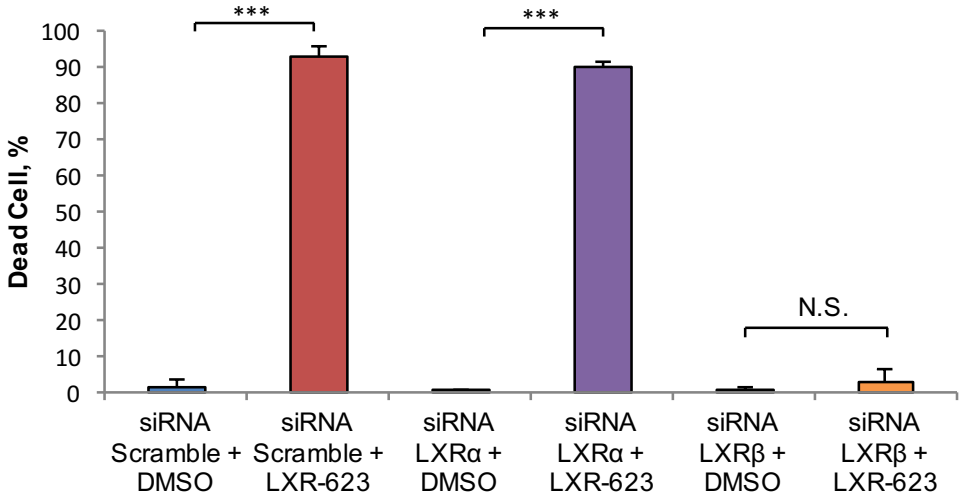
***
***
N.S.
Dead Cell, %
100
90
80
70
60
50
40
30
20
10
0
siRNA Scramble + DMSO
siRNA Scramble + LXR-623
siRNA LXRα + DMSO
siRNA LXRα + LXR-623
siRNA LXRβ + DMSO
siRNA LXRβ + LXR-623

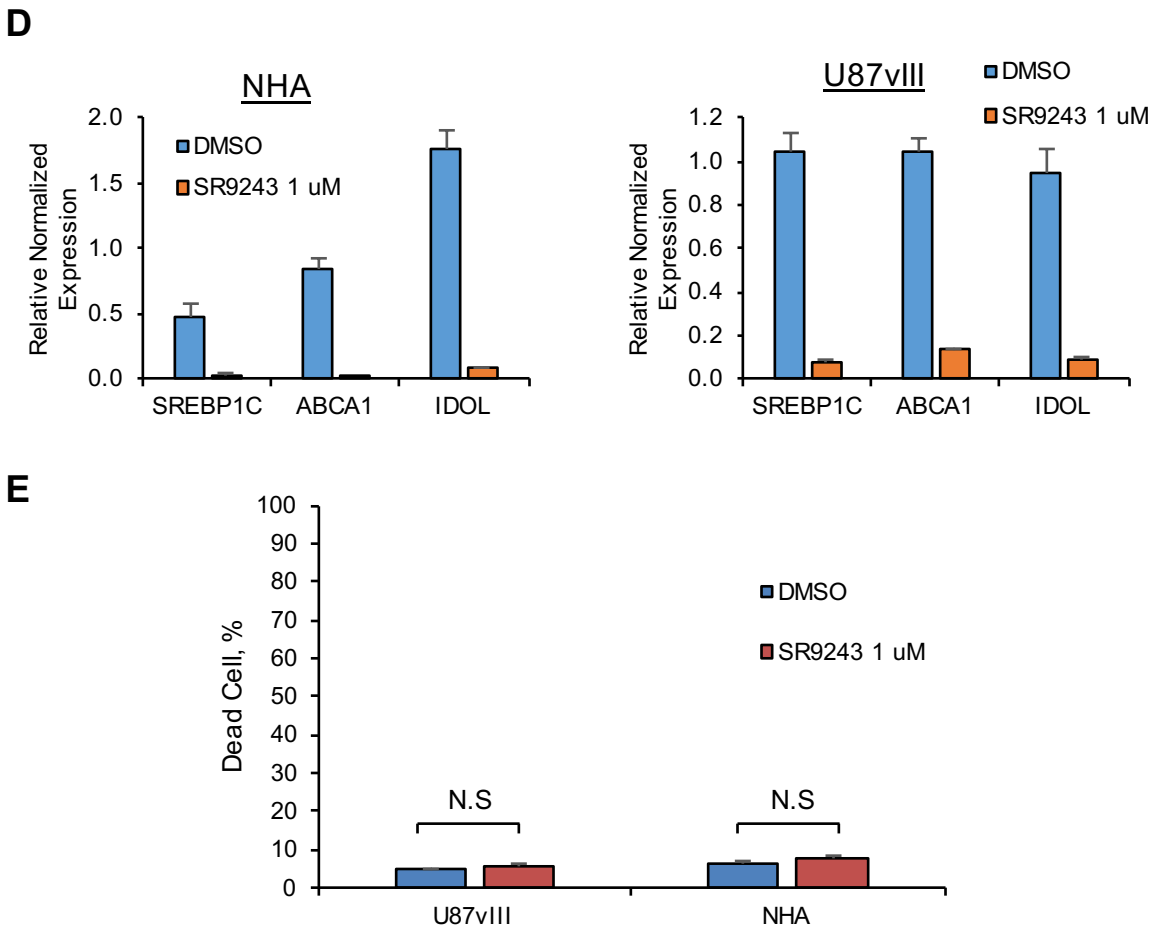

Figure 3-9. **LXR-623 induces GBM cell death through activation of LXRβ**. (**A**) U87EGFRvIII cells were transfected with siRNA targeting LXRα or LXRβ. After 48 hr RNA was extracted and qPCR was performed. *Gene expression was normalized for scramble control. (**B**) Cells were transfected with siRNA as in (**A**) and treated with LXR-623 for 24 hr. Immunoblotting was performed with the indicated antibodies. (**C**) U87EGFRvIII cells were transfected with siRNA and treated with LXR-623. Trypan blue exclusion assay was performed after three days of treatment. (**D**) NHA and U87vIII were treated with the inverse LXR agonist, SR9243, for 24 hr after which RNA was collected and qPCR was performed. (**E**) Cell death assessment of NHA and U87vIII treated with SR9243 for 24 hr.* *$p < 0.05$; **$p < 0.01$; ***$p < 0.001$; N.S. = not significant.

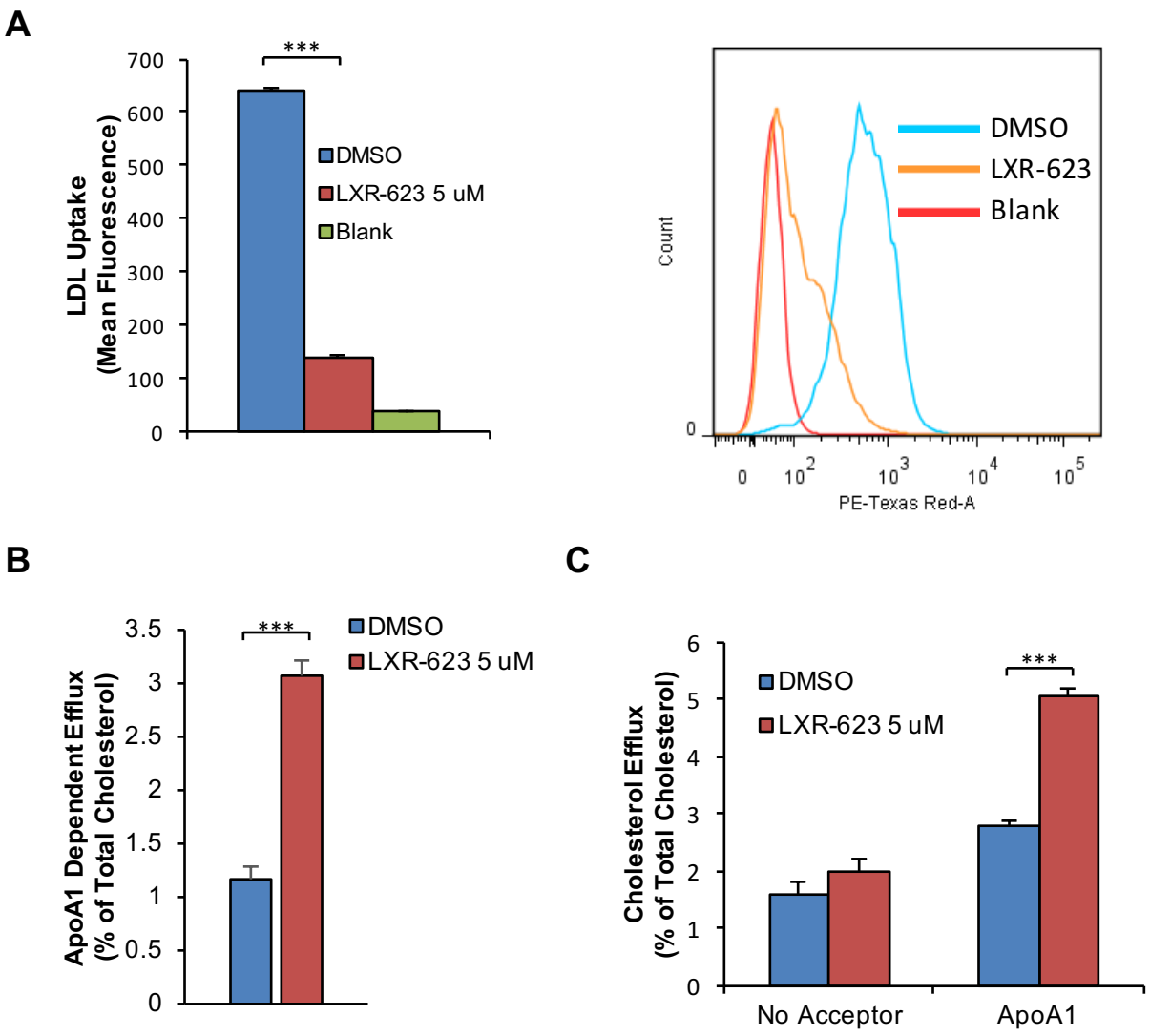

Figure 3-10. **LXR-623 inhibits uptake and induces efflux of cholesterol**. (**A**) U87EGFRvIII cells were treated with LXR-623 for a total of 48 hr. Cells were incubated with fluorescently labeled LDL for four hours and LDL uptake was quantified (left panel) via flow cytometry (right panel. (**B**) U87EGFRvIII cells were loaded with 3H-cholesterol and treated with LXR-623 5 uM. Cholesterol efflux was determined by scintillation counting. (**C**) Data from (**B**) reorganized to show differences between no acceptor and ApoA1. *$p < 0.05$; **$p < 0.01$; ***$p < 0.001$.

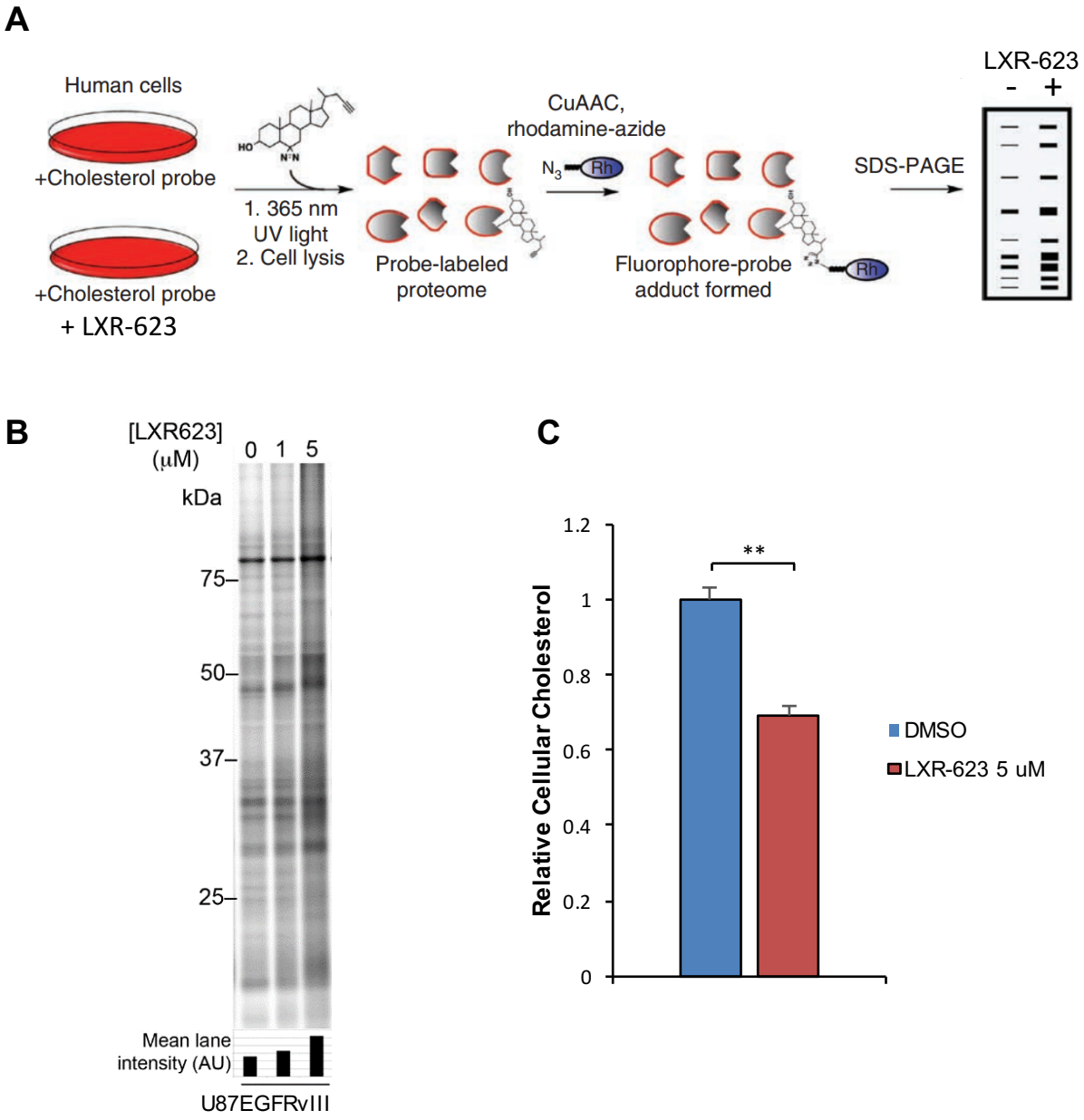

Figure 3-11. **LXR-623 depletes GBM cells of cholesterol**. (**A**) Scheme for treatment of live cells with sterol probes and LXR-623 treatment (Hulce et al., 2013). (**B**) Sterol probe labeling profile (10 μM probe, 30 min) of U87vIII cells pre-treated with DMSO or the indicated concentrations of LXR-623 for 48 hr. (**C**) U87EGFRvIII cells were treated for 48 hr with LXR-623 5 uM and total cholesterol levels were assessed by LC/MS. **$p < 0.01$.

A

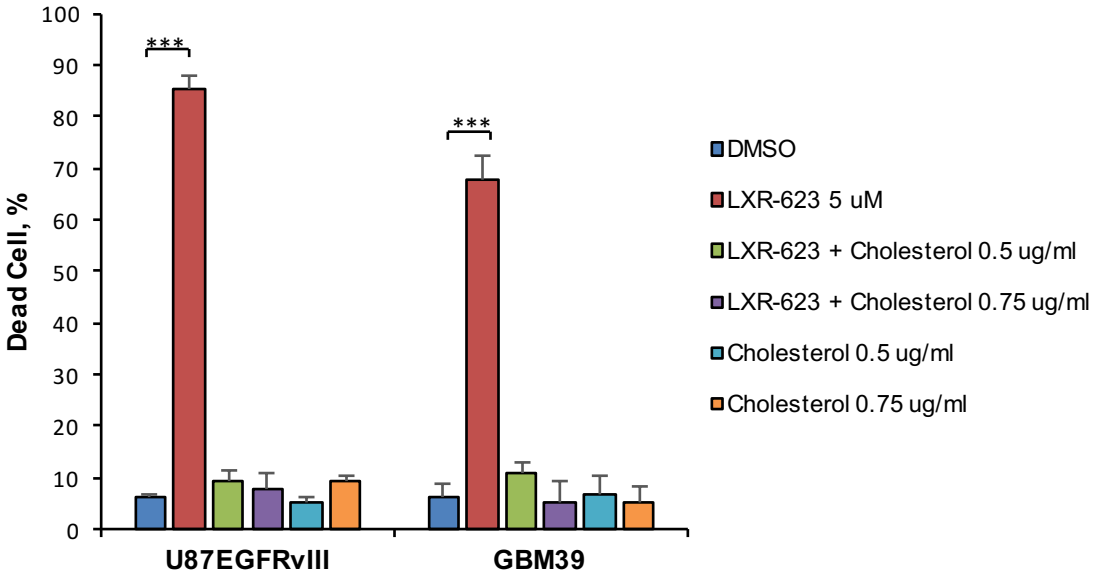
100
90
80
70
60
50
40
30
20
10
0
Dead Cell, %
***
***
U87EGFRvIII
GBM39
DMSO
LXR-623 5 uM
LXR-623 + Cholesterol 0.5 ug/ml
LXR-623 + Cholesterol 0.75 ug/ml
Cholesterol 0.5 ug/ml
Cholesterol 0.75 ug/ml

B

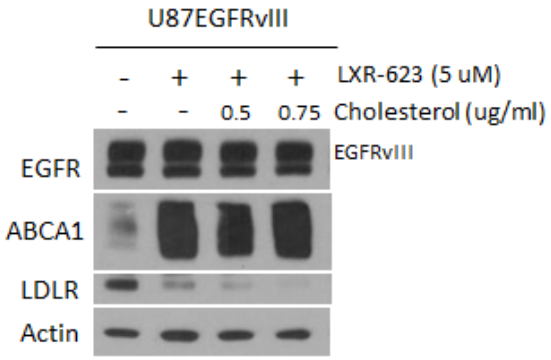
U87EGFRvIII
- + + + LXR-623 (5 uM)
- - 0.5 0.75 Cholesterol (ug/ml)
EGFR
EGFRvIII
ABCA1
LDLR
Actin

C

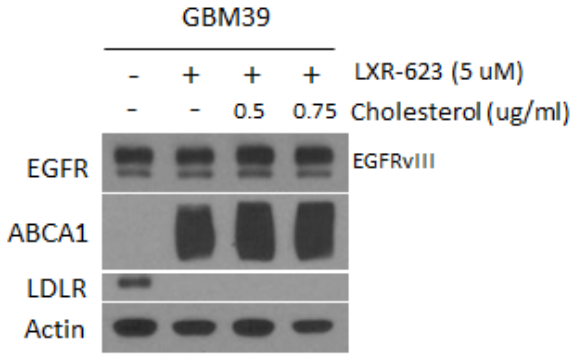
GBM39
- + + + LXR-623 (5 uM)
- - 0.5 0.75 Cholesterol (ug/ml)
EGFR
EGFRvIII
ABCA1
LDLR
Actin

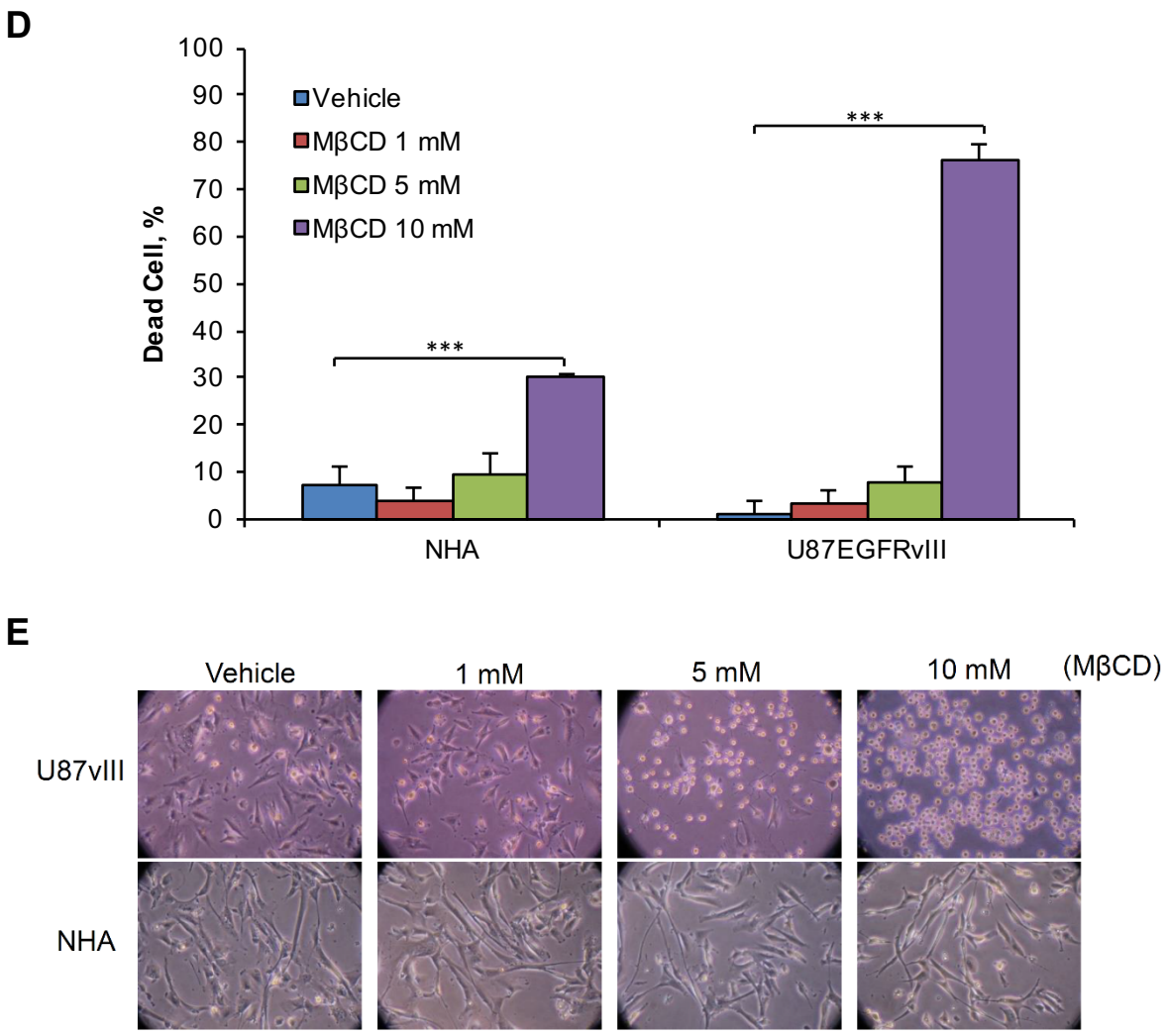

Figure 3-12. **LXR-623 kills GBM cells through cholesterol depletion**. (**A**) U87EGFRvIII and GBM39 cells were treated with LXR-623 in the presence or absence of methyl-β-cyclodextrin complexed to cholesterol at the indicated concentrations (final concentration of cholesterol is shown). Cell death was assessed via Annexin/PI staining on day three for U87vIII and via trypan blue staining on day five for GBM39. (**B**) U87EGFRvIII or (**C**) GBM39 were treated with LXR-623 for 48 hr in the presence or absence of MβCD-Cholesterol. Immunoblotting was performed with the indicated antibodies. (**D**) NHA and U87EGFRvIII were treated with the indicated concentrations of methyl-β-cyclodextrin (MβCD) for 1 hr and cell death was assessed by trypan blue exclusion assay (**E**) Representative images from (**D**). *$p < 0.05$; **$p < 0.01$; ***$p < 0.001$.

DISCUSSION

The anti-tumor activity of LXR modulators, a recent and intense subject of interest, has been described against melanoma, intestinal cancers, squamous cell cancers, prostate cancers, and breast cancers (Flaveny et al., 2015; Gabitova et al., 2015; Lin and Gustafsson, 2015; Lo Sasso et al., 2013; Nguyen-Vu et al., 2013; Pencheva et al., 2014; Pommier et al., 2013). However, a new, unanticipated, and important result from our studies is the critical role that tissue type and organ context seems to play in determining the activity of a specific LXR modulator. In peripheral melanomas, activation of LXRβ by GW3965 potently suppresses metastasis by transcriptional induction of tumoral and stromal ApoE (Pencheva et al., 2014). In the same study, however, GW3965 did not kill melanoma cells. In contrast, we show that LXR-623 kills GBM cells specifically by depleting them of cholesterol (3-12), independent of any effect on ApoE (Figure 3-5).

To further investigate the role of cholesterol, we examined the following three potential mechanisms by which depletion of cholesterol might alter tumor cell viability: 1) by regulating steroid biogenesis; 2) by activating endoplasmic reticulum (ER) stress and 3) by causing a rise in cellular reactive oxygen species (ROS).

First, cholesterol is the precursor of the five major classes of steroid hormones: progestagens, glucocorticoids, mineralocorticoids, androgens, and estrogens (Manna et al., 2016). Whether steroid hormones are critical in the etiology or pathogenesis of GBM is not well understood (Kabat et al., 2010). Given that LXR-623 depletes cellular cholesterol (Figures 3-10, 3-11), synthesis of steroid hormones may also be affected. Second, the lipogenic and cholesterol lowering activity of LXR agonists (Chu et al., 2006; Joseph et al., 2002) could perturb the

function of the ER, resulting programmed cell death (Borradaile et al., 2006). Third, LXR agonist-mediated modulation of lipid species requires NADPH, a key reducing agent in relatively short supply (Pavlova and Thompson, 2016), which may lead to a deficit in buffering ROS.

Preliminary studies examining each of the aforementioned potential mechanisms failed to define the process underlying GBM cell sensitivity to LXR-623 mediated cholesterol depletion (data not shown). Notably, our observation that LXR agonism does not induce ER stress is in agreement with recent literature (Rong et al., 2013). While a deeper assessment of each potential mechanism is warranted, investigation into other cholesterol regulated processes, such as membrane fluidity, may also expand our understanding of LXR-623 mediated cell death.

We also found that the LXR inverse agonist SR9243, which has activity against a variety of cancer cell lines through its ability to inhibit the Warburg effect (Flaveny et al., 2015), has no anti-tumor effect on GBM cells, despite robust LXR target gene inhibition (Figures 3-9D, 3-9E). Of course, differences in the transcriptional regulation/cofactor recruitment profiles of specific LXR modulators and the expression of LXR isoforms may contribute to the gamut of responses to LXR agonists and inverse agonists observed thus far in cancer models. Alternatively, it is also plausible that individual cancers respond differently to the same drugs as a consequence of the interplay between their specific genotype, metabolic state, and the tissue context to which they are exposed. Importantly, actionable metabolic co-dependencies are likely to be shaped both by specific tumor cell oncogenes that reprogram cellular metabolism and by the local biochemical environment to which the tumor cells must adapt their metabolic circuitry for growth and survival (Galluzzi et al., 2013). LXR-623 showed considerable activity against GBMs and

EGFR-driven brain metastases (Figures 3-1, 3-2, 3-3, 3-4), meriting investigation of its potential efficacy against these tumor cells in their native environment.

EXPERIMENTAL PROCEDURES

Antibodies and Reagents

Antibodies used include mouse anti-ABCA1 (Abcam, ab18180), rabbit anti-LDLR (Abcam, ab30532), rabbit anti-EGFR (Millipore, 06847MI), mouse anti-ACTIN (Sigma, A4700), rabbit anti-HER2 (Cell Signaling, 2165), mouse anti-LXRβ (Perseus Proteomics, PP-K8917-00), HRP-linked anti-rabbit IgG antibody (Cell Signaling, 7074), and HRP-linked anti-mouse IgG antibody (Cell Signaling, 7076). Reagents used include bexarotene (Sigma, SML0282), [^{3}H] cholesterol (PerkinElmer, NET139001MC), acyl-CoA:cholestrol O-acyltransferase inhibitor (Sigma, Sandoz 58-035), fatty acid free bovine serum albumin (BSA) (Sigma, A8806), ApoA-I (Meridian life science, A95120H), methyl-β-cyclodextrin (Sigma, M7439), and cholesterol–methyl-β-cyclodextrin (Sigma, C4951). LXR-623 and SR9243 were synthesized by Sundia MediTech (Shanghai, China).

Cell Culture

The U87EGFRvIII isogenic GBM cell line was obtained as described previously (Wang et al., 2006). U87EGFRvIII, U251, T98, U373 and A172 GBM cell lines were cultured in Dulbecco's Modified Eagle Media (DMEM, Cellgro), and PC9 BRM cells were cultured in RPMI1640 (Gibco), supplemented with 10% fetal bovine serum (FBS, Hyclone) and 1% penicillin/streptomycin/glutamine (Invitrogen) in a humidified 5% CO2 incubator at 37°C. MDA-MB-361 cells were cultured in Leibovitz's L-15 media (Cellgro) supplemented with 20% FBS in a humidified 0% CO2 incubator at 37°C. Normal human astrocytes were purchased from Lonza and cultured per manufacturer's guidelines. GBM39, GBM6, HK301, GSC11, and GSC23

were cultured in Neurocult media (Stemcell Technologies) supplemented with EGF (Sigma), FGF (Sigma) and heparin (Sigma) in a humidified 5% CO2 incubator at 37°C.

Western Blotting

Cultured cells were lysed and homogenized with RIPA lysis buffer from Boston BioProducts (50mM Tris-HCl, 150mM NaCl, 1% NP-40, 0.5% Sodium deoxycholate, 0.1% SDS) supplemented with protease and phosphatase inhibitor cocktail (Thermo Scientific). Protein concentration of each sample was determined by BCA assay using the BCA kit (Pierce) per manufacturer's instructions. Equal amounts of protein extracts were separated by electrophoresis on 4-12% NuPAGE Bis-Tris Mini Gel (Invitrogen), and then transferred to a nitrocellulose membrane (GE Healthcare) with XCell II Blot Module (Invitrogen). The membrane was probed with various primary antibodies, followed by secondary antibodies conjugated to horseradish peroxidase. The immunoreactivity was detected with Super Signal West Pico Chemiluminescent Substrate or Super Signal West Femto Kit (Thermo Scientific).

Real-Time RT-PCR

Total RNA was extracted by using the RNeasy Plus Mini Kit (QIAGEN). First-strand cDNA was synthesized using the using the SuperScript VILO cDNA synthesis kit (Invitrogen). Real-time RT-PCR was performed using the iQ SYBR Green Supermix (Bio-Rad) on the the CFX96 Touch Real Time PCR Detection system (Bio-Rad) following the manufacturer's instructions. Results were normalized to the GAPDH reference gene for *in vitro* studies. Primer sequences are available upon request.

Microarray Analysis

Total RNA was isolated in triplicate for each condition using the RNeasy Plus Mini Kit (QIAGEN). Primeview affymetrix arrays were obtained from Affymetrix, and labeled samples were hybridized and scanned, and gene expression was analyzed in the UCSD VA/VMRF Microarray and NGS Core. The data were robust multiarray average (RMA) normalized in R using the "affy" package.

TCGA Data Analysis

Processed TCGA data were downloaded through the TCGA data portal. The EGFR status of TCGA GBM samples are designated as euploid, regionally amplified, focally amplified, or EGFRvIII based on annotations previously published (Brennan et al., 2013). Specifically, EGFRvIII samples are samples with non-zero Δ2–7 values, and euploid / regionally amplified / focally amplified samples are non-EGFRvIII samples labeled as “Euploid” / “Regional gain” / “Focal Amplification.”

Cell Viability Assay

Cells were seeded in triplicate for each condition in 24-well culture plates at 10,000 cells per well. DMSO or LXR-623 was added to cells in DMEM media containing 0.5%-1% FBS for established cell lines or Neurocult media without supplement for patient derived neurosphere lines. Total and live cells in each well were quantified by Trypan blue (Gibco) assay using a TC10 automatic cell counter (Bio-Rad).

Apoptosis Assay

Cells were seeded at a density of 80,000-100,000 in each well of 6-well plate. The following day, DMSO or LXR-623 was added to cells in DMEM media containing 0.5%-1% FBS or Neurocult media without supplement. Annexin V/Propidium Iodide (PI) staining was carried out using the FITC Annexin V Apoptosis Detection Kit II (BD Biosciences). Flow cytometry was performed using the BD LSR II Flow Cytometer System (BD Biosciences). Data analyses were performed using FlowJo.

LDL Uptake

For FACS analysis, cells were seeded at a density of 80,000-100,000 in each well of 6-well plates and treated as above with 5 ug/ml Dil-LDL 5 for 4 h with or without pretreatment of LXR-623 for 48h. After treatment, cells were washed twice with PBS, harvested, and LDL uptake was assessed via flow cytometry recording signals using the PE channel. Data analyses were performed using FlowJo.

Cholesterol Efflux

Cholesterol efflux was performed as described (Hong C et al. J Lipid Research, 2012). Briefly, 80% to 100% confluent cells were labeled with [^{3}H] cholesterol (1.0 uCi/ml) in the presence of acyl-CoA:cholesterol O-acyltransferase inhibitor (2 g/ml) either with DMSO or with LXR-623 for 24 hr. After equilibrating the cholesterol pools, cells were washed with PBS and incubated in DMEM containing 0.2% fatty acid free BSA in the absence or presence of ApoA-I (15 g/ml) for 4 h. Radioactivity of both medium and cell samples were determined by scintillation counting.

Cholesterol Measurement

Cells were plated in 10 cm dishes and harvested, pelleted, suspended in PBS, counted, and then lysed by probe sonication. Lipid metabolites were extracted with 2:1 chloroform and the extract was separated by centrifugation and then concentrated under N_2 gas. The residue was solubilized ethanol and the supernatant was transferred to high pressure liquid chromatography (HPLC) inserts. Cholesterol levels were measured by using liquid chromatography (2.1 x 50m C8, Agilent) coupled to an Agilent 6490 triple quadrupole mass spectrometer.

Sterol Probe Labeling

Sterol probe labeling was performed as described (Hulce et al., 2013). Briefly, sterol probe was complexed in aqueous solution to mβCD (Sigma-Aldrich) for at least 12 h before dilution in culture medium for labeling at working concentrations. The desired amount of sterol probe was added to a saturated aqueous mβCD (38 mM) solution to generate a concentrated stock, and the mixture was agitated at room temperature overnight; solutions were filtered through a 0.22um filter before use the following day. Aqueous stock solutions of the trans-sterol probe were prepared at 2 mM. For live-cell labeling, cells were plated 10 cm dishes in 1% FBS DMEM and treated with DMSO or LXR-623 for 48 h. At 48 h, culture medium was then removed from the cells and replaced with probe-containing medium under dim ambient light. Cells were then incubated at 37 °C for 30 min in the dark to load the cells with sterol probe. After this time, cells were washed quickly with cold PBS and then irradiated for 5 min in cold PBS under 365-nm UV light in a Stratalinker 2400 UV cross-linker (Stratagene). Cells were then collected by scraping, and the cell pellet was frozen at −80 °C until processing for gel-based analysis.

Sterol probe sample processing for analysis by SDS-PAGE

Frozen cell pellets were thawed on ice and lysed in PBS by sonication. Protein concentrations of cell lysates were determined using the BCA protein assay on a microplate reader. Click chemistry was then performed as previously described (Martin et al., 2012) directly in whole-cell lysates in PBS. For analysis by gel, each sample was adjusted to a protein concentration of 1 mg/ml (50 μl) and a total of 50 μg of protein was used,Samples were mixed with 20 μM rhodamine-azide, 1 mM Tris(2-carboxyethyl)phosphine (TCEP, Sigma-Aldrich), 100 μM Tris[(1-benzyl-1H-1,2,3-triazol-4-yl)methyl]amine (TBTA) (Sigma-Aldrich) and 1 mM $CuSO_4$ in PBS at room temperature. After 1 h, samples were mixed with SDS sample loading buffer and loaded without boiling on a 10% SDS-PAGE gel, separated and imaged using a Hitachi FMBIO-II flatbed fluorescence scanner. Fluorescence images are shown in grayscale and quantitative densitometry was performed using ImageJ.

siRNA Transfection

Transient knockdown experiments using siRNA were performed as described (Akhavan et al., 2013). Briefly, reverse transfection of siRNA (10 nM) into cell lines was carried out using Lipofectamine RNAiMAX (Invitrogen) in full serum, with medium change after 24 hours. siRNA scramble, LXRα, and LXRβ were purchased from Thermo Scientific.

Data Analysis

Statistical comparisons were carried out using Student's t-tests. Throughout all figures, $*p < 0.05$, $**p < 0.01$, and $***p < 0.001$. Significance was concluded at $p < 0.05$.

REFERENCES

Bendell, J.C., Domchek, S.M., Burstein, H.J., Harris, L., Younger, J., Kuter, I., Bunnell, C., Rue, M., Gelman, R., and Winer, E. (2003). Central nervous system metastases in women who receive trastuzumab-based therapy for metastatic breast carcinoma. Cancer *97*, 2972–2977.

Borradaile, N.M., Han, X., Harp, J.D., Gale, S.E., Ory, D.S., and Schaffer, J.E. (2006). Disruption of endoplasmic reticulum structure and integrity in lipotoxic cell death. J. Lipid Res. *47*, 2726–2737.

Brennan, C.W., Verhaak, R.G.W., McKenna, A., Campos, B., Noushmehr, H., Salama, S.R., Zheng, S., Chakravarty, D., Sanborn, J.Z., Berman, S.H., et al. (2013). The somatic genomic landscape of glioblastoma. Cell *155*, 462–477.

Caliceti, C., Zambonin, L., Prata, C., Vieceli Dalla Sega, F., Hakim, G., Hrelia, S., and Fiorentini, D. (2012). Effect of plasma membrane cholesterol depletion on glucose transport regulation in leukemia cells. PloS One *7*, e41246.

Calkin, A.C., and Tontonoz, P. (2012). Transcriptional integration of metabolism by the nuclear sterol-activated receptors LXR and FXR. Nat. Rev. Mol. Cell Biol. *13*, 213–224.

Chen, J., Zhang, X., Kusumo, H., Costa, L.G., and Guizzetti, M. (2013). Cholesterol efflux is differentially regulated in neurons and astrocytes: implications for brain cholesterol homeostasis. Biochim. Biophys. Acta *1831*, 263–275.

Christian, A.E., Haynes, M.P., Phillips, M.C., and Rothblat, G.H. (1997). Use of cyclodextrins for manipulating cellular cholesterol content. J. Lipid Res. *38*, 2264–2272.

Chu, K., Miyazaki, M., Man, W.C., and Ntambi, J.M. (2006). Stearoyl-coenzyme A desaturase 1 deficiency protects against hypertriglyceridemia and increases plasma high-density lipoprotein cholesterol induced by liver X receptor activation. Mol. Cell. Biol. *26*, 6786–6798.

Ciriello, G., Miller, M.L., Aksoy, B.A., Senbabaoglu, Y., Schultz, N., and Sander, C. (2013). Emerging landscape of oncogenic signatures across human cancers. Nat. Genet. *45*, 1127–1133.

Clayton, A.J., Danson, S., Jolly, S., Ryder, W.D.J., Burt, P.A., Stewart, A.L., Wilkinson, P.M., Welch, R.S., Magee, B., Wilson, G., et al. (2004). Incidence of cerebral metastases in patients treated with trastuzumab for metastatic breast cancer. Br. J. Cancer *91*, 639–643.

Flaveny, C.A., Griffett, K., El-Gendy, B.E.-D.M., Kazantzis, M., Sengupta, M., Amelio, A.L., Chatterjee, A., Walker, J., Solt, L.A., Kamenecka, T.M., et al. (2015). Broad Anti-tumor Activity of a Small Molecule that Selectively Targets the Warburg Effect and Lipogenesis. Cancer Cell *28*, 42–56.

Gabitova, L., Restifo, D., Gorin, A., Manocha, K., Handorf, E., Yang, D.-H., Cai, K.Q., Klein-Szanto, A.J., Cunningham, D., Kratz, L.E., et al. (2015). Endogenous Sterol Metabolites Regulate Growth of EGFR/KRAS-Dependent Tumors via LXR. Cell Rep. *12*, 1927–1938.

Galluzzi, L., Kepp, O., Vander Heiden, M.G., and Kroemer, G. (2013). Metabolic targets for cancer therapy. Nat. Rev. Drug Discov. *12*, 829–846.

Guo, D., Prins, R.M., Dang, J., Kuga, D., Iwanami, A., Soto, H., Lin, K.Y., Huang, T.T., Akhavan, D., Hock, M.B., et al. (2009). EGFR signaling through an Akt-SREBP-1-dependent, rapamycin-resistant pathway sensitizes glioblastomas to antilipogenic therapy. Sci. Signal. *2*, ra82.

Guo, D., Reinitz, F., Youssef, M., Hong, C., Nathanson, D., Akhavan, D., Kuga, D., Amzajerdi, A.N., Soto, H., Zhu, S., et al. (2011). An LXR agonist promotes glioblastoma cell death through inhibition of an EGFR/AKT/SREBP-1/LDLR-dependent pathway. Cancer Discov. *1*, 442–456.

Hulce, J.J., Cognetta, A.B., Niphakis, M.J., Tully, S.E., and Cravatt, B.F. (2013). Proteome-wide mapping of cholesterol-interacting proteins in mammalian cells. Nat. Methods *10*, 259–264.

Janowski, B.A., Willy, P.J., Devi, T.R., Falck, J.R., and Mangelsdorf, D.J. (1996). An oxysterol signalling pathway mediated by the nuclear receptor LXR alpha. Nature *383*, 728–731.

Joseph, S.B., Laffitte, B.A., Patel, P.H., Watson, M.A., Matsukuma, K.E., Walczak, R., Collins, J.L., Osborne, T.F., and Tontonoz, P. (2002). Direct and indirect mechanisms for regulation of fatty acid synthase gene expression by liver X receptors. J. Biol. Chem. *277*, 11019–11025.

Kabat, G.C., Etgen, A.M., and Rohan, T.E. (2010). Do steroid hormones play a role in the etiology of glioma? Cancer Epidemiol. Biomark. Prev. Publ. Am. Assoc. Cancer Res. Cosponsored Am. Soc. Prev. Oncol. *19*, 2421–2427.

Kandoth, C., McLellan, M.D., Vandin, F., Ye, K., Niu, B., Lu, C., Xie, M., Zhang, Q., McMichael, J.F., Wyczalkowski, M.A., et al. (2013). Mutational landscape and significance across 12 major cancer types. Nature *502*, 333–339.

Lin, C.-Y., and Gustafsson, J.-Å. (2015). Targeting liver X receptors in cancer therapeutics. Nat. Rev. Cancer *15*, 216–224.

Lin, N.U., Diéras, V., Paul, D., Lossignol, D., Christodoulou, C., Stemmler, H.-J., Roché, H., Liu, M.C., Greil, R., Ciruelos, E., et al. (2009). Multicenter phase II study of lapatinib in patients with brain metastases from HER2-positive breast cancer. Clin. Cancer Res. Off. J. Am. Assoc. Cancer Res. *15*, 1452–1459.

Lo Sasso, G., Bovenga, F., Murzilli, S., Salvatore, L., Di Tullio, G., Martelli, N., D'Orazio, A., Rainaldi, S., Vacca, M., Mangia, A., et al. (2013). Liver X receptors inhibit proliferation of human colorectal cancer cells and growth of intestinal tumors in mice. Gastroenterology *144*, 1497–1507, 1507.e1–e13.

Manna, P.R., Stetson, C.L., Slominski, A.T., and Pruitt, K. (2016). Role of the steroidogenic acute regulatory protein in health and disease. Endocrine *51*, 7–21.

Martin, B.R., Wang, C., Adibekian, A., Tully, S.E., and Cravatt, B.F. (2012). Global profiling of dynamic protein palmitoylation. Nat. Methods *9*, 84–89.

Nguyen, D.X., Chiang, A.C., Zhang, X.H.-F., Kim, J.Y., Kris, M.G., Ladanyi, M., Gerald, W.L., and Massagué, J. (2009). WNT/TCF signaling through LEF1 and HOXB9 mediates lung adenocarcinoma metastasis. Cell *138*, 51–62.

Nguyen-Vu, T., Vedin, L.-L., Liu, K., Jonsson, P., Lin, J.Z., Candelaria, N.R., Candelaria, L.P., Addanki, S., Williams, C., Gustafsson, J.-Å., et al. (2013). Liver × receptor ligands disrupt breast cancer cell proliferation through an E2F-mediated mechanism. Breast Cancer Res. BCR *15*, R51.

Patel, A.P., Tirosh, I., Trombetta, J.J., Shalek, A.K., Gillespie, S.M., Wakimoto, H., Cahill, D.P., Nahed, B.V., Curry, W.T., Martuza, R.L., et al. (2014). Single-cell RNA-seq highlights intratumoral heterogeneity in primary glioblastoma. Science *344*, 1396–1401.

Pavlova, N.N., and Thompson, C.B. (2016). The Emerging Hallmarks of Cancer Metabolism. Cell Metab. *23*, 27–47.

Pencheva, N., Buss, C.G., Posada, J., Merghoub, T., and Tavazoie, S.F. (2014). Broad-spectrum therapeutic suppression of metastatic melanoma through nuclear hormone receptor activation. Cell *156*, 986–1001.

Pommier, A.J.C., Dufour, J., Alves, G., Viennois, E., De Boussac, H., Trousson, A., Volle, D.H., Caira, F., Val, P., Arnaud, P., et al. (2013). Liver x receptors protect from development of prostatic intra-epithelial neoplasia in mice. PLoS Genet. *9*, e1003483.

Rangachari, D., Yamaguchi, N., VanderLaan, P.A., Folch, E., Mahadevan, A., Floyd, S.R., Uhlmann, E.J., Wong, E.T., Dahlberg, S.E., Huberman, M.S., et al. (2015). Brain metastases in patients with EGFR-mutated or ALK-rearranged non-small-cell lung cancers. Lung Cancer Amst. Neth. *88*, 108–111.

Repa, J.J., Turley, S.D., Lobaccaro, J.A., Medina, J., Li, L., Lustig, K., Shan, B., Heyman, R.A., Dietschy, J.M., and Mangelsdorf, D.J. (2000). Regulation of absorption and ABC1-mediated efflux of cholesterol by RXR heterodimers. Science *289*, 1524–1529.

Rong, X., Albert, C.J., Hong, C., Duerr, M.A., Chamberlain, B.T., Tarling, E.J., Ito, A., Gao, J., Wang, B., Edwards, P.A., et al. (2013). LXRs regulate ER stress and inflammation through dynamic modulation of membrane phospholipid composition. Cell Metab. *18*, 685–697.

Venkateswaran, A., Laffitte, B.A., Joseph, S.B., Mak, P.A., Wilpitz, D.C., Edwards, P.A., and Tontonoz, P. (2000). Control of cellular cholesterol efflux by the nuclear oxysterol receptor LXR alpha. Proc. Natl. Acad. Sci. U. S. A. *97*, 12097–12102.

Vivanco, I., Robins, H.I., Rohle, D., Campos, C., Grommes, C., Nghiemphu, P.L., Kubek, S., Oldrini, B., Chheda, M.G., Yannuzzi, N., et al. (2012). Differential sensitivity of glioma- versus lung cancer-specific EGFR mutations to EGFR kinase inhibitors. Cancer Discov. *2*, 458–471.

Wang, M.Y., Lu, K.V., Zhu, S., Dia, E.Q., Vivanco, I., Shackleford, G.M., Cavenee, W.K., Mellinghoff, I.K., Cloughesy, T.F., Sawyers, C.L., et al. (2006). Mammalian target of rapamycin inhibition promotes response to epidermal growth factor receptor kinase inhibitors in PTEN-deficient and PTEN-intact glioblastoma cells. Cancer Res. *66*, 7864–7869.

Zelcer, N., Hong, C., Boyadjian, R., and Tontonoz, P. (2009). LXR regulates cholesterol uptake through Idol-dependent ubiquitination of the LDL receptor. Science *325*, 100–104.

Zhang, Y., Breevoort, S.R., Angdisen, J., Fu, M., Schmidt, D.R., Holmstrom, S.R., Kliewer, S.A., Mangelsdorf, D.J., and Schulman, I.G. (2012). Liver LXRα expression is crucial for whole body cholesterol homeostasis and reverse cholesterol transport in mice. J. Clin. Invest. *122*, 1688–1699.

Chapter 4

LXR-623 Efficacy in an Intracranial Patient-Derived GBM Xenograft Model

INTRODUCTION

Adult brain cancers are almost universally fatal, in part because of the physicochemical segregation and biochemical composition of the central nervous system (CNS). The brain cholesterol pool is virtually separate from cholesterol metabolism in the periphery. Because cholesterol cannot be transported across the blood-brain barrier into the CNS, almost all brain cholesterol is synthesized de novo. Here we exploit this unique feature of neural physiology and show that EGFR-mutant glioblastoma (GBM) cells suppress *de novo* cholesterol and liver X receptor (LXR) ligand synthesis (Figures 1-1, 1-6), making them entirely dependent on exogenous cholesterol for survival (Figure 1-5). This physiological property renders GBMs highly and selectively vulnerable to the brain penetrant LXR agonist, LXR-623, in an LXRβ- and cholesterol-dependent fashion (Figures 3-9, 3-12). Thus, next critical step is to test the efficacy of LXR-623 in a clinically relevant, patient-derived GBM xenograft model.

Much of what we know about glioblastoma, and cancer in general, has come through studying established tumor cell lines in culture. Adherent GBM cell lines in serum-containing culture have been used to identify most of the oncogenes and tumor suppressors that we know are important in GBM, including EGFR/EGFRvIII (Huang et al., 1997), PTEN (Chiariello et al., 1998), and INK4ARF (Zhu et al., 2009). Further, studies in these established GBM cell lines have yielded important insights into the behavior and function of these tumor cells, including some aspects of the molecular determinants of response to treatments (Mellinghoff et al., 2005). The Cancer Cell Line Encyclopedia, a pioneering effort using established cancer cell lines further illustrates this point (Barretina et al., 2012).

However, these established GBM cell lines have a number of significant limitations. They are less heterogeneous than the tumors from which they are derived; they often lack the invasive growth pattern characteristic of GBMs in orthotopic xenografts; and some of the signature genetic alterations, including EGFR amplification and mutations such as EGFRvIII, are lost within a small number of *in vitro* passages (Schulte et al., 2012).

Patient-derived, *ex vivo* tumor neurosphere cultures, which maintain the cellular heterogeneity and phenotypic characteristics that are more reflective of GBM biology in patients, have been a significant advancement in the field (Galli et al., 2004; Shu et al., 2008; Singh et al., 2004; Tunici et al., 2004). Orthotopic implantation of these cells into the brain in mice produces a patient-derived xenograft (PDX) model, which is a valuable preclinical tool that better represents human tumor biology and patient response to therapy (Joo et al., 2013; Sarkaria et al., 2007; Xie et al., 2015). Here, we determine the efficacy of LXR-623 *in vivo* using a clinically relevant, patient-derived GBM intracranial xenograft model we recently developed.

RESULTS

LXR-623 efficacy in intracranial patient-derived GBM xenograft models

The relative efficacy (Figure 3-1, Figure 3-2) and specificity (Figure 1-10) of LXR-623 against GBM cells, as well as the high brain penetrance of the drug (Figures 2-1, 2-2), inspired us to assess the potential efficacy and toxicity of this drug in a relevant pre-clinical animal model of GBM. Therefore, we investigated the therapeutic impact of LXR-623 in mice bearing patient-derived GBM orthotopic xenografts (Figure 4-1A). Oral administration of LXR-623 (400 mg/kg) to mice bearing GBM39 cells engineered to express the infrared fluorescent protein 720

(IRFP720) caused a striking inhibition of tumor growth (Figure 4-1B-C) and highly significant prolongation of survival (Figure 4-1D).

Immunohistochemical analysis revealed a significant increase in ABCA1 protein expression ($p < 0.01$) and a significant decrease in LDLR protein expression, ($p < 0.001$) in GBM tumors from LXR-623-treated mice (Figure 4-2). LXR-623 induced a greater than ten-fold increase in TUNEL staining, ($p < 0.001$) (Figure 4-2), demonstrating that it induces substantial apoptosis in GBM tumors. Importantly, no change in the number of neurons in the brain was seen in response to LXR-623 and no drug-induced cell death was detected in normal brain (Figures 4-3). Further, mice bearing GBMs maintained their body weights throughout LXR-623 treatment (Figure 4-4A), and showed no evidence of fatty liver (Figure 4-4B), a known consequence of LXR-target gene activation in the periphery (Chisholm et al., 2003). These findings are consistent with the high penetration of LXR-623 into the brain relative to the periphery (Figures 2A, 2B) and the relative lack of LXR-target gene induction in peripheral tissues (Figures 2C, 2D). Taken together, these results demonstrate that LXR-623 selectively kills GBM cells with excellent efficacy *in vivo* and prolongs survival in a clinically relevant, patient-derived GBM model.

A

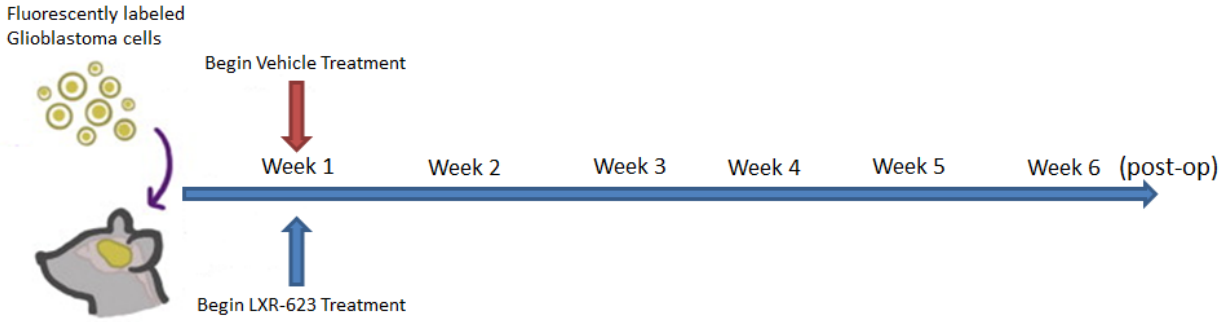
Fluorescently labeled
Glioblastoma cells
Begin Vehicle Treatment
Week 1
Week 2
Week 3
Week 4
Week 5
Week 6
(post-op)
Begin LXR-623 Treatment

B

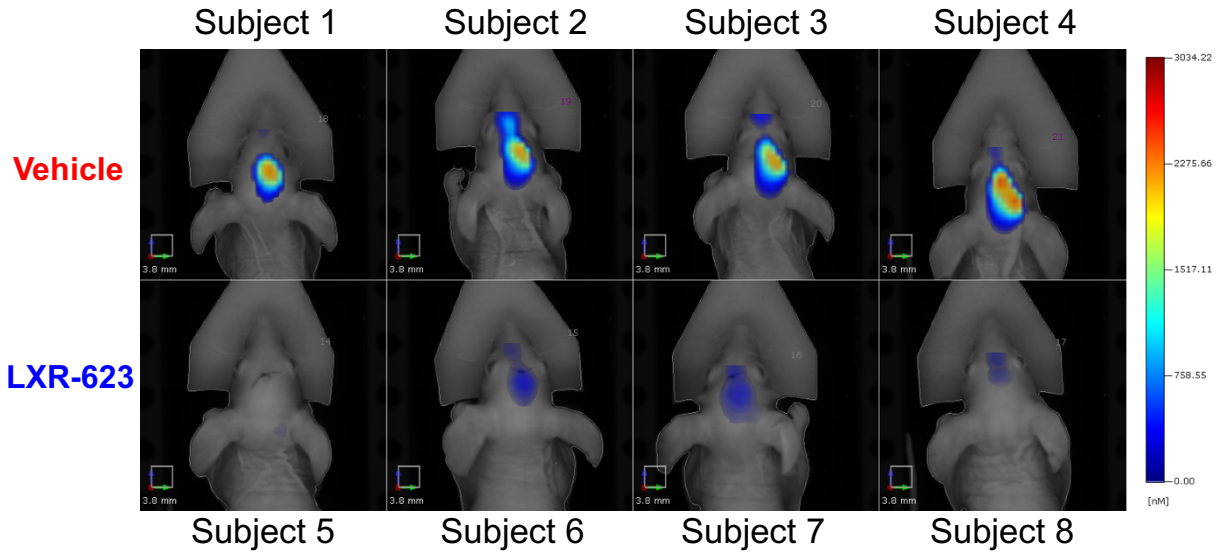
Subject 1
Subject 2
Subject 3
Subject 4
Vehicle
LXR-623
3034.22
2275.66
1517.11
758.55
0.00
[nM]
Subject 5
Subject 6
Subject 7
Subject 8

C

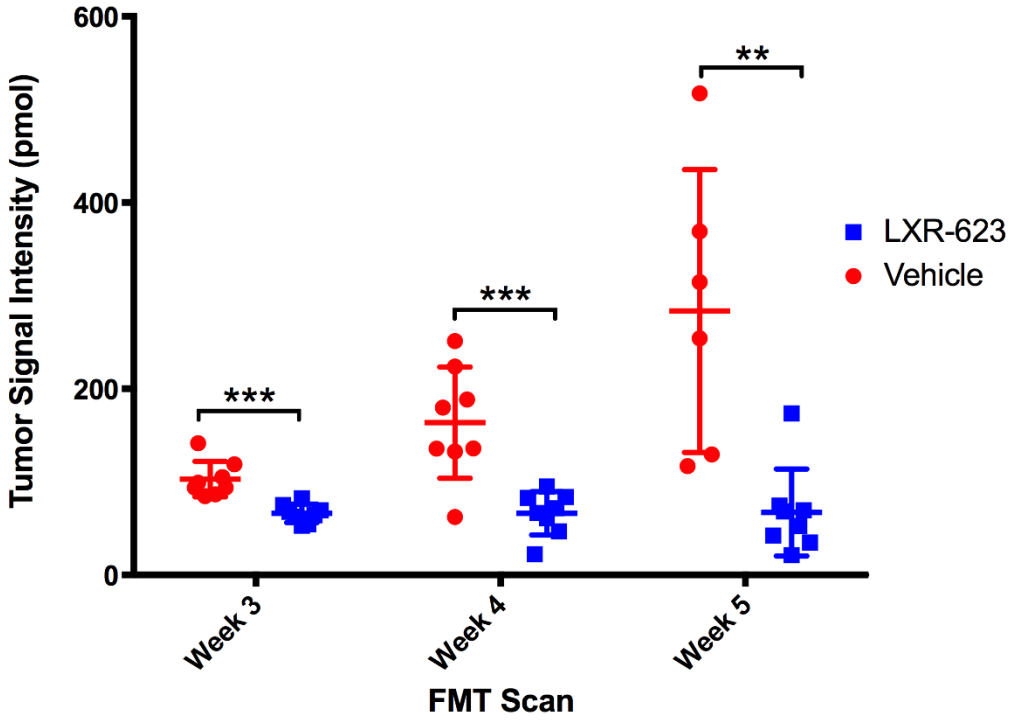
600
400
200
0
Tumor Signal Intensity (pmol)
***
***
**
Week 3
Week 4
Week 5
FMT Scan
LXR-623
Vehicle

D

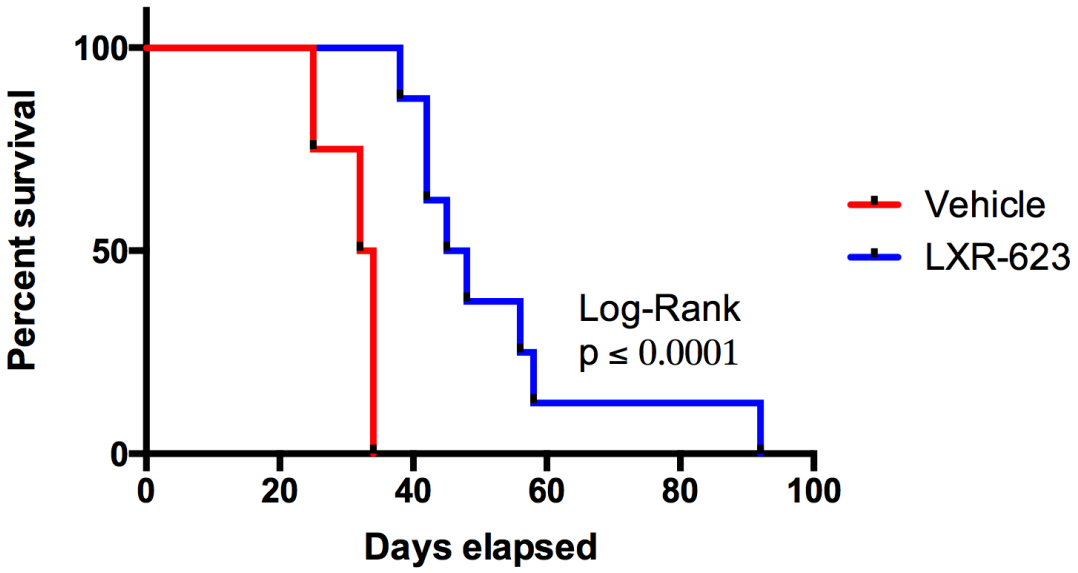
100
50
0
Percent survival
0
20
40
60
80
100
Days elapsed
Log-Rank
p ≤ 0.0001
Vehicle
LXR-623

Figure 4-1. **LXR-623 inhibits tumor growth and prolongs survival in mice bearing intracranial patient-derived GBMs**. (**A**) Schematic of experimental setup for assessment of LXR-623 in an orthotopic GBM xenograft mouse model modified from (Joo et al., 2013). 1.0 x 10^5 GBM39 patient-derived neurosphere cells, engineered to stably express the infrared protein 720 (IRFP 720), were orthotopically injected in the five-week-old mice. Mice were treated with vehicle or LXR-623 400 mpk p.o. daily (n = 8 for each group) and tumor size was assessed by fluorescence molecular tomography (FMT) technology. (**B**) FMT images of mice at week five of treatment. (**C**) Tumor size was assessed via FMT weekly. Two-way ANOVA was used to assess statistical significance. **$p < 0.01$; ***$p < 0.001$. (**D**) Kaplan-Meier curves assessing overall survival of mice from (**B**). Log-rank (Mantel-Cox) test: $p = 0.0001$, Gehan-Breslow-Wilcoxon test: $p = 0.0002$.

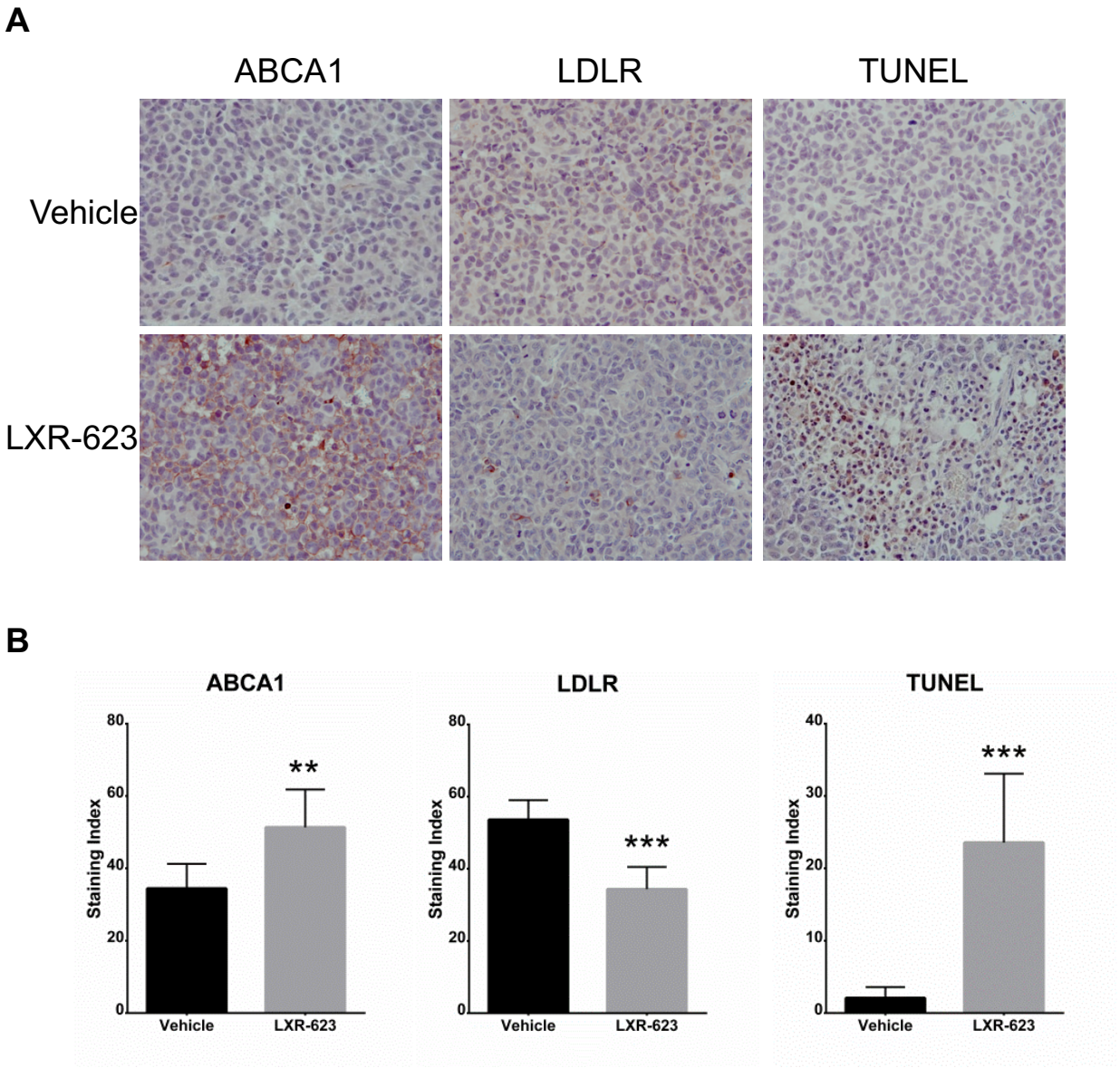

Figure 4-2. **LXR-623 induces LXR target gene expression and tumor cell death in orthotopic GBM xenografts**. (**A**) Tumors were excised and immunohistochemistry analysis was performed with the indicated antibodies. (**B**) Quantification of the immunohistochemistry performed in (**A**). *$p < 0.05$; **$p < 0.01$; ***$p < 0.001$. Values shown are ± SEM.

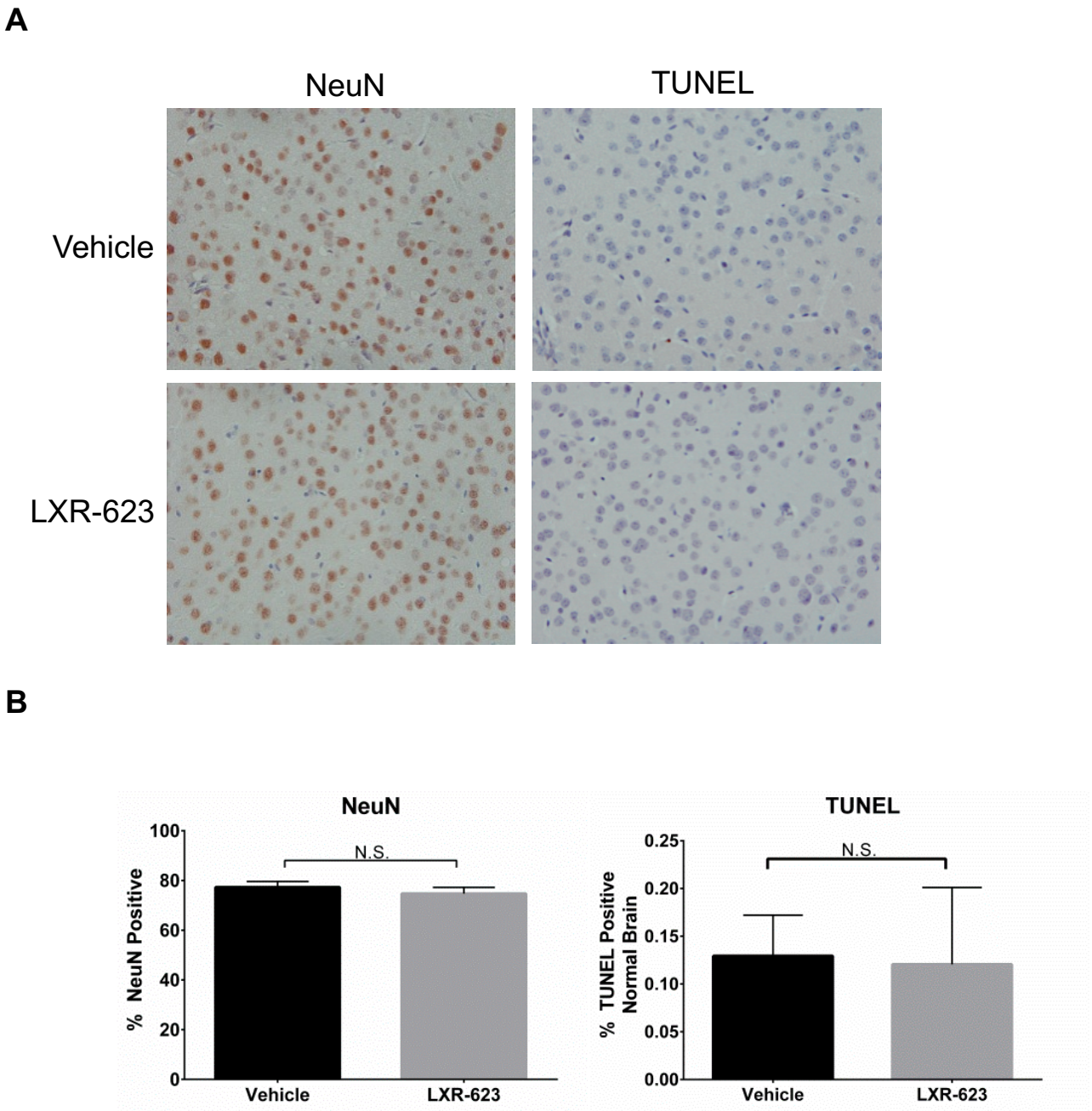

Figure 4-3. **LXR-623 does not cause cerebral cell death in mice bearing orthotopic GBMs**. (**A**) Normal brain sections from mice in Figure 4-1 were stained with the neuronal marker NeuN (left panel) or TUNEL (right panel) and percent positive cells were quantified (**B**). Values shown are +/- SEM. N.S. = not significant.

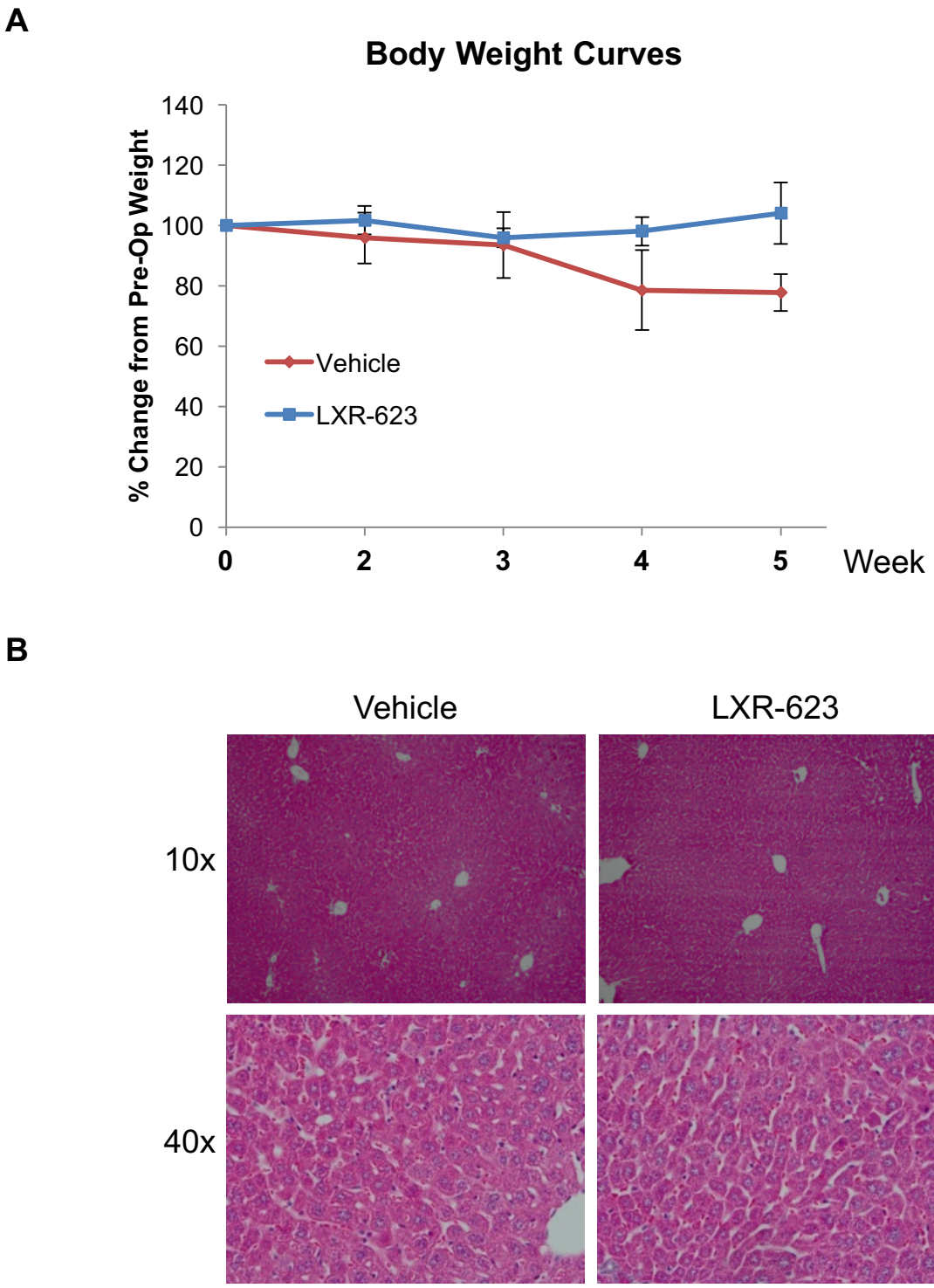

Figure 4-4. **LXR-623 does not cause weight loss or hepatic steatosis**. (**A**) Body weights of mice from Figure 4-1 treated with vehicle or LXR-623 400 mpk p.o. daily. (**B**) Representative hematoxylin and eosin (H&E) stains of mouse livers from mice in Figure 4-1.

DISCUSSION

LXR-623 showed a remarkably specific activity against GBMs *in vivo* (Figures 4-1, 4-2), sparing normal cells, including neurons, in the brain and failing to elicit obvious toxicity in peripheral tissues (Figures 4-3, 4-4). Three features may contribute to the specificity we found in our *in vitro* and *in vivo* models (Figures 1-10, 4-1, 4-3). First, the intact cellular cholesterol homeostasis machinery that is present in neurons and glia, but absent in GBM cells, may render normal brain cells less sensitive to LXR-623. Astrocytes rely on *de novo* cholesterol synthesis for survival and are not dependent on cholesterol uptake, rendering them vulnerable to statins, but not to LXR-623 (Figure 1-2). Similarly, no decrease in neuron number was seen and no neuronal cell death was detected in LXR-623-treated mice *in vivo* (Figure 4-3), indicating that neurons were less sensitive to the LXR-623 than were GBM cells. Second, the relatively high LXR-623 brain to plasma ratio limits the dose needed to reach therapeutic levels in tumor cells in the brain, thus limiting peripheral drug exposure. Third, LXR-623 is an LXRα-partial/LXRβ-full agonist (Wrobel et al., 2008) and many of the undesirable effects of synthetic LXR agonists are mediated through LXRα, including hepatic lipogenesis (Bradley et al., 2007; Joseph et al., 2002a, 2002b; Schultz et al., 2000). On this note, we did not detect fatty livers in tumor-bearing mice treated with LXR-623 at a dose that dramatically shrunk GBMs in the brain (Figure 4-4).

Taken together, our data suggest that LXR-623 could offer a viable pharmacological therapy for GBM patients who currently have no effective treatment options. Similar to GBMs, tumors that metastasize to the brain also commonly contain amplification and gain-of-function mutations of EGFR and erbB family members, including HER2 (Brastianos et al., 2015). LXR-623 effectively killed EGFR-mutated PC9 BRM lung cancer cells and HER2-amplified MDA-MB-231 breast cancer cells that were derived from a brain metastasis (Figures 3-3, 3-4), raising the possibility

that LXR-623 might further be used to treat systemic tumors that migrate to the brain. Future studies are warranted to determine the potential efficacy of this drug for the treatment of an array of brain cancers.

EXPERIMENTAL PROCEDURES

Cell Culture

GBM39 and GBM39 infrared Fluorescent Protein 720 (iRFP720) cells were cultured as neurospheres in Neurocult media (Stemcell Technologies) supplemented with EGF (Sigma), FGF (Sigma) and heparin (Sigma) in a humidified 5% CO2 incubator at 37°C.

Antibodies and Reagents

Antibodies used include mouse anti-ABCA1 (Abcam, ab18180), rabbit anti-LDLR (Abcam, ab30532), rabbit anti-NeuN (Abcam, ab104225), and sheep anti-digoxigenin (Roche, 11207733910). Reagents used include TdT (invitrogen, 10533-065), Digoxigenin-11-dUTP (Roche, 11558706910), Hematoxylin QS (Vector, H-3404), and Eosin (Fischer, 314-631). LXR-623 was synthesized by Sundia MediTech (Shanghai, China).

Lentivirus Production and Infection

The infrared Fluorescent Protein 720 cDNA (Shcherbakova and Verkhusha, 2013) was PCR-cloned into the Nhe I and Xho I restriction enzyme sites of the lentiviral plasmid vector pLV. The construct was then co-transfected with lentivirus packaging plasmids to Lenti-X 293T cells (Clontech), using X-tremeGENE DNA transfection reagents (Roche). Supernatants containing high titer lentiviruses were collected between 24-72 hours after transfection and were filtered through a 0.45 μm syringe filter before use. For infection experiments, $5x10^5$ GBM39 cells were seeded. The following day, 1/10 volume of high titer lentivirus and 12.5 ng/ml (final concentration) of polybrene were mixed and added to cultured cells. After 8 hours of incubation in 37 °C, the supernatant containing virus was replaced by fresh culture media

(DMEM/10%FBS). Infected cells were selected by blasticidin (2 μg /ml) and then fluorescence-activated cell sorting (FACS) using the Sony Sorter SH800Z was used to enrich the top 5% of total fluorescent cell population.

Intracranial Xenograft

Five week old female athymic nu/nu mice were purchased from Harlan Sprague Dawley Inc. 1×10^5 GBM39 IRFP720 cells in 5 μl of phosphate-buffered saline (PBS) were intracranially injected into the mouse brain as described previously (Ozawa and James, 2010). Tumor growth was monitored using an FMT 2500 Fluorescence Tomography System (PerkinElmer). For drug treatment studies, vehicle (0.5% methylcellulose, 2% Tween-80 in water) or LXR-623 (400 mg/kg) resuspended in vehicle were administered to mice via oral gavage daily starting at day seven post-injection. All procedures were reviewed and approved by the Institutional Animal Use and Care Committee at University of California, San Diego.

Data Analysis

The Mantel-Cox log-rank and Gehan-Breslow-Wilcoxon tests were used for statistical comparisons in survival analyses. All other statistical comparisons were carried out using Student's t-tests. Throughout all figures, $*p < 0.05$, $**p < 0.01$, and $***p < 0.001$. Significance was concluded at $p < 0.05$.

Immunohistochemistry

Formalin-fixed, paraffin-embedded (FFPE) tissue sections were prepared by the Histology Core Facility at UCSD Moores Cancer Center. Immunohistochemistry was performed according to standard procedures. Antigen was retrieved by boiling slides in 0.01 M of sodium citrate (pH

6.0) in a microwave for 15 min. Sections were incubated with primary antibodies at 4 °C overnight, followed by incubation with biotinylated secondary antibodies at room temperature for 30 min. For TUNEL staining, sections were incubated in TdT/dUTP for 30 min at 37 degrees, washed, and then incubated with HRP-conjugated Anti-Digoxigenin for 30 min at room temperature. Immunostained sections underwent immunohistochemical analysis by a pathologist blinded to treatment and vehicle groups. Three representative images from each immunostained section were captured using DP 25 camera mounted on an Olympus BX43 microscope at 40x magnification. Quantitative analysis of the IHC images was performed using image analyzing software (Visiopharm).

REFERENCES

Barretina, J., Caponigro, G., Stransky, N., Venkatesan, K., Margolin, A.A., Kim, S., Wilson, C.J., Lehár, J., Kryukov, G.V., Sonkin, D., et al. (2012). The Cancer Cell Line Encyclopedia enables predictive modelling of anticancer drug sensitivity. Nature *483*, 603–607.

Bradley, M.N., Hong, C., Chen, M., Joseph, S.B., Wilpitz, D.C., Wang, X., Lusis, A.J., Collins, A., Hseuh, W.A., Collins, J.L., et al. (2007). Ligand activation of LXR beta reverses atherosclerosis and cellular cholesterol overload in mice lacking LXR alpha and apoE. J. Clin. Invest. *117*, 2337–2346.

Brastianos, P.K., Carter, S.L., Santagata, S., Cahill, D.P., Taylor-Weiner, A., Jones, R.T., Van Allen, E.M., Lawrence, M.S., Horowitz, P.M., Cibulskis, K., et al. (2015). Genomic Characterization of Brain Metastases Reveals Branched Evolution and Potential Therapeutic Targets. Cancer Discov. *5*, 1164–1177.

Chiariello, E., Roz, L., Albarosa, R., Magnani, I., and Finocchiaro, G. (1998). PTEN/MMAC1 mutations in primary glioblastomas and short-term cultures of malignant gliomas. Oncogene *16*, 541–545.

Chisholm, J.W., Hong, J., Mills, S.A., and Lawn, R.M. (2003). The LXR ligand T0901317 induces severe lipogenesis in the db/db diabetic mouse. J. Lipid Res. *44*, 2039–2048.

Galli, R., Binda, E., Orfanelli, U., Cipelletti, B., Gritti, A., De Vitis, S., Fiocco, R., Foroni, C., Dimeco, F., and Vescovi, A. (2004). Isolation and characterization of tumorigenic, stem-like neural precursors from human glioblastoma. Cancer Res. *64*, 7011–7021.

Huang, H.S., Nagane, M., Klingbeil, C.K., Lin, H., Nishikawa, R., Ji, X.D., Huang, C.M., Gill, G.N., Wiley, H.S., and Cavenee, W.K. (1997). The enhanced tumorigenic activity of a mutant epidermal growth factor receptor common in human cancers is mediated by threshold levels of constitutive tyrosine phosphorylation and unattenuated signaling. J. Biol. Chem. *272*, 2927–2935.

Joo, K.M., Kim, J., Jin, J., Kim, M., Seol, H.J., Muradov, J., Yang, H., Choi, Y.-L., Park, W.-Y., Kong, D.-S., et al. (2013). Patient-specific orthotopic glioblastoma xenograft models recapitulate the histopathology and biology of human glioblastomas in situ. Cell Rep. *3*, 260–273.

Joseph, S.B., Laffitte, B.A., Patel, P.H., Watson, M.A., Matsukuma, K.E., Walczak, R., Collins, J.L., Osborne, T.F., and Tontonoz, P. (2002a). Direct and indirect mechanisms for regulation of fatty acid synthase gene expression by liver X receptors. J. Biol. Chem. *277*, 11019–11025.

Joseph, S.B., McKilligin, E., Pei, L., Watson, M.A., Collins, A.R., Laffitte, B.A., Chen, M., Noh, G., Goodman, J., Hagger, G.N., et al. (2002b). Synthetic LXR ligand inhibits the development of atherosclerosis in mice. Proc. Natl. Acad. Sci. U. S. A. *99*, 7604–7609.

Mellinghoff, I.K., Wang, M.Y., Vivanco, I., Haas-Kogan, D.A., Zhu, S., Dia, E.Q., Lu, K.V., Yoshimoto, K., Huang, J.H.Y., Chute, D.J., et al. (2005). Molecular determinants of the response of glioblastomas to EGFR kinase inhibitors. N. Engl. J. Med. *353*, 2012–2024.

Sarkaria, J.N., Yang, L., Grogan, P.T., Kitange, G.J., Carlson, B.L., Schroeder, M.A., Galanis, E., Giannini, C., Wu, W., Dinca, E.B., et al. (2007). Identification of molecular characteristics correlated with glioblastoma sensitivity to EGFR kinase inhibition through use of an intracranial xenograft test panel. Mol. Cancer Ther. *6*, 1167–1174.

Schulte, A., Günther, H.S., Martens, T., Zapf, S., Riethdorf, S., Wülfing, C., Stoupiec, M., Westphal, M., and Lamszus, K. (2012). Glioblastoma stem-like cell lines with either maintenance or loss of high-level EGFR amplification, generated via modulation of ligand concentration. Clin. Cancer Res. Off. J. Am. Assoc. Cancer Res. *18*, 1901–1913.

Schultz, J.R., Tu, H., Luk, A., Repa, J.J., Medina, J.C., Li, L., Schwendner, S., Wang, S., Thoolen, M., Mangelsdorf, D.J., et al. (2000). Role of LXRs in control of lipogenesis. Genes Dev. *14*, 2831–2838.

Shu, Q., Wong, K.K., Su, J.M., Adesina, A.M., Yu, L.T., Tsang, Y.T.M., Antalffy, B.C., Baxter, P., Perlaky, L., Yang, J., et al. (2008). Direct orthotopic transplantation of fresh surgical specimen preserves CD133+ tumor cells in clinically relevant mouse models of medulloblastoma and glioma. Stem Cells Dayt. Ohio *26*, 1414–1424.

Singh, S.K., Hawkins, C., Clarke, I.D., Squire, J.A., Bayani, J., Hide, T., Henkelman, R.M., Cusimano, M.D., and Dirks, P.B. (2004). Identification of human brain tumour initiating cells. Nature *432*, 396–401.

Tunici, P., Bissola, L., Lualdi, E., Pollo, B., Cajola, L., Broggi, G., Sozzi, G., and Finocchiaro, G. (2004). Genetic alterations and in vivo tumorigenicity of neurospheres derived from an adult glioblastoma. Mol. Cancer *3*, 25.

Xie, Y., Bergström, T., Jiang, Y., Johansson, P., Marinescu, V.D., Lindberg, N., Segerman, A., Wicher, G., Niklasson, M., Baskaran, S., et al. (2015). The Human Glioblastoma Cell Culture Resource: Validated Cell Models Representing All Molecular Subtypes. EBioMedicine *2*, 1351–1363.

Zhu, H., Acquaviva, J., Ramachandran, P., Boskovitz, A., Woolfenden, S., Pfannl, R., Bronson, R.T., Chen, J.W., Weissleder, R., Housman, D.E., et al. (2009). Oncogenic EGFR signaling cooperates with loss of tumor suppressor gene functions in gliomagenesis. Proc. Natl. Acad. Sci. U. S. A. *106*, 2712–2716.

Future Directions

The work herein identifies a surprising aspect of tumor cell biology at the interface of oncogenic signaling and metabolism. By upregulating the LDLR and suppressing endogenous LXR-ligand synthesis, GBM cells obtain access to a nearly limitless supply of cholesterol with minimal energy expenditure. However, this tumor cell metabolic dependency, namely, the ability of GBM cells to behave in a "parasitic" fashion with regard to cholesterol, renders them selectively sensitive to a brain-penetrant LXR agonist. Thus, through basic and translational research we have discovered a potentially compelling opportunity to treat refractory brain cancers. A number of exciting questions remain.

Suppression of a Cholesterol Negative Feedback

Mass spectrometric analysis of GBM cell lines and NHAs revealed endogenous LXR ligands, negative regulators of cholesterol uptake, were significantly reduced in GBM cells relative to NHAs (Figure 1-6). Further, the mRNA levels of the enzymes that catalyze that catalyze the production of these ligands were also significantly reduced in both cell culture and the TCGA dataset. In particular, CYP46A1, the most highly expressed enzyme that catalyzes oxysterol synthesis in the brain, was reduced nearly 10-fold in GBM samples (Figure 1-7). Notably, the regulatory axes that control expression of CYP46A1, the enzyme responsible for producing 24-OHC from cholesterol, are not well understood (Ohyama et al., 2006). These data indicate that the mRNA levels of oxysterol-synthesizing enzymes are suppressed in GBM, however, the mechanistic basis for this observation remains unknown.

We recently discovered the SOX9 and FOXG1 transcription factors as critical mediators of EGFRvIII-dependent tumorigenesis (Appendix; Liu et al., 2015). SOX9 and FOXG1 were studied primarily for their ability to upregulate gene expression in an EGFRvIII-dependent manner, although the specific downstream effectors regulating their activity are unknown.

Nevertheless, SOX9 and FOXG1 have also been shown to act as transcriptional repressors (Blache et al., 2004; Dou et al., 2000; Leung et al., 2011; Seoane et al., 2004), and our preliminary data suggest that these master regulators of EGFR-mediated GBM tumorigenesis may also function, directly or indirectly, to negatively regulate the expression of metabolic enzymes detrimental to tumor growth. Chromatin immunoprecipitation-qPCR (ChIP-qPCR) coupled to RNA-interference analyses involving SOX9 and FOXG1 should be undertaken to determine if either transcription factor has a role in suppressing oxysterol synthetic enzyme gene expression in GBM. Because other transcription factors cannot be excluded, genome-wide screening studies may also be undertaken to identify additional potential transcriptional suppressors of the aforementioned enzymes. Given that 24-OHC, the product of CYP46A1 mediated cholesterol oxidation, induced GBM cell death while sparing NHAs (Figure 1-8), studies dissecting the regulatory factors affecting CYP46A1 expression may yield an alternative therapeutic strategy for patients with GBM.

Cholesterol Depletion Mediates LXR-623 Induced Cell Death

Our finding that LXRβ activation significantly reduced cellular cholesterol content (Figure 3-11), concomitant with promotion of tumor cell death (Figure 1-10), raised the possibility that LXR-623 kills GBM cells by depleting cholesterol. Consistent with this hypothesis, adding cholesterol to cultures fully rescued LXR-623-induced cell death in both established and patient-derived GBM cell lines (Figure 3-12A). However, the precise mechanism by which LXR-623-mediated cholesterol depletion induces GBM cell death has yet to be established.

LXR agonists have been shown to alter plasma membrane fluidity (Ito et al., 2015; Rong et al., 2013), which is determined in part by cholesterol content (Ikonen, 2008; Simons and Toomre, 2000). Cholesterol is critical to micro-environments in the plasma membrane (Pike, 2003), also

known as lipid rafts, which form concentrating platforms for individual membrane-bound receptors (Simons and Toomre, 2000). Consequently, changes in plasma membrane cholesterol content could alter cellular signaling critical to tumor growth (Orr et al., 2005; Prasanna et al., 2014). In support of this notion, LXR activation downregulates AKT phosphorylation in prostate cancer, resulting in cell death (Pommier et al., 2010)

Thus, an integrative analysis of plasma membrane dynamics and cellular signaling may expose the mechanism underlying LXR-623-mediated cell death. Biochemical studies assessing cellular signaling may initially be directed toward EGFR and downstream effectors critical for GBM cell growth, including AKT, mTORC1, and mTORC2, and also utilize kinase signaling arrays for a more broad evaluation (Akhavan et al., 2013).

LXR-623 Structure and Pharmacology

LXR-623 showed a remarkably specific activity against GBMs in vivo (Figures 4-1, 4-2), sparing normal cells, including neurons, in the brain and failing to elicit obvious toxicity in peripheral tissues (Figures 4-3, 4-4). The relatively high LXR-623 brain to plasma ratio (Figure 2-1) contributed to this specificity. However, pharmacokinetic data concerning the entry of LXR-623 into the human CNS are lacking.

Functional molecular imaging has enhanced our understanding, diagnosis, and management of illnesses such as cancer, heart diseases, and brain disorders (Preshlock et al., 2016; Willmann et al., 2008). Positron emission tomography (PET) in particular is increasingly being used for the study of CNS drug development (Cunha et al., 2014; Fowler et al., 1999; Rudin and Weissleder, 2003). PET radionuclides are most commonly isotopes of carbon, oxygen, nitrogen, and fluorine. The structure of LXR-623 (Figure 1-9) contains multiple fluorine groups, which may be

amenable to ^{18}F-fluorination via nucleophilic substitution (Rokka et al., 2013). Because ^{18}F may directly substitute a stable isotope of fluorine in LXR-623, the molecular structure and consequently the chemical properties of ^{18}F-LXR-623 could be nearly identical to that of the parent compound. Should preclinical studies validate this hypothesis, PET radiotracer development of LXR-623 would readily allow for a phase zero evaluation of CNS penetration in GBM patients.

Broader Implications

We have found that the most common genetic alterations in GBM converge to promote tumor growth by reprogramming cellular metabolism. The current work here indicates it is possible to exploit GBM cell-type selective vulnerabilities that are generated by the special metabolic environment of the brain. Cancer cells utilize glucose, glutamine or acetate-derived acetyl-CoA to provide the precursors for lipid biogenesis. However, the influence of oncogenic signaling on the enzymes that regulate the flux of these nutrients into the synthesis of a specific lipids, and whether these lipids are required for tumor growth in its native environment, is not well understood. It is possible that there may be distinct lipid species that maintain oncogenic signaling through plasma membrane remodeling, providing a feed-forward mechanism for tumor growth. Isotope labeling of nutrients, coupled to patient-derived orthotopic xenografts, and subsequent mass-spectrometry analysis would allow for the identification of these lipids. Together, these studies may generate a deeper understanding of the role of oncogenic signaling and metabolism, and potentially identify a set of targetable vulnerabilities.

Concluding Remarks

Glioblastoma is a complex disease, and the epigenetic, transcriptional, and metabolic networks that drive tumor cell growth are only starting to be elucidated. What is illustrated here is that there may be unknown and unappreciated metabolic dependency pathways that are critical to growth factor receptor-mediated tumorigenesis. Dissecting the molecular circuitry, including discovery of more dependency pathways, will greatly expand the target landscape for treating genetically defined cancer and translate into better care for patients.

REFERENCES

Akhavan, D., Pourzia, A.L., Nourian, A.A., Williams, K.J., Nathanson, D., Babic, I., Villa, G.R., Tanaka, K., Nael, A., Yang, H., et al. (2013). De-repression of PDGFRβ transcription promotes acquired resistance to EGFR tyrosine kinase inhibitors in glioblastoma patients. Cancer Discov. *3*, 534–547.

Blache, P., van de Wetering, M., Duluc, I., Domon, C., Berta, P., Freund, J.-N., Clevers, H., and Jay, P. (2004). SOX9 is an intestine crypt transcription factor, is regulated by the Wnt pathway, and represses the CDX2 and MUC2 genes. J. Cell Biol. *166*, 37–47.

Cunha, L., Szigeti, K., Mathé, D., and Metello, L.F. (2014). The role of molecular imaging in modern drug development. Drug Discov. Today *19*, 936–948.

Dou, C., Lee, J., Liu, B., Liu, F., Massague, J., Xuan, S., and Lai, E. (2000). BF-1 interferes with transforming growth factor beta signaling by associating with Smad partners. Mol. Cell. Biol. *20*, 6201–6211.

Fowler, J.S., Volkow, N.D., Wang, G.J., Ding, Y.S., and Dewey, S.L. (1999). PET and drug research and development. J. Nucl. Med. Off. Publ. Soc. Nucl. Med. *40*, 1154–1163.

Ikonen, E. (2008). Cellular cholesterol trafficking and compartmentalization. Nat. Rev. Mol. Cell Biol. *9*, 125–138.

Ito, A., Hong, C., Rong, X., Zhu, X., Tarling, E.J., Hedde, P.N., Gratton, E., Parks, J., and Tontonoz, P. (2015). LXRs link metabolism to inflammation through Abca1-dependent regulation of membrane composition and TLR signaling. eLife *4*, e08009.

Leung, V.Y.L., Gao, B., Leung, K.K.H., Melhado, I.G., Wynn, S.L., Au, T.Y.K., Dung, N.W.F., Lau, J.Y.B., Mak, A.C.Y., Chan, D., et al. (2011). SOX9 governs differentiation stage-specific gene expression in growth plate chondrocytes via direct concomitant transactivation and repression. PLoS Genet. *7*, e1002356.

Liu, F., Hon, G.C., Villa, G.R., Turner, K.M., Ikegami, S., Yang, H., Ye, Z., Li, B., Kuan, S., Lee, A.Y., et al. (2015). EGFR Mutation Promotes Glioblastoma through Epigenome and Transcription Factor Network Remodeling. Mol. Cell *60*, 307–318.

Ohyama, Y., Meaney, S., Heverin, M., Ekström, L., Brafman, A., Shafir, M., Andersson, U., Olin, M., Eggertsen, G., Diczfalusy, U., et al. (2006). Studies on the transcriptional regulation of cholesterol 24-hydroxylase (CYP46A1): marked insensitivity toward different regulatory axes. J. Biol. Chem. *281*, 3810–3820.

Orr, G., Hu, D., Ozçelik, S., Opresko, L.K., Wiley, H.S., and Colson, S.D. (2005). Cholesterol dictates the freedom of EGF receptors and HER2 in the plane of the membrane. Biophys. J. *89*, 1362–1373.

Pike, L.J. (2003). Lipid rafts: bringing order to chaos. J. Lipid Res. *44*, 655–667.

Pommier, A.J.C., Alves, G., Viennois, E., Bernard, S., Communal, Y., Sion, B., Marceau, G., Damon, C., Mouzat, K., Caira, F., et al. (2010). Liver X Receptor activation downregulates AKT survival signaling in lipid rafts and induces apoptosis of prostate cancer cells. Oncogene *29*, 2712–2723.

Prasanna, X., Chattopadhyay, A., and Sengupta, D. (2014). Cholesterol modulates the dimer interface of the β_2-adrenergic receptor via cholesterol occupancy sites. Biophys. J. *106*, 1290–1300.

Preshlock, S., Tredwell, M., and Gouverneur, V. (2016). (18)F-Labeling of Arenes and Heteroarenes for Applications in Positron Emission Tomography. Chem. Rev. *116*, 719–766.

Rokka, J., Federico, C., Jurttila, J., Snellman, A., Haaparanta, M., Rinne, J.O., and Solin, O. (2013). 19F/18F exchange synthesis for a novel [18F]S1P3-radiopharmaceutical. J. Label. Compd. Radiopharm. *56*, 385–391.

Rong, X., Albert, C.J., Hong, C., Duerr, M.A., Chamberlain, B.T., Tarling, E.J., Ito, A., Gao, J., Wang, B., Edwards, P.A., et al. (2013). LXRs regulate ER stress and inflammation through dynamic modulation of membrane phospholipid composition. Cell Metab. *18*, 685–697.

Rudin, M., and Weissleder, R. (2003). Molecular imaging in drug discovery and development. Nat. Rev. Drug Discov. *2*, 123–131.

Seoane, J., Le, H.-V., Shen, L., Anderson, S.A., and Massagué, J. (2004). Integration of Smad and forkhead pathways in the control of neuroepithelial and glioblastoma cell proliferation. Cell *117*, 211–223.

Simons, K., and Toomre, D. (2000). Lipid rafts and signal transduction. Nat. Rev. Mol. Cell Biol. *1*, 31–39.

Willmann, J.K., van Bruggen, N., Dinkelborg, L.M., and Gambhir, S.S. (2008). Molecular imaging in drug development. Nat. Rev. Drug Discov. *7*, 591–607.

Appendix

The work described here is the result of collaborative efforts that have advanced the understanding of how oncogenic epidermal growth factor receptor signaling converges to promote tumor growth and survival through reprogramming of epigenetic, transcriptional, and metabolic networks in glioblastoma. My contributions were to the conception, design and execution of specific experiments in each of the following studies.

Glioblastoma epigenome and transcription factor network remodeling

Until recently, the impact of EGFR alteration on the transcriptional and enhancer landscape of glioblastoma (GBM) was not known. To better understand this process, we performed ChIP-seq and RNA-seq in GBM cells with, or without, stable expression of EGFRvIII (Liu et al., 2015). FOXG1 and SOX9 transcription factors were among the most highly enriched enhancer motifs and mRNA levels of both were highly elevated by EGFRvIII expression. Further integrated epigenome, transcriptome, and genetic analyses in genotyped clinical samples, TCGA data, and xenografts revealed EGFR mutations remodel the activated enhancer and transcriptional landscape of GBM and promote tumorigenesis in a FOXG1- and SOX9-dependent manner. *In vitro* and *in vivo* pharmacologic studies indicated that EGFRvIII sensitizes GBM cells to the BET-bromodomain inhibitor JQ1 in a SOX9, FOXG1-dependent manner. Together, this study identified the role of transcriptional and epigenetic remodeling in EGFR-dependent pathogenesis and suggested a mechanistic basis for epigenetic therapy (Figure 1).

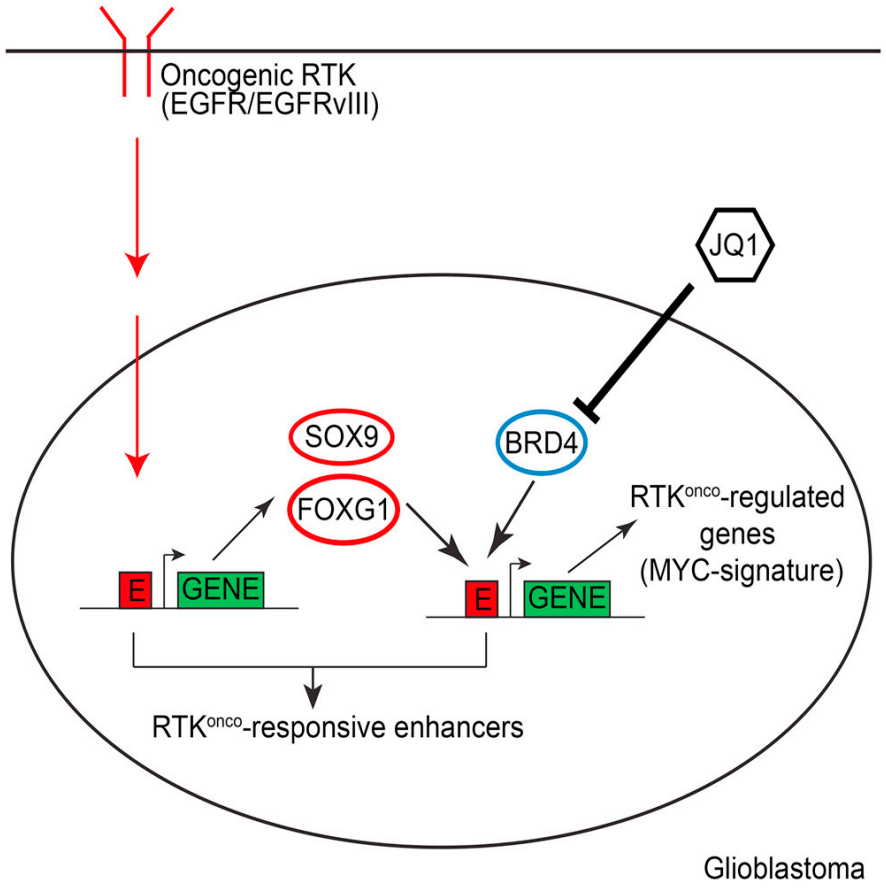

Figure 1. **EGFR Mutation Promotes Glioblastoma through Epigenome and Transcription Factor Network Remodeling**. Oncogenic EGFR/EGFRvIII signaling promotes tumorigenesis through SOX9- and FOXG1-dependent epigenome and transcriptional network remodeling. See text for additional detail. Figure from (Liu et al., 2015).

EGFR mutation-induced alternative splicing contributes to glycolytic GBM tumor growth

In the last decade, alternative splicing was identified as a means for cancer cells to induce expression of genes who protein products reprogram cellular metabolism and suppress apoptosis (Clower et al., 2010; David et al., 2010). However, the effects of oncogenes on genome-wide alternative splicing and the contribution of alternative splicing to alterations in metabolism were not well understood. Therefore, we performed genome-wide splicing and expression analysis of GBM EGFRvIII and EGFRvIII-null xenografts (Babic et al., 2013). Expression analysis revealed an EGFRvIII-dependent upregulation of the heterogeneous nuclear ribonucleoprotein A1 (hnRNPA1) splicing factor and subsequent bioinformatics analyses indicated hnRNPA1 promotes the splicing of the max transcript to generate delta max. Delta max is an obligate binding partner of c-Myc, a master regulator of metabolic gene expression. Ensuing metabolic and genetic analyses revealed delta Max promotes Myc-dependent glycolysis and tumor growth *in vivo*. Thus, we discovered an important role for alternative splicing in GBM and identified Delta Max as a mediator of Myc-dependent tumor cell metabolism (Figure 2).

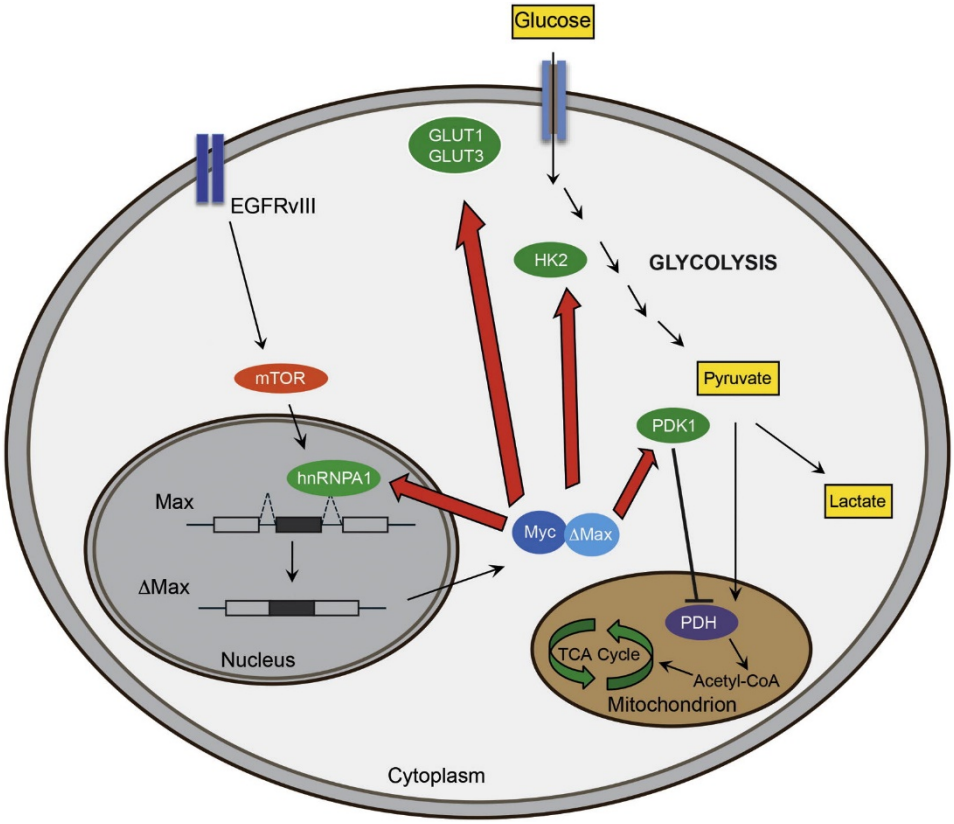

Figure 2. **EGFR mutation-induced alternative splicing of max contributes to growth of glycolytic tumors in GBM**. EGFRvIII induces the expression of the splicing factor, hnRNPA1, which promotes the splicing of the Max transcript to generate delta max. Delta Max interacts with Myc to promote glycolysis and tumor growth *in vivo*. See text for additional detail. Figure from (Babic et al., 2013).

mTOR Complex 2 Controls Glycolytic Metabolism in GBM through FoxO Acetylation and Upregulation of c-Myc

Metabolic reprogramming is a hallmark of cancer (Pavlova and Thompson, 2016). Many cancer cell types, including those derived from GBM, convert the majority of their glucose into lactate to provide carbon-containing precursors for macromolecular biosynthesis, even in the presence of sufficient oxygen to support oxidative phosphorylation (Babic et al., 2013; Dang, 2012; Warburg, 1956). However, precisely how oncogenic EGFR signaling drives this biochemical adaptation known as the Warburg effect, including which downstream effectors are critical for glucose-dependent GBM growth, is not well understood. Through integrated metabolic and genetic analyses of GBM cell lines and patient-derived xenografts, we show that the mammalian target of rapamycin complex 2 (mTORC2), an EGFR-activated downstream kinase complex, is required for GBM cell growth in the presence of glucose (Masui et al., 2013). We further demonstrate that mTORC2 regulates levels of c-Myc to drive glycolytic metabolism via inhibition of class IIa histone deacetylases (HDACs), which leads to the sustained acetylation of FoxO1 and FoxO3. Acetylation of FoxO1 and FoxO3 inhibits their ability increase expression of the microRNA, miR-34c, which antagonizes c-Myc. Thus, c-Myc levels and glycolytic metabolism are sustained by mTORC2. These results nominate mTORC2 as a critical regulator of glycolytic metabolism in GBM (Figure 3).

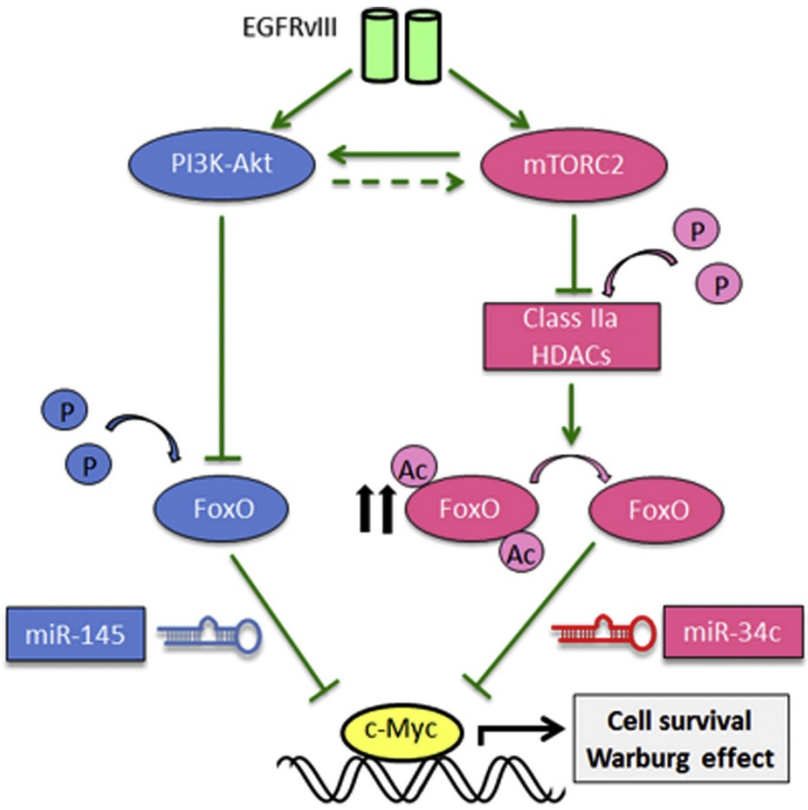

Figure 3. **mTORC2 controls glycolytic metabolism by sustaining c-Myc expression**. EGFRvIII signaling activates mTORC2, which inhibits class IIa HDACs. Inhibition of HDACs sustains acetylation and thus repression of FoxO function. Acetylated FoxO can no longer drive expression of c-Myc repressive miR-34c, allowing c-Myc to drive cell proliferation and utilization of glucose. See text for additional detail. Figure from (Masui et al., 2013).

Glucose-dependent acetylation of Rictor promotes targeted cancer therapy resistance

Growth factor receptor mutations drive cancer cells to reprogram their metabolism. However, whether the environment in which cancers reside can alter oncogenic signaling is not well understood. Here, we demonstrate that two abundant resources in brain, namely glucose and acetate, promote EGFRvIII-dependent activation of mTORC2 by acetylation of rapamycin-insensitive companion of mammalian target of rapamycin (RICTOR), a component of this kinase complex (Masui et al., 2015). Acetylation of RICTOR is mediated through elevated levels of acetyl-CoA, which result from EGFRvIII-driven metabolic programming, rendering mTORC2 constitutively active. A fascinating implication of our work here is that glucose or acetate can contribute to targeted therapy resistance by maintaining oncogenic activation of downstream effectors, even when upstream components of EGFR signaling are inhibited (Figure 4). Thus, we uncover unexpected role for metabolic reprogramming at the interface of oncogenic signaling and the environment in which GBMs reside.

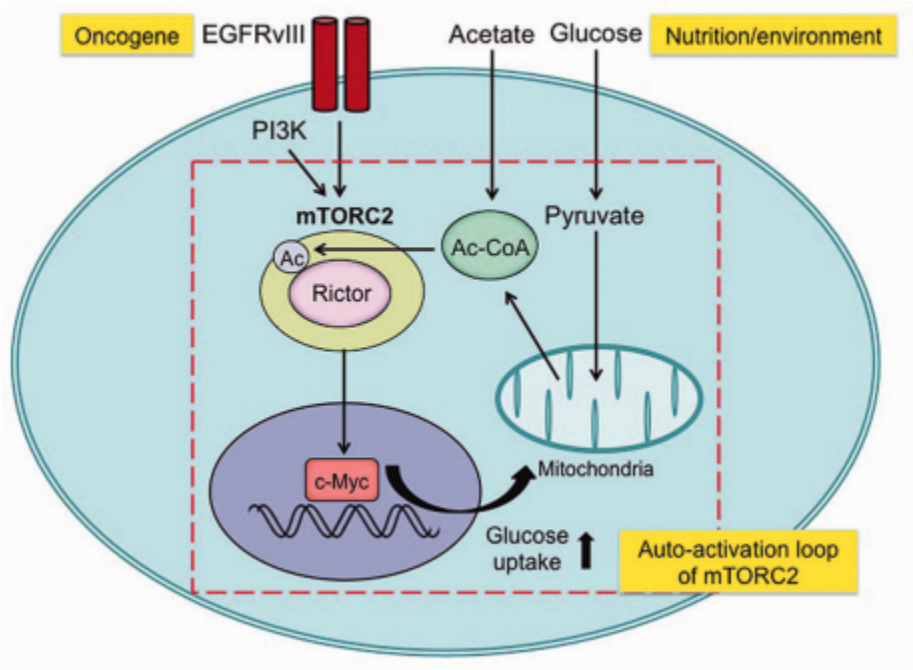

Figure 4. **Glucose-dependent acetylation of mTORC2 promotes targeted therapy resistance**. EGFRvIII activates downstream effectors, including mTORC2, to drive metabolic reprogramming. Glucose and acetate are converted into acetyl-CoA, which is utilized to acetylate mTORC2, rendering it constitutively active as a result of mTORC2 mediated inhibition of class II histone deacetylases (Figure 3). See text for additional detail. Figure from (Masui et al., 2015).

REFERENCES

Babic, I., Anderson, E.S., Tanaka, K., Guo, D., Masui, K., Li, B., Zhu, S., Gu, Y., Villa, G.R., Akhavan, D., et al. (2013). EGFR mutation-induced alternative splicing of Max contributes to growth of glycolytic tumors in brain cancer. Cell Metab. *17*, 1000–1008.

Clower, C.V., Chatterjee, D., Wang, Z., Cantley, L.C., Vander Heiden, M.G., and Krainer, A.R. (2010). The alternative splicing repressors hnRNP A1/A2 and PTB influence pyruvate kinase isoform expression and cell metabolism. Proc. Natl. Acad. Sci. U. S. A. *107*, 1894–1899.

Dang, C.V. (2012). Links between metabolism and cancer. Genes Dev. *26*, 877–890.

David, C.J., Chen, M., Assanah, M., Canoll, P., and Manley, J.L. (2010). HnRNP proteins controlled by c-Myc deregulate pyruvate kinase mRNA splicing in cancer. Nature *463*, 364–368.

Liu, F., Hon, G.C., Villa, G.R., Turner, K.M., Ikegami, S., Yang, H., Ye, Z., Li, B., Kuan, S., Lee, A.Y., et al. (2015). EGFR Mutation Promotes Glioblastoma through Epigenome and Transcription Factor Network Remodeling. Mol. Cell *60*, 307–318.

Masui, K., Tanaka, K., Akhavan, D., Babic, I., Gini, B., Matsutani, T., Iwanami, A., Liu, F., Villa, G.R., Gu, Y., et al. (2013). mTOR complex 2 controls glycolytic metabolism in glioblastoma through FoxO acetylation and upregulation of c-Myc. Cell Metab. *18*, 726–739.

Masui, K., Tanaka, K., Ikegami, S., Villa, G.R., Yang, H., Yong, W.H., Cloughesy, T.F., Yamagata, K., Arai, N., Cavenee, W.K., et al. (2015). Glucose-dependent acetylation of Rictor promotes targeted cancer therapy resistance. Proc. Natl. Acad. Sci. U. S. A. *112*, 9406–9411.

Pavlova, N.N., and Thompson, C.B. (2016). The Emerging Hallmarks of Cancer Metabolism. Cell Metab. *23*, 27–47.

Warburg, O. (1956). On respiratory impairment in cancer cells. Science *124*, 269–270.